Republic of Iraq

Ministry of Higher Education and Scientific Research

University of Babylon / College of Science

Department of Physics

Influence of the Laser Radiation on the Structural and Optical Properties of an Organic Pigment

A Thesis

Submitted to the Physics Department, College of Science, University of Babylon in Partial Fulfillment of the Requirements for the Degree of Master of Science in Physics.

By

Ahmed Ali Jassim Mohammed

B.Sc. in physics 2019

Supervised By

Asst. Prof. Dr.

Nihal Abdullah AbdulWahhab

2022 A.D. **1444 A.H.**

بسم الله الرحمن الرحيم

(اللَّهُ نُورُ السَّمَاوَاتِ وَالْأَرْضِ ۚ مَثَلُ نُورِهِ كَمِشْكَاةٍ فِيهَا مِصْبَاحٌ ۖ الْمِصْبَاحُ فِي زُجَاجَةٍ ۖ الزُّجَاجَةُ كَأَنَّهَا كَوْكَبٌ دُرِّيٌّ يُوقَدُ مِنْ شَجَرَةٍ مُبَارَكَةٍ زَيْتُونَةٍ لَا شَرْقِيَّةٍ وَلَا غَرْبِيَّةٍ يَكَادُ زَيْتُهَا يُضِيءُ وَلَوْ لَمْ تَمْسَسْهُ نَارٌ ۚ نُورٌ عَلَىٰ نُورٍ ۗ يَهْدِي اللَّهُ لِنُورِهِ مَنْ يَشَاءُ ۚ وَيَضْرِبُ اللَّهُ الْأَمْثَالَ لِلنَّاسِ ۗ وَاللَّهُ بِكُلِّ شَيْءٍ عَلِيمٌ)

صَدَقَ اللهُ العَلِيُّ العَظيم

سورة النور الآية (٣٥)

Supervisor Certification

I certify that this thesis entitled "***Influence of the Laser Radiation on the Structural and Optical Properties of an Organic Pigment***" was prepared under my supervision at the Department of Physics, College of Science, University of Babylon as partial requirement for the degree of Master of Science in physics.

Signature:

Supervisor

Name: Dr. Nihal Abdullah AbdulWahhab

Title: Asst. Prof.

Address: Department of Physics/ College of Science/ University of Babylon

Date: / / 2022

Recommendation of Head of Physics Department

In view of the available recommendations, I forwarded this thesis for debate by the examining committee.

Signature:

Name : Dr. Samira Adnan Mahdi

Title : Asst. Prof.

Address : Head of the Department of Physics/ College of Science/ University of Babylon

Date : / / 2022

Dedication

To…

My Uncle's Soul

My Father
My Mother
My Brothers

And My Teachers

With My love and Respect

Ahmed Ejam

Acknowledgments

At first, I am grateful to the God for the good health and wellbeing that were necessary to complete this thesis.

I would like to express my deep appreciation to my supervisor ***Asst. Prof. Dr. Nihal Abdullah AbdulWahhab****, for suggesting the topic of this thesis and the unceasing guidance throughout the course of this work with kind, wisdom and experience.*

Many thanks to the deanery of the College of Sciences at the University of Babylon and the Department of Physics for offering me the opportunity to complete my thesis.

I also register my gratitude to all, who directly or indirectly lent their hands on this project, especially, to the distinguished professor, ***Dr.Adnan H. Al-Aarajiy****.*

Ahmed Ejam

Summary

This thesis describes the influence of the laser irradiation on an organic pigment. The measurements are taken for the Copper phthalocyanine (CuPc) pigment solutions first and then to the thin film prepared by spin coating deposition technique. The samples are irradiated by lasers with varying multiple parameters (wavelength λ). The optical properties are measured for the solution and the thin film. Also, the structural properties are studied including X-Ray and FTIR measurements. The structural parameters such as the grain size, roughness, root main square are calculated and compared between the non-irradiated and laser irradiated samples.

Copper phthalocyanine solution is prepared with different concentrations $0.05, 0.1, 0.15, and\ 0.2\ g/l$. Then, the thin film are prepared using the spin coating technique with thickness $\sim 219.12\ nm$. The samples solution and thin film are irradiated by different semiconductor laser with wavelengths $650, 532, and\ 405 nm$ for different irradiation times $0, 4, , 8\ , and\ 16\ min$ for solution samples, and $0, 10, 20, and\ 30 min$ for thin film samples.

The optical properties for CuPc solution with 0.15 g/l concentration show decreasing in the absorption and reflectance with increasing the laser irradiation times while the transmission increases. The energy gap is increased with increasing the irradiation times. The optical constants (absorptivity, molar absorptivity, absorption coefficient, refractive Index, extinction coefficient, real dielectric constant, imaginary dielectric constant, optical conductivity) are decreased.

Concentrations effect on the optical properties of the CuPc before and after laser exposure of different wavelengths $650, 532, and\ 405\ nm$, for different

irradiation times $0, 4, 8, and\ 16\ min$. The results show that the band gap decreases with increasing the solution concentration. The band gap is measured in both Tauc and fluorescence method and the values are compared at concentration $0.2\ g/l$. The optical parameters are decreasing with increasing laser time irradiation for all solution concentrations.

CuPc thin films that deposited on a glass substrate with thickness $\sim 219.12\ nm$ at room temperature are irradiated by different laser wavelengths $650, 532, and\ 405\ nm$ for different times $0, 10, 20, and\ 30\ min$. The results show decreasing in the absorbance and the reflectance with increasing the irradiation times.

The structural properties are examined and the XRD results show a decrease in the peaks height with increasing the time irradiation. Also, the material tends towards amorphous as a result of the breaking of intermolecular bonds. AFM data show an obvious impact on the thin films morphology by laser irradiation. The fluctuation in values is due to the heterogeneity of the thin films surface that belong to the deposition method, but it is clearly proved that the laser is affected the thin films.

Contents

List of Figures

List of Tables

List of Symbols

Symbol	Description
A	Absorbance
α	Absorption Coefficient
r	Constant in Tauc Formula
θ	Diffraction Angle
E	Dielectric Constant
e	Electric Charge
E_g	Energy Gap
E	Electric Filed
E_P	Energy of an Absorbed or Emitted Phonon.
k	Extinction Coefficient
v	Frequency
$\varepsilon_{im.}$	Imaginary Part of Dielectric Constant
$\sigma_{Optical}$	Optical Conductivity
hv	Photon Energy
h	Plank Constant
I_o	Incident Photon Intensity
ρ_m	Material Density
n	Refractive Index
ε_{Real}	Real Part of Dielectric Constant
ρ	Resistivity
R	Reflectance
P	Radiation Power
I	Transmitted Photon Intensity
T	Transmittance
t	Thickness of Thin Film
d_{hkl}	The Inter Planar Distance
c	Velocity of Light in Vacuum
λ	Wavelength

List of Abbreviations

Abbrev	Term
CuPc	Copper Phthalocyanine
C. B.	Conduction Band
FTIR	Fourier Transform Infrared
FWHM	Full Width at Half Maximum
HOMO	High Occupied Molecular Orbit
IR	Infrared Radiation
LOMO	Lowest Occupied Molecular Orbit
H_2Pc	Metal Free Phthalocyanine
MPc	Metal Phthalocyanine
PL	Photoluminescence
Pcs	Phthalocyanines
PD	Photo Detector
UV	Ultra Violet
V. B.	Valence Band
Vis	Visible
XRD	X-Ray Diffraction

CHAPTER ONE

GENERAL INTRODUCTION

1 Introduction

Phthalocyanines (Pcs) are macrocyclic chemicals that have drawn a lot of interest because of their unusual physical and chemical features [1]. Phthalocyanine is an organic semiconductor with excellent light, moisture, and oxygen resistance that is frequently employed in sensors applications and transistor production [2].

Phthalocyanine and its derivatives are porphyry derivatives that cover a wide variety of compounds with similar structures. Since their first synthesis in the early twentieth century, phthalocyanines have been highly sought-after compounds in the industry. Their attraction stemmed from their vivid coloring properties, which led to their widespread use as pigments. However, since 1948, when their semiconducting capabilities were discovered, phthalocyanines have piqued the interest of a considerably larger spectrum of industrial applications [3].

Phthalocyanines have a rich hue and are chemically and thermally stable. Due to its particularly high thermal and chemical stability, it is suitable for usage in a wide range of technical applications, including digital cameras, mobile phones, and personal computers [4].

Metal phthalocyanine (MPc) structure can be found in a variety of crystalline phases, [5–7] and deposition circumstances, such as substrate temperature or annealing temperature, which might affect the outcome, the difference in structure of MPc displays multiple crystallographic phases and diverse shapes. The MPc phase is a metastable phase that can be thermally changed into a stable phase. Furthermore, both the electrical and optical properties of MPcs have been impacted by their structural attributes [8,9].

1.2 Semiconductors

Semiconductors and their physics have become one of the most important topics of solid-state physics in terms of applications as a result of its astonishing progress [10].

Semiconductors are so named because their capacity to carry electricity is moderate. Indeed, temperature may alter the conductivity of a typical semiconductor to the point that most of them appear to be insulators at low temperatures and metals at high temperatures. Impurities can also be an effective factor. Intrinsic semiconductors are free of substantial impurities, while extrinsic semiconductors are doped with impurities. Both of these featues are necessary for microelectronic devices operation [11].

A semiconductor is often characterized as a material having an electrical resistivity of $10^{-2} - 10^{9}\ \Omega.cm$. Materials with zero band gap are classified as metals or semimetals, whereas insulators have a higher energy gap than $3\ eV$ [12].

1.3 Organic Semiconductors

Organic semiconductors usually consist of hydrocarbons (hydrogen and carbon atoms bonding, sometimes with other atoms of oxygen and nitrogen, depending on the structures of organic molecules). Organic solids are formed by the weak Van der Waals forces, leading to frail bonding caused by the weak overlap of the electronic wave functions between neighboring molecules. The weak bonding in the organic molecules means the inter-molecular separation in organic solids is usually much greater than that in inorganic solids, leading to far narrower electronic bands than in inorganic solids, and hence the energies of the

valence and conduction bands of solids can be well approximated by those of the highest occupied molecular orbitals (HOMO) and lowest unoccupied molecular orbitals (LUMO) of individual molecules, respectively [13].

Organic semiconductors are especially fascinating since they combine unique semiconducting optical and electrical qualities with ease of manufacture and control of organic material properties. Unlike inorganic semiconductors, organic semiconductors' electrical and optical properties are mostly determined by their chemical structure; therefore they do not require well organized crystals. This simplifies device manufacture, for example, using solution deposition, and is projected to result in lower final device costs. Furthermore, it allows for the production of many devices side by side, OLEDs (organic light-emitting diodes) [14].

Semiconducting properties of organic semiconductors are determined, or at least largely influenced, by π electrons in π bonds. Since π bonds are weaker than σ bonds and, furthermore, π electrons are delocalized throughout a network of connected p-orbitals, it is much easier to add an electron to and extract one from π electrons as well as to excite π electrons with a visible light. The p_z-orbitals of sp^2-hybridized C-atoms in the molecules create a conjugated π-electron system in both, as shown in Fig. (1-1). Therefore, the lowest electronic excitations of conjugated molecules are the π-π*-transitions with an energy gap typically between 1.5 and 3 eV leading to absorption bands observed in a range from near infrared to near ultraviolet. The energy gap can be controlled by the degree of conjugation in a molecule [13,15].

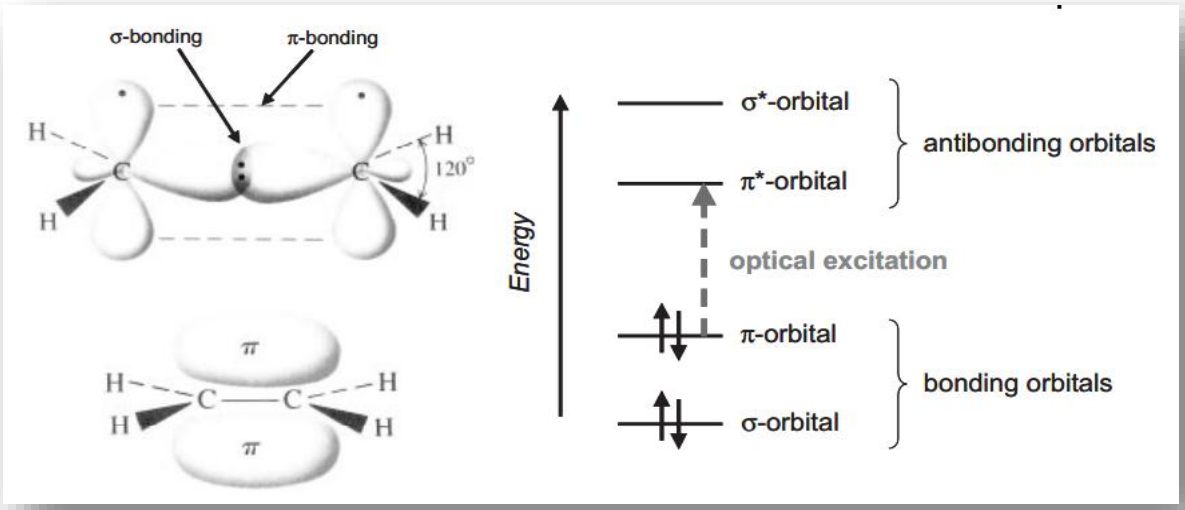

Figure 1-1: The simplest conjugated π-electron system in ethane, which has left *σ*- and π-bonds. The energy levels of a π-conjugated molecule are shown in the right viewgraph. Between the π-π* orbital and the orbital lies the lowest electronic excitation [15]

1.4 Phthalocyaninces (Pcs, MPcs)

In 1907, the first Pc synthesis was reported. Pc and metal Pcs (MPcs) molecular structures were discovered and confirmed in 1930. Pcs were discovered to have a number of appealing properties, including highest purity availability due to the ease with which it crystallizes and sublimates; exceptional chemical and thermal stability; attractive optical features (high absorption in the red and blue spectrum region, resulting in exceptionally pure blue pigments); and a huge number of compounds accessible (over 70 MPcs have been identified) [16]. Pcs derivatives, with a structure comparable to porphyrin, are used in a variety of significant functional materials. The efficient electron transport abilities (an aromatic system with 18π - electrons) are credited with their beneficial features [17]. The core cavity of phthalocyanines has been shown to hold 63 distinct

elemental ions, hydrogens, for example (metal-free phthalocyanine, H_2Pc). A metal phthalocyanine (MPc) is a phthalocyanine that contains one or two metal ions [18], as shown in Fig. (1-2). There are three phases of phthalocyanines: α, β, and γ phases. Phosphocyanines, metal-substituted as well as metal-free, Gas sensors, photocapacitive and photoresistive detectors, organic thin film transistors (OTFTs), color filters, and organic laser materials all use active layers [19, 20].

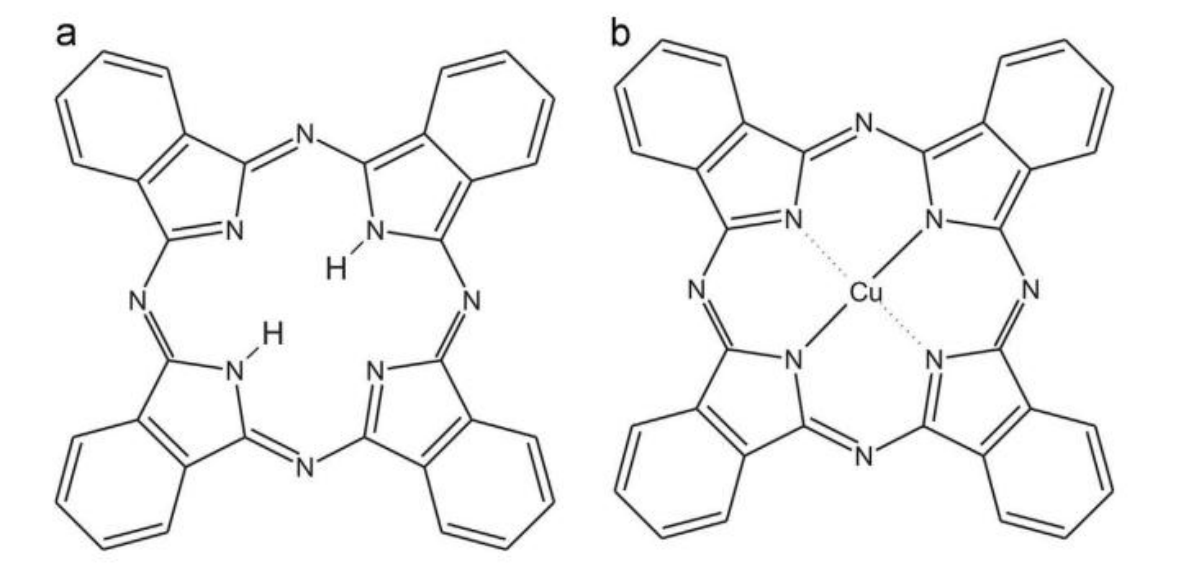

Figure 1-2: Molecular structures of (a) H_2Pc and (b) CuPc [20]

Due to their excellent electron transfer abilities having been utilized in numerous disciplines in recent decades, molecular electronics, optoelectronics, and photonics are examples, see Fig. (1-3). MPcs have an 18π electron conjugated ring system in their chemical structure; their functionalities are virtually exclusively predicated on electron transfer reactions. Furthermore, because they have a high absorption of far-red light between $(600\ and\ 850)\ nm$, which has better tissue penetration qualities, as well as suitable photosensitization of singlet oxygen,

certain derivatives are known to have potential as second-generation photosensitizers for cancer photodynamic therapy (PDT) [21]. Vacuum-sublimed films of metal phthalocyanine in general are p-type semiconductor [6,22].

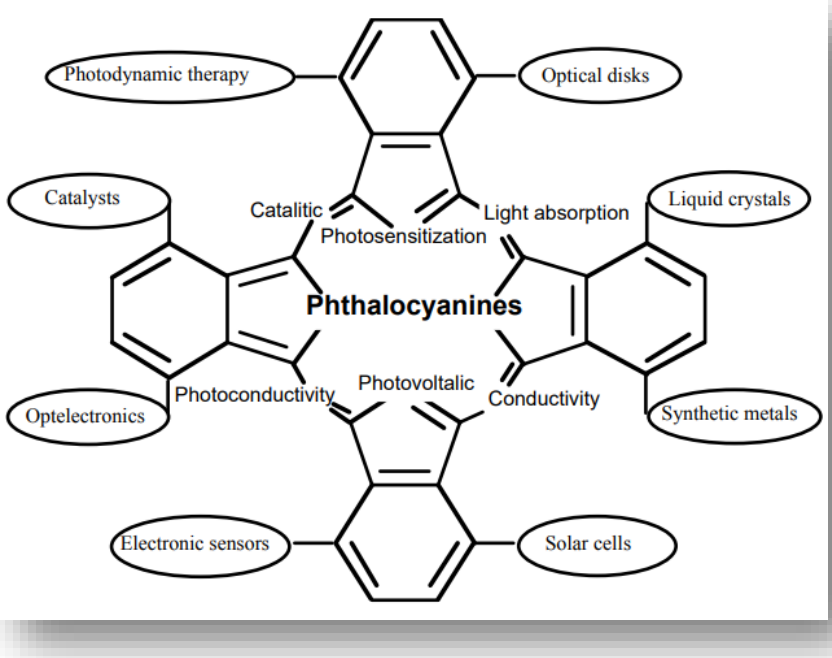

Figure 1-3: Typical function of phthalocyanine derivatives [21]

1.5 Copper Phthalocyanine (CuPc)

Copper Phthalocyanine (CuPc) Blue is the copper(II) complex of tetraazatetrabenzoporphine. The mesomeric structures indicate that all of the pyrrole rings simultaneously contribute to the aromatic system [23].

The most common polymorphic forms are known as α-and β-forms, and they differ slightly in structure and electrical characteristics. Both the molecular structure and molecular orientation influence their physical properties [8]. Because

the intermolecular force of the molecular crystals is very weak, the α-form crystalline CuPc can transform to the β-form crystalline (the most stable in terms of temperature) at temperatures above $200°C$. The molecules in the herringbone structure of the two α- and β-phases create stacks held together by Van der Waals forces and aligned at angles of 63.5^{o} *and* 44.2^{o} degrees, respectively, between the column direction (b-axis) and the molecular plane Fig (1-4) [24]. The α-phase crystallites are formed when phthalocyanine films are deposited at room temperature under low pressure, The β-phase, on the other hand, is formed at higher pressures and temperatures. $T > 210$ ˚C [25]. The crystal structure of both polymorphs, α and β, are very similar to each other. A copper-phthalocyanine molecule has a square-planar configuration with a metal ion in its center, large CuPc molecules (with a diagonal greater than 1.3 nm), facing parallel to one another, stack themselves in crystals so that they form closely packed columns in both modifications [5].

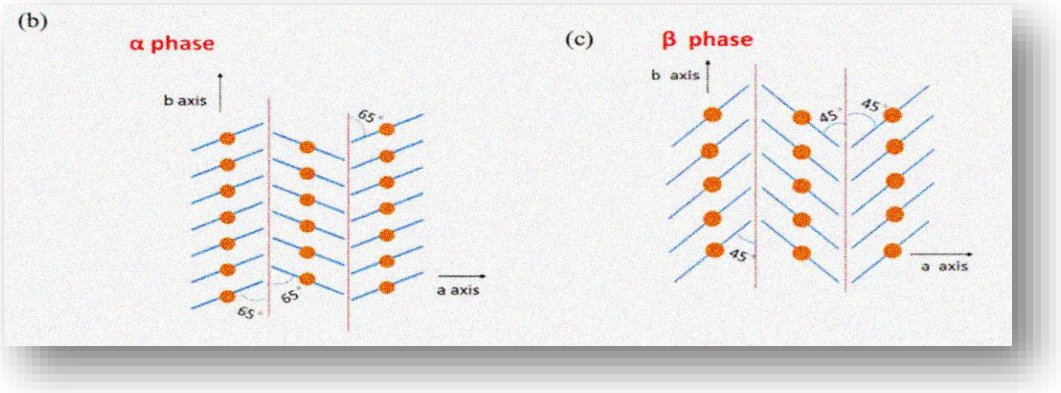

Figure 1-4: The stacked structures of (a) α-phase (b) and β-phase [24]

CuPc, is an extensively used chemicals in both basic research and technological applications. It is a big polyaromatic molecule with a planar shape [26]. Table (1-1) shows some properties of CuPc.

Table (1-1) Properties of CuPc blue pigment [1]

Name	Copper Phthalocyanine Blue (Alpha)
Molecular Structure	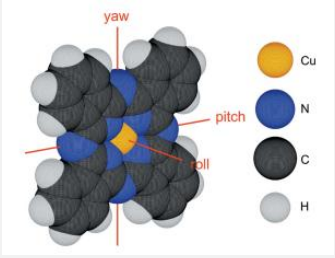 [27]
Molecular Formula	**$C_{32}H_{16}CuN_8$**
Molecular Weight	**576.08 g/mol**
Heat Fastness	**300 °C (5 min)**
Water Solubility (Max)	**0.5 %**
Crystal system	**Triclinic (anorthic)**
Cell Parameters	**a= 12.88600 Å, b= 3.76900 Å, and c= 12.06100 Å, α= 96.220°, β= 90.620 °, and γ= 90.320 °**
Density	**1.64300 g/cm³**

1.6 Literature Survey

There are many previous studies which have been investigated before starting the work, the most relevant research to our topic are.

- **In (2007), A.A.M. Farag.** [28] examined the optical absorption of thermally evaporated (CuPc) thin film. Concerning the absorption spectra of the cupper phthalocyanine molecules, it can see two distinct absorption bands which may be seen in the UV-Vis spectrum., the Soret B-band and the Q-band. Two indirect allowed transitions with appropriate energies were discovered by analyzing the spectrum behavior of the absorption coefficient (α) in the absorption zone $2.95 \pm 0.03, and\ 1.55 \pm 0.02\ eV$. The infrared absorption spectra may be used to characterize the powder's vibration modes, CuPc thin films annealed at 150 °C for two hours.

- **In (2007), Santanu Karan, *et al*.** [29] investigated the effects of annealing on the morphology and optical property of CuPc thin films, deposited at room temperature on indium tin oxide (ITO) substrates. The temperature of post-deposition annealing under normal atmospheric conditions caused a change in their surface shape. The X-ray diffractograms of CuPc thin films formed at room temperature indicated the presence of the α-phase. The α-phase is also present in thin films formed at room temperature and annealed at $100, 200, and\ 240$ ºC. When annealing temperatures are $275\ and\ 310$ ˚C, a β-phase of CuPc thin films was observed. The UV–Vis. spectrum of MPcs. is hypothesized to come from molecular orbitals inside aromatic molecules 18π-electron system and overlapping orbitals on the central metal, based on CuPc thin film optical absorption spectrum. The B-band or Soret band in the near-UV region, as well as each sample film's absorption band in the visible spectrum, is referred to as the Q-band. The energy gap shrinks as the annealing temperature rises, according to the findings. Variations in the structure of these films' crystals are related to changes in the energy gap at various annealing temperatures**.**

- **In (2008), Hassan, H, *et al*.** [30] examined the potential of the organic material (CuPc) in the solar cell as a p-type organic material. CuPc films were made on a Si-n substrate using a spin coating process, at room temperature. In the spectral region $300 - 800\ nm$, the optical characteristics of CuPc thin film were investigated using a UV-Vis-NIR spectrometer. To investigate the optical characteristics of CuPc, it was growing on a glass substrate. The UV-Vis-NIR spectrum was used to assess the absorption and transmission qualities of each film. The direct electronic transition from $\pi\ -$

π^* orbitals in the 350 to 500 nm region in the UV region creates the absorption edge of an intense band known as the Soret Band B-Band. The Q-Band, which occurs in the visible area between $550\ and\ 750\ nm$, is the other band. The transfer of charge from the highest occupied molecular orbit (HOMO) to the lowest unoccupied molecular orbit (LUMO) is connected to the Q-Band edge that appears in two trapping levels (LUMO). The energy gap created by vacuum coating a CuPc thin layer on glass and annealing at 300 ^{o}C with a thickness of $280\ nm$ is $2.75\ eV$. Meanwhile, the energy gap value was calculated using a CuPc thin film on a glass substrate $102\ nm$ which is generated by thermal evaporation and annealed at 250 ^{o}C for 1 hour $2.64\ eV$.

- **In (2009), M Della Pirriera, *et al.*** [31] studied the structural and optical properties of thermally produced CuPc thin films at various substrate temperatures. The results of XRD for the films thickness $700\ nm$ deposited on glass at various substrate temperatures, illustrate all the patterns the CuPc polymorphous structure's distinguishing properties, which are defined by a single sharp reflection at $2\theta = 6.9^{o}$, $d = 12.9$ Å. The intensity of the (200) peak increases as the substrate temperature rises, indicating that the crystal phase rather than the amorphous phase is growing. The grain of the crystals grows as the temperature of the substrate rises. The optical characteristics, on the other hand, show no substantial alterations. High optical absorption coefficients $(more\ than\ 5\ x\ 10^{-5}\ cm^{-1})$ are present in the films. The absorption coefficient in the sub-gap area is quite low, and it has a little temperature dependency.

- **In (2012), Sawanta S. Mali *et al.*** [32] used various spectroscopy approaches to explore the optical characteristics of CuPc thin layers. The visible absorption spectra of CuPc thin films formed at room temperature using vacuum deposition made up of two different bands Q-band and B-band. Spectrophotometry, reflectometry, FTIR, UV-Vis. and other techniques were used to analyze the CuPc thin films that had been deposited. High optical absorption coefficients are seen in the films, which are greater than $5\ x\ 10^{-5} cm^{-1}$. At energy levels between $1.7\ and\ 1.5\ eV$, there is an exponential reduction in optical absorption.

- **In (2013), C. Defeyt *et al.*** [33] contributed to the identification of α- and β-copper phthalocyanine blue pigments by X-ray powder diffraction and attenuated total reflectance micro-fourier transform infrared spectroscopy This study focuses on the CuPc polymorphs commonly used corresponding to the stabilized and un-stabilized α- and β- polymorphic modifications. The Colour Index generic name used for the CuPc blue pigments is Pigment Blue 15 (PB15). More specifically, PB15:0 is used for the un-stabilized α-CuPc, PB15:1 for the non-crystallizing α-CuPc, PB15:3 for the un-stabilized β-CuPc, PB15:4 for the non-flocculating β-CuPc. Diffractograms of CuPc samples having the same crystalline structure do not differ much from each other's. The averaged d values and diffractogram patterns are very close and cannot be considered as reliable markers to discriminate PB15:0 from PB15:1 and PB15:3 from PB15:4. The similarity of the d spacing. The FTIR results show that polymorphic markers underlined for dry pigments are reliable for the CuPc identification crystalline structure in artists' paints. The CuPc

polymorphs have been identified for every analyzed artists' paint by using the discriminating band positions observed in FTIR spectra.

- **In (2015), H. A. Afify *et al.*** [34] demonstrated the structural and optical properties of deposited and annealed CuPc thin films. Spectrophotometric measurements in the spectral range $200 - 2500\ nm$ were used to analyze the optical constants and lattice dielectric constant of spin coated CuPc thin films before and after annealing. The values of the direct optical band gap at $1.52, and\ 2.85\ eV$ were red shifted to $1.4, and\ 2.42\ eV$ for the annealed film. For near-infrared photonics, this change is significant.

- **In (2015), Ali H.A. Jalaukhan.** [35] Thin films of Copper Phthalocyanine (CuPc) of about 200 nm thicknesses have been deposited by thermal evaporation method on a glass substrate at 303 ^{o}K and 403 ^{o}K substrate temperature (Ts) and under pressure better than 10^{-5} mbar. This study concentrated on the effect of substrate temperature on some physical properties of CuPc thin films such as optical properties within the visible range. The spectra have been characterized by two major bands i.e. B and Q bands, both corresponding to $\pi - \pi^*$ transitions. It is found that the optical band gap decreases from 3.29 eV for the film deposited at 303 ^{o}K to 3.23 eV for film deposited at 403 ^{o}K. This can be attributed to the increasing of localized states in the forbidden gap which is due to increasing of the films defects (such as voids) between grain boundaries with increasing substrate temperature or due the phase transition from β –phase to α –phase.

- **In (2016), M. T. Hussein *et al.*** [36] deposited the CuPc thin films on glass and silicon substrates by thermal evaporation and pulsed laser deposition

(PLD) methods. CuPc thin films were made at various annealing temperatures $25, 50, 75, 100, and\ 150$ °C. It was discovered that as the annealing temperature was changed, the crystallinity and surface morphology changed and improved. The goal of their research is to determine the ideal temperature at which the CuPc thin film generates the greatest structural features for the production of organic field effect transistors.

- **In (2017), Xiaowei Ai, *et al.*** [24] evaluated the crystal structures of both the powder and the films by the XRD technique for the CuPc that deposited by a thermal evaporation method on glass substrates in a high vacuum. CuPc films only display one peak at $2\theta = 6.84^{o}$, suggesting a strong α-phase texture along the (200) orientation CuPc powder, on the other hand, exhibits a succession of peaks, which are corroborated by the mixing of both α- and β-phases. All of the films are α-phase, and when the substrate temperature rises, the complete width of half maximum for the (200) diffraction peak narrows. The average grain size computed by Scherrer's formula for the film without annealing which is $(33.63\ nm)$, then increases to (58.29 nm) with the film annealed at 200 °C. The spectrum of CuPc films exhibits two intense distinctive bands: B band $\pi-\pi^{*}$ transition in the UV region and Q band ($\pi-\pi^{*}$ transition) in the visible area, as seen in the UV–Vis absorption spectra. The free electron oscillation around the Cu center is likely to be affected by increased particle size with rising substrate temperature, resulting in a red shift in light absorption.

- **In (2017), JING XU, *et al.*** [37] investigated the morphology of CuPc thin films produced by solvent–vapour annealing (SVA). XRD data for CuPc thin films of 40 nm thickness coated on bare quartz for 1 h at room temperature

20 ºC with various SVAs and then dried under ambient conditions. A single sharp reflection can be noticed at $2\theta = 6.9^{o}$, $d = 12.8\,\text{Å}$ which corresponds to the (200) lattice plane of the α-phase of CuPc. Because the location of the diffraction peak does not vary, the solvent–vapour is different, confirming that the CuPc thin films have the same polycrystalline structure. The reflection intensity at $2\theta = 6.9^{o}$ with varied solvent–vapours, there is a commensurate rise and sharpness, indicating greater ordering and crystallinity within CuPc thin films.

- **In (2019), M. T. Hussein *et al*.** [38] examined the optical absorption spectrum, Photoluminesces, and non-linear optical properties for CuPc thin films $150, 300, and\ 450\ nm$ respectively using a pulsed laser deposition (PLD) approach. The absorption spectra revealed two bands, one in UV about $330\ nm$, known as B-band, and the other in visible around $650\ nm$, known as Q-band.

- **In (2020), Hubert Gojzewski *et al*.** [39] deposited CuPc thin films on silicon substrates at room temperature using four different solution processing methods: drop-casting, dip-coating, spin-casting, and spray-coating. AFM investigated the CuPc films. The film morphology varies based on the concentration of the solution, the number of layers, and the manner of deposition. For example, the morphology of films created by dip-coating ranges from very broad $600\ nm$ yet flat $1\ nm$ ribbons to crystalline rod-like characteristics (multi-layered ribbons) when formed by spray-coating.

- **In (2021), Ameer F. Abdulameer, *et al.*** [40] studied the structural and optical properties of CuPc thin films doped with fullerene; the films'

properties were obviously altered by the annealing temperatures, which reduced grain size as demonstrated by XRD and AFM studies, resulting in an increase in the optical energy gap. The remarkable thermal stability of the blended film was validated by FTIR measurements, which showed no breakdown when the annealing temperature was increased. The structural investigations of annealed and as deposited samples revealed a polymorphism structure dominated by CuPc, with a preferred orientation of the plane (100) of $2\theta = 7^{o}$ except at 150 ^{o}C, when a minor peak around $2\theta = 31^{o}$ for C_{60} was seen. The presence of a tight packing sheet with a smooth surface was shown by AFM observations. The FTIR spectra emphasized the bonding between CuPc and C_{60}. UV-Vis Absorption spectroscopy confirmed that the CuPc was dominating the optical properties with a small shift in Q band towards higher wavelengths.

- **In (2021), R. R. Mohammed *et al*.** [41] prepared CuPc thin films with various thicknesses $150, 300\ and\ 450\ nm$ utilizing pulsed laser deposition technique using Q – Switched Nd:YAG laser pulses at $1.64\ \mu m$ wavelength, 6 Hz frequency, 9 ns width, and $240\ mJ$ energy at room temperature. The optical absorption spectra of CuPc thin films revealed two bands of absorption, one in the visible range at roughly $635\ nm$, referred to as Q-band, and the other in the UV region at $330\ nm$, referred to as B-band. CuPc thin films were discovered to exhibit straight band gaps of roughly $1.81\ and\ 3.14\ eV$.

- **In (2021), Lekshmi Vijayan *et al*.** [42] investigated the light affectability of a CuPc thin layer using a UV–Visible spectrophotometer. The UV–Vis spectra for thermally evaporated thin films of CuPc on a glass surface with a

thickness of $50\,nm$. The absorption spectra demonstrated that the material was exceptionally sensitive to light across the visible range, with maximal sensitivity at $300 - 400\,nm$ and $550 - 750\,nm$. The CuPc layer was able to absorb light and produce a large number of charge carriers while also acting as a transport route for photo-generated carriers.

1.7 The Aims of the Project

The following objectives are examined during the research:

1. Characterizing the copper phthalocyanine solution and thin films.
2. Investigating the influence of the laser irradiation on the optical properties of copper phthalocyanine solution and thin films with different laser wavelengths for different irradiation times.
3. Studying the laser irradiation effect on the structural properties of the deposited thin films.

CHAPTER TWO

THEORETICAL PART

CHAPTER THREE

EXPERIMENTAL PART

2 Introduction

This chapter presents a brief overview of the underlying principles for the relevant theoretical topics to the work of this thesis starting from laser interaction with matter until the diagnostic techniques including UV-Vis spectroscopy, fluorescence, surface morphology and structural properties.

2.2 Laser Interaction with Matter

Lasers are unique types of light with incredible properties. "LASER" stands for “Light Amplification by Stimulated Emission of Radiation” [43]. Since their invention in 1960, lasers have been shown to be extremely valuable in industry, medicine, technology, and the military. Scientists have been inspired to do studies on this topic due to its widespread application in society. Lasers are valuable because they are coherent, monochromatic, and have other features that allow them to be focused at a point and induce ionization, excitation, and scattering when passed through matter, which can be used to examine the properties of some materials [44,45].

Some electromagnetic energy is reflected, some is absorbed, and some is transmitted when it hits a surface. It will be absorbed in accordance with the Beer–Lambert equation, when it flows through the new medium [43]:

$$I = I_o e^{-\alpha t} \qquad (2-1)$$

Where α is the absorption coefficient, which is influenced by the medium, the wavelength, and the intensity.

As seen in Fig. (2-1), the radiation of the electromagnetic (EM) wave is represented by the electric and a magnetic field vector.

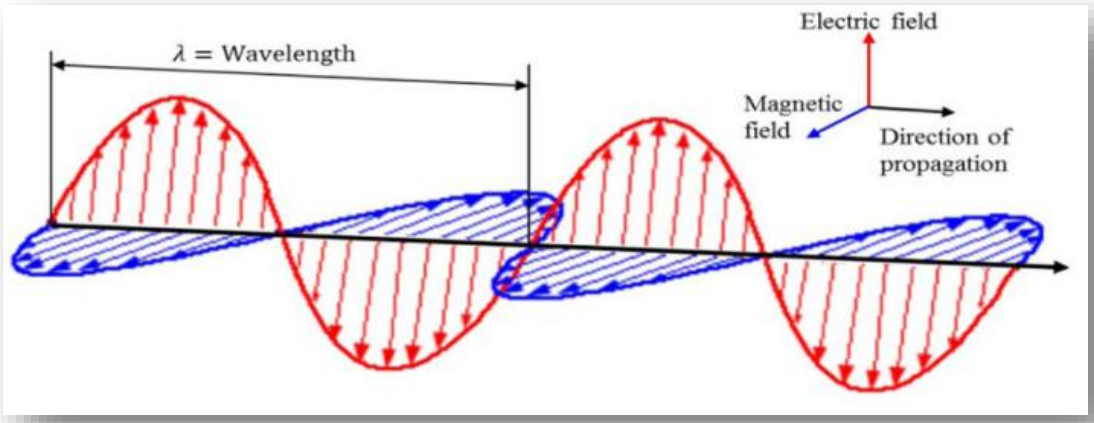

Figure 2-1: The vectors of the electric and magnetic fields in the electromagnetic wave [46]

When an (EM) wave passes through a small elastically bound ionized particle, the electric field (E) is exerted on the particle by the electric force which causes it to move. The force is so weak that it cannot vibrate an atomic nucleus. The "Inverse Bremsstrahlung Effect" describes the process of photons being absorbed by electrons. The electron will be reradiated in all directions or be limited by the lattice phonon as it vibrates [47,48].

2.3 Fourier Transform Infrared Spectrometer (FTIR)

The infrared (IR) ranges of $14000 - 4\,cm^{-1}$ is splited into three regions: near-infrared $14000 - 4000\,cm^{-1}$, mid-infrared $4000 - 400\,cm^{-1}$ and far-infrared $400 - 4cm^{-1}$. IR light was first discovered in the nineteenth century [49–51]. Since then, scientists have discovered a variety of applications for infrared light. They used infrared absorption spectroscopy to determine the structures of molecules by observing how they absorb IR light. The vibrational spectrum of molecules is represented by infrared light. When specimens are exposed to IR radiation, particular wavelengths are absorbed, as a result, the moment of dipole

changes. As a consequence, the vibrational energy levels of the sample molecules change from ground to excited. The vibrational band gap controls the frequency of the absorption peak. The number of absorption edge determines the molecule's vibration freedom. The intensity of absorption peaks is related to the dipole moment shift and the probability of energy level transitions. As a consequence, studying the infrared spectrum provides copious structural information about a molecule. IR absorption spectroscopy is considerably more beneficial since it can analyze any gas, liquid, and solid materials. Because most organic compounds' absorption radiation occurs within this region, it is the most commonly used region for IR absorption spectroscopy $4000 - 400\ cm^{-1}$ [52].

The advantages of FTIR spectrometers are numerous [50]:

(1) The signal-to-noise ratio of spectrum is significantly higher than the previous generation infrared spectrometers.
(2) The accuracy of wavenumber is high. The error is within the range of $\pm\ 0.01\ cm^{-1}$.
(3) The scan time of all frequencies is short (approximately 1 s).
(4) The resolution is extremely high $0.1 \sim 0.005\ cm^{-1}$.
(5) The scan range is wide $1000 \sim 10\ cm^{-1}$.
(6) The interference from stray light is reduced. Due to these advantages, FTIR Spectrometers have replaced dispersive IR spectrometers.

An interferometer, a sample container, a detector, an amplifier, an A/D converter, and a computer are all components of a standard FTIR spectrometer. The source's radiation went through a sample, via the interferometer, and into the detector. The amplifier and analog-to-digital converter then amplifies and converts

the signal to digital. After that, the signal is sent to a computer, which executes the Fourier transform [49].

2.4 Optical Properties of Semiconductors

The optical characteristics of semiconductors at low enough light intensities are referred to as linear properties. A semiconductor's absorbance or other optical characteristics are controlled by a variety of physical processes [1]. These processes, in turn, are impacted by external factors like as pressure, temperature, and other wavelengths of light. As a result, one may distinguish between intrinsic optical qualities of semiconductors, which are dependent on their flawless crystalline state, and extrinsic optical properties, which are introduced when the sample is subjected to a laser beam, or flaws [53].

Semiconductors absorb photons from incident beams; absorption is proportional to photon energy ($E = hv$); The electronic transition between the material's valence band and conduction band (h is Plank's constant, v is incoming photon frequency) is linked to absorption [12].

The relationship between the photon energy and wavelength, $E = hv = hc/\lambda$ so the energy gap is given by [10]:

$$E_g(eV) = \frac{hc}{\lambda(nm)} = \frac{1240}{\lambda(nm)} \qquad (2-2)$$

The absorbed energy is proportional to the thickness of the specimen in most situations of optical absorption. The relationship (2 – 1) describes the intensity variation inside the absorptive medium [54]. The absorption coefficient is given by the following formula:

$$\alpha = \frac{4\pi k}{\lambda} \qquad (2-3)$$

We should clarify that a (measured in cm^{-1}) refers to the attenuation of the radiation intensity, not the electric field [53]. The commencement of absorption at the area of inter band transitions from valence to conduction bands is the energy dependence of the absorption coefficient $\alpha(h\nu)$, which we are interested in.

For simplicity, the energy dependence of at the band edge for band-to-band and exciton transitions is described as follows:

1. Allowed direct transitions, with ignoring the exciton effects:

$$\alpha(h\nu) = B\ (h\nu - Eg)^{\frac{1}{2}} \qquad (2-4)$$

Amorphicity is inversely proportional to B. The transition is called allowed if it happens between states with the same wave vector, but not equal to zero.

2. Forbidden Direct transition, which obeys the following relation:

$$\alpha(h\nu) = B(h\nu - Eg)^{\frac{3}{2}} \qquad (2-5)$$

Because there is a considerable momentum difference between the sites in the valence and conduction bands where the transition occurs in an indirect transition, the valence band maxima do not have the same k value as the conduction band maxima Fig. (2-2). Phonons aid is required to conserve momentum [55]:

$$h\nu = E_{gap} \pm E_P \qquad (2-6)$$

Where E_{photon} is the energy of an absorbed or emitted phonon.

Indirect transmission is achieved by using the absorption coefficient data, by using the equation [56,57]:

$$\alpha E = \acute{B}(E - E_g)^2 \qquad (2-7)$$

Reflectivity data is used to evaluate the refractive index by [58]:

$$n = \left[\frac{4R}{(R-1)^2} - k^2\right]^{1/2} - \frac{(R+1)}{(R-1)} \qquad (2-8)$$

The extinction coefficient is determined by the following equation [59]:

$$k = \frac{\alpha\lambda}{4\pi} \qquad (2-9)$$

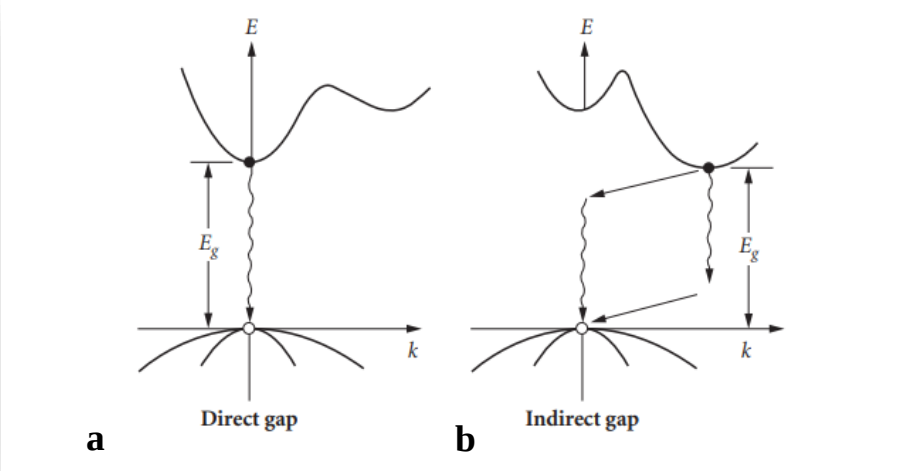

Figure 2-2: (a) Direct transition (b) Indirect transition [53]

The optical conductivity is calculated using the following equation:

$$\sigma = \frac{\alpha\, n\, c}{4\pi} \qquad (2-10)$$

Where c is the speed of light.

The phenomenological formula are used to compute the real and imaginary components of the optical dielectric constant, ε_{real} and $\varepsilon_{im.}$ which make up the complex refractive index [1]:

$$\acute{n} = n_1 - in_2 \qquad (2-11)$$

k, is used to represent the imaginary component of the index of refraction, n_2.

$$\acute{n} = n_1 - ik \qquad (2-12)$$

The index of refraction $\acute{n} = \sqrt{\varepsilon}$, $\acute{n}^2 = \varepsilon$ presides over most optical phenomena like refraction and reflection [60].

From (2-12):

$$\varepsilon = (n - ik)^2 \qquad (2-13)$$

$$= n^2 + 2ink - i^2k^2 \qquad (2-14)$$

$$\varepsilon_{real} = n^2 - k^2 \qquad (2-15)$$

and

$$\varepsilon_{Im.} = 2nk \qquad (2-16)$$

The optical constants, n and k, are the real and imaginary components of the refractive index. They represent the material's linear optical properties. The existence of k, the imaginary component, indicates that the semiconductor absorbs optical radiation. Coefficients of reflection, transmission, and absorption. k is relatively small in spectral areas where absorptive processes are weak or nonexistent, such as the sub-band gap range, but it is quite big in regions of significant absorption [53].

2.5 Fluorescence

Fluorescence is based on photoluminescence (PL), which is a glow and light emission phenomena. It is the physical process of light being released after being absorbed by a material. The PL is formed by fluorescent molecules called fluorophores that absorb energy (light). The absorbed energy enhances the energy level of electrons. When electrons return to their ground state, they emit light, this excited state becomes unstable [61].

The required energy to excite an electron is always greater than the energy necessary to fall back. The emission wavelength is usually longer than the excitation light because higher-wavelength radiation is less energetic than short-wavelength radiation. The Stokes shift is the distance between the maximums of excitation and emission (peaks). Figure (2-3).

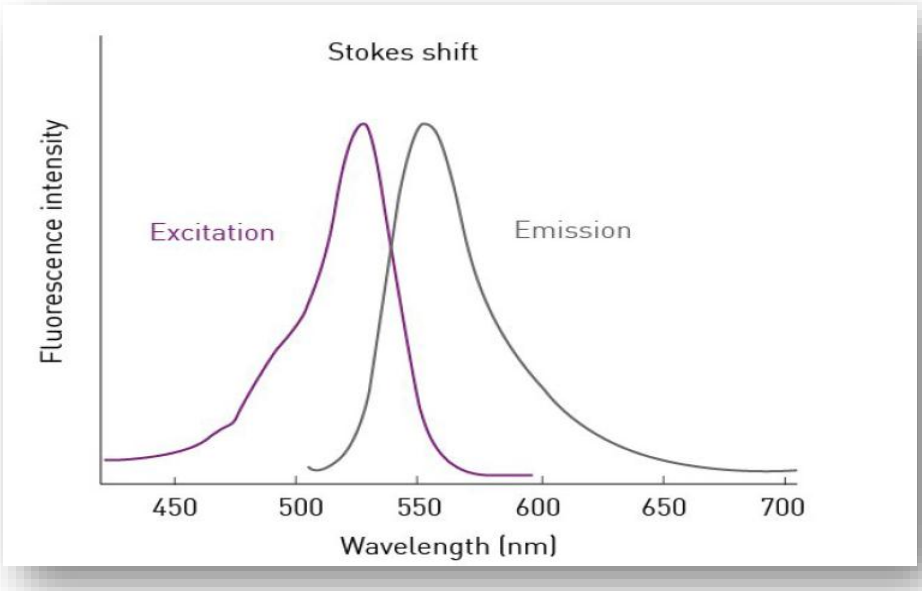

Figure 2-3: The wavelength difference between the excitation (absorption) and emission peaks which is known as the Stokes shift [61]

2.6 X-ray Diffraction (XRD)

XRD is a powerful non-destructive approach for material characterization can be applied to identify crystal structure, orientations, and crystal size. For the description, a typical XRD wavelength that corresponds to the crystal's interatomic distance is utilized. The normal spacing d_{hkl} around neighboring crystal orientations within the planes indices (hkl) is determined by using Bragg's formula [12]:

$$2d \sin\theta = n\lambda \qquad (2-17)$$

Fig. (2-4 a) shows the wavelength of the X-ray beam that strikes a film, as well as its angle of incidence and reflective. Because the first-order reflected beam is used to do the measurement. $n = 1$ in (2-17). As shown in Fig. (2-4 b), the intensity $I(\theta)$ of the dispersed x-ray beam is typically measured as a function of 2θ. For a crystal with low defect density, the material's periodicity results in relatively narrow intensity peaks in the scattered x-ray field at angles where constructive interference occurs. According to the $I(\theta)$ versus 2θ plot, the location 2θ of the first order peak is utilized to calculate (d_{hkl}) from values of λ and θ (2-17). For the crystallographic direction indicated by (hkl), this measured value is frequently referred to as the 'd-spacing' [62].

This is the diffraction Bragg condition. In the corresponding directions, the intensity of the reflected beam exhibits distinct peaks. Bragg peaks are what they're called. Changing the detector's angle, 2θ will reveal the Bragg peak. The investigation of grain size backs up the observed difference in crystallization in the films, the grain size of crystallite is calculated using Scherer's equation [63].

$$\left(D = \frac{0.9\,\lambda}{\beta\,cos\theta}\right) \qquad (2-18)$$

Where 0.9 is the Schere constant, λ is the X-ray wavelength, β is the FWHM, and θ is the Bragg angle.

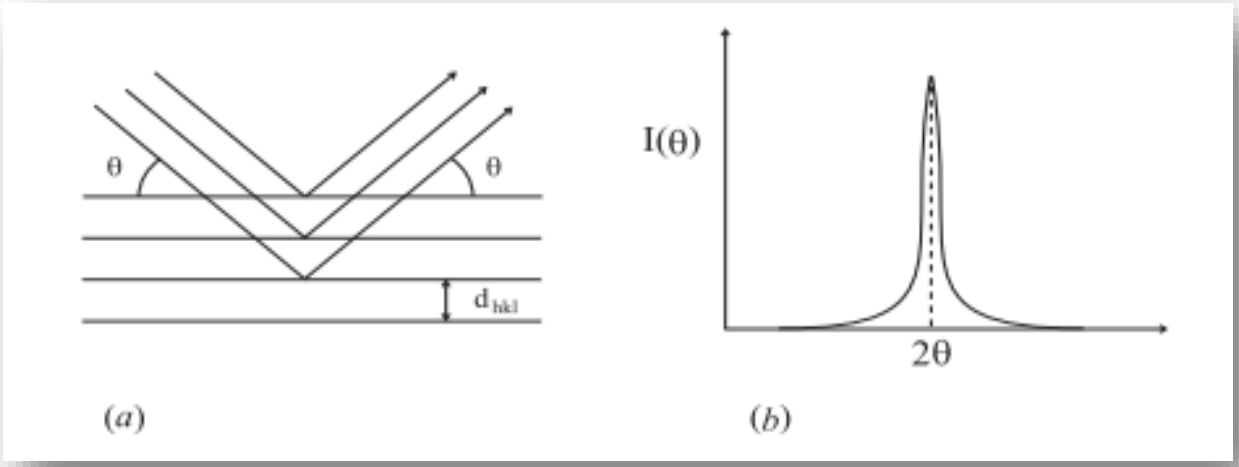

Figure 2-4: (a) The reflection of x-rays by crystallographic planes, (b) Plot of x-ray beam intensity I(θ) versus 2θ [62]

2.7 Atomic Force Microscopy (AFM)

In 1986, Binnig, Quate, and Gerber introduced the atomic force microscopy technique [64]. Because of the ability to get three-dimensional morphology maps using sub-nanometer of specimens, atomic force microscopy has emerged as one of the most powerful and adaptable single molecule methods [63,65].

The AFM consists of a small needle on the end of a micro machined flexible cantilever that raster scans the surface of the sample. When the tip is placed closer to the specimen surface, the cantilever is deflected due to attraction and repulsion forces. To construct topographical pictures, this deflection is recognized and

processed as a function of position in the (x, y) plane. The AFM may operate in contact (the tip is always in touch with the surface), non-contact (the cantilever vibrates and changes in its resonance frequency are utilized to make pictures), and intermittent modes (the cantilever vibrates and variations in its resonance frequency are used to generate images), with a high oscillation between repulsive and attractive forces, the cantilever travels quickly [66].

3 Introduction

This chapter includes a description of the materials and devices used in this research, in addition to the method of thin film deposition and thickness measurement. There are many techniques and devices are used to characterize the samples such as spectrophotometers, fluorescence, XRD, AFM and FTIR. Figure (3-1) shows the schematic diagram for the experimental work.

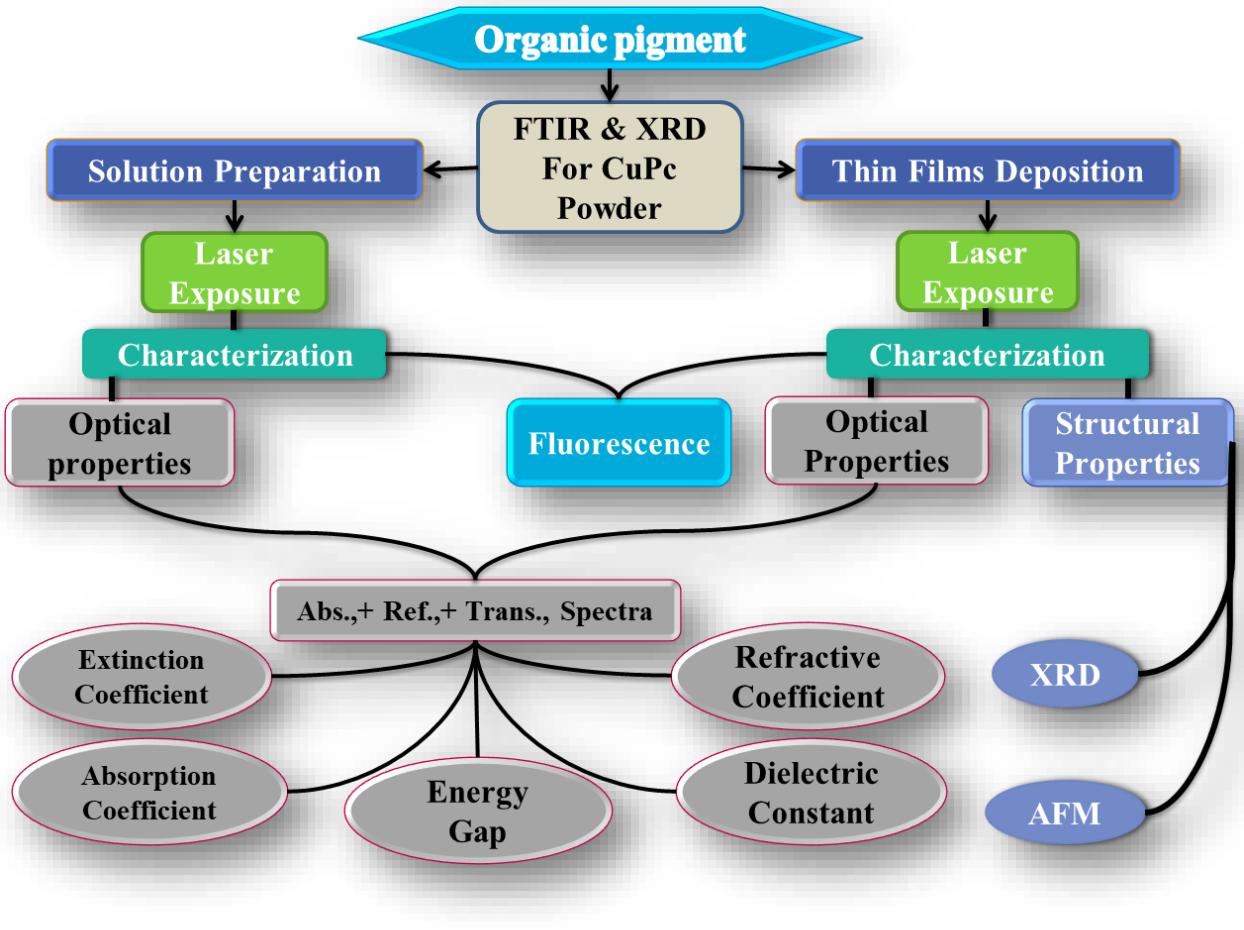

Figure 3-1: Schematic diagram of the experimental work

3.2 Laser Irradiation System

The laser irradiation are carried out using different lasers wavelengths $650, 532, and\ 405\ nm$ with different powers. The laser irradiation is achieved for both the solution, with different concentrations, and thin films, with different thicknesses, for different times. Figure (3-2) shows the laser irradiation system that is located in the organic devices laboratory in the department of Physics/ College of Science/ University of Babylon.

The properties of the semiconductor lasers that used are listed in Table (3-1)

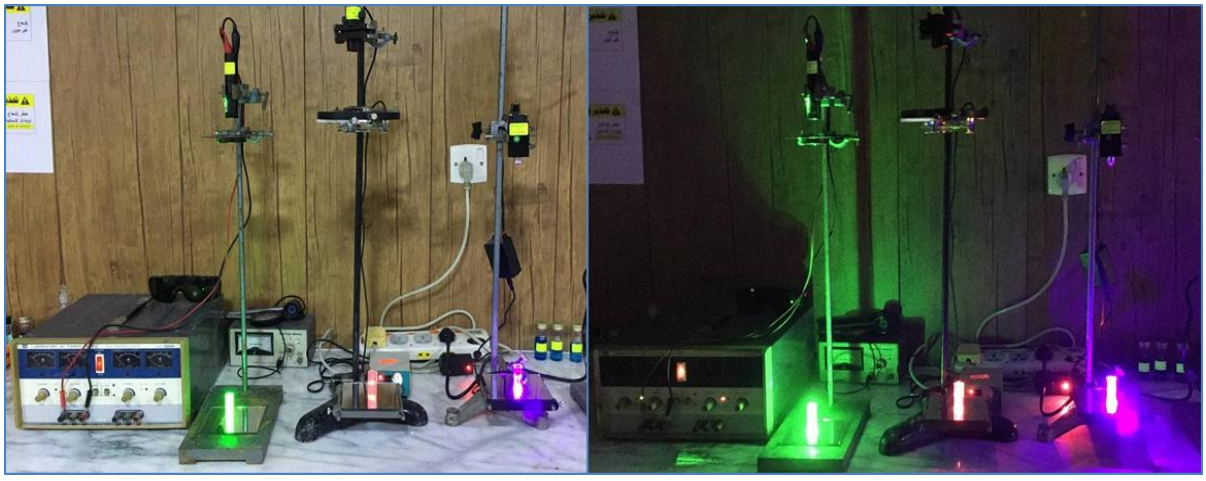

Figure 3-2: Laser irradiation system

Table 3-1. Lasers with the wavelength, power and intensity

Laser	Wavelength (nm)	Power (mW)	Intensity (W/m^2)
Red	650	1.9	0.03
Green	532	32	0.36
Violet	405	60	0.69

3.3 Solution Preparation

The solution is prepared by dissolving $50\,mg$ of Copper phthalocyanine (blue CuPc) in $100\,ml$ chloroform solvent to obtain a concentration of $0.5\,g/l$, then it is diluted to other concentrations $0.05, 0.1, 0.15, and\ 0.2\ g/l$. Figure (3-2) shows the different concentrations.

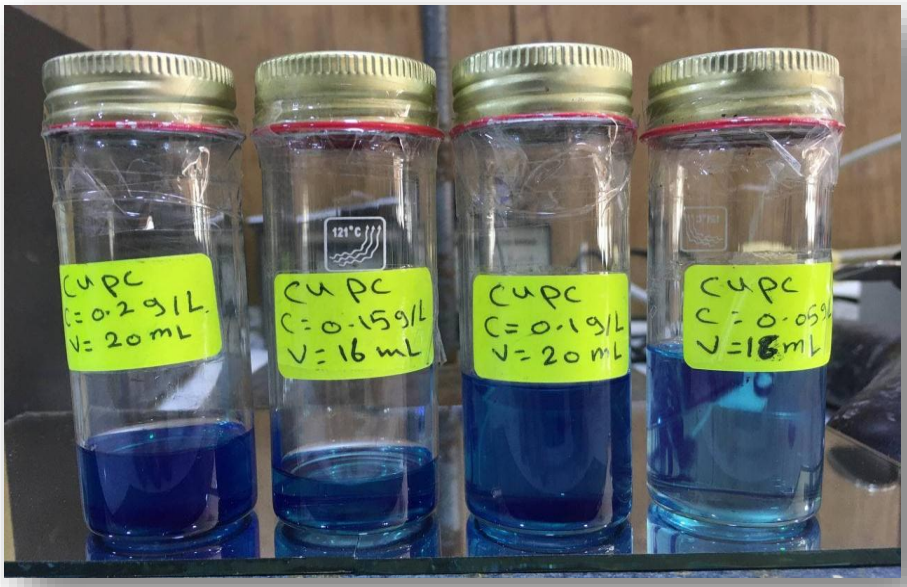

Figure 3-3: The prepared concentrations of CuPc

3.4 The Blue CuPc Thin Films Deposition

CuPc thin film is prepared by spin coating deposition technique at room temperature with thickness $\sim 219.12\ nm$ on the glass substrate as shown in Fig. (3-4). That was obtained from VOXCO company (blue CuPc alpha phase).

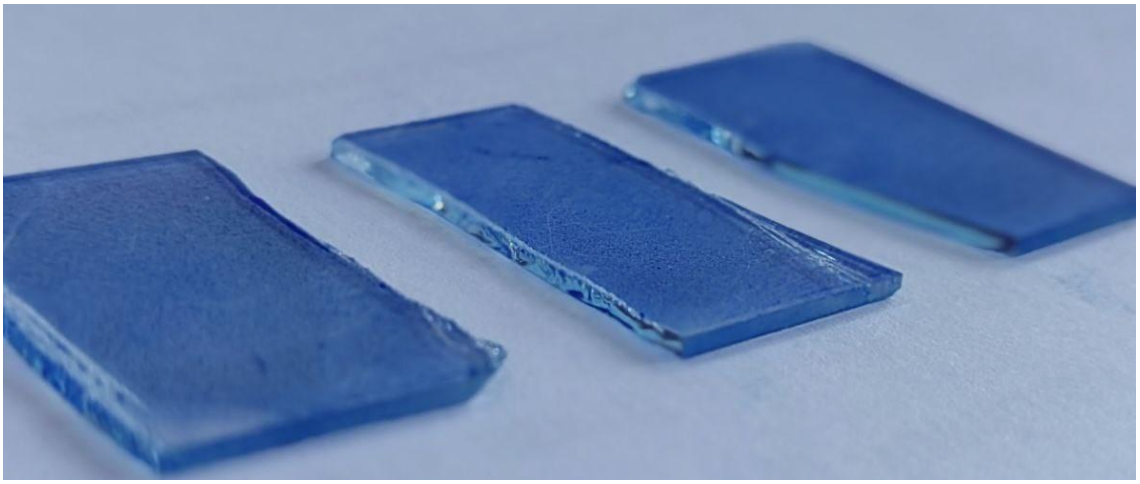

Figure 3-4: The prepared thin film of CuPc

Figure (3-5) shows spin coating technique for depositing a thin layer, homogeneous coatings onto flat surfaces. A tiny quantity of coating material is usually placed to the substrate's center, it is either whirling slowly or not at all. The substrate is then spin up to 1,000 times per minute to disperse the coating material using centrifugal force [67].

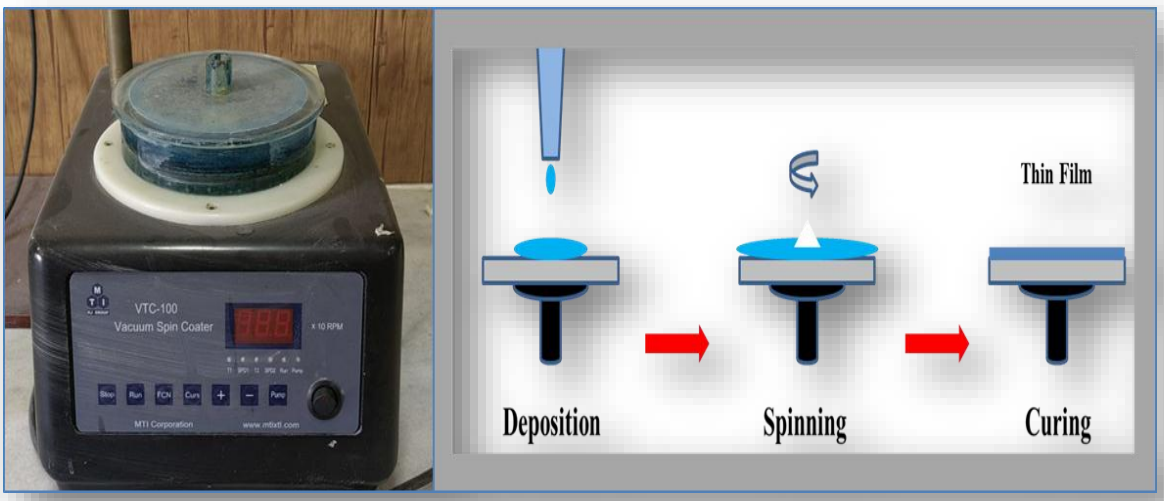

Figure 3-5: Spin coating method

3.5 Measurements and Characterization

3.5.1 Thickness Measurements:

Thickness of the prepared thin film was measured by Ellipsometry as shown in Fig.(3-6), in University of Babylon/ College of Science for Women WSCI. A diode laser of 5 mW output power and wavelength 532 nm is used as a source. It is a sensitive technique for measuring the thickness of thin films and electronics[68]. Ellipsometers are used to analyze a multi-layer or single-layer thin film material on a substrate non-invasively using polarized light. It may also investigate the substrate's bulk. Single wavelength Ellipsometers are typically employed for simple systems like a single layer non-absorbing material, although they are limited to just giving two parameters. There are two different variants of the approach that provide additional information. The Ellipsometry technique is best used to measure the thickness of thin coatings on a silicon wafer or other typical highly absorbent substrate [69].

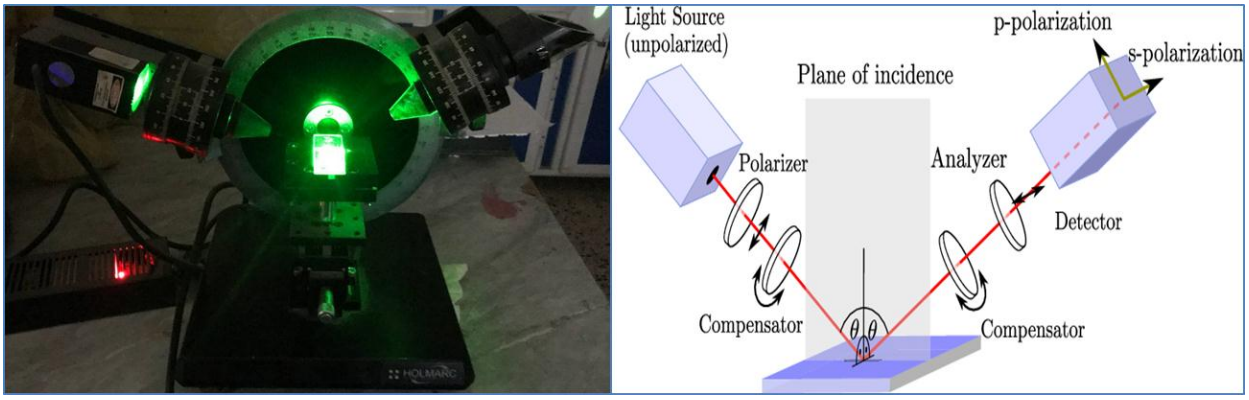

Figure 3-6: Conventional configuration of an Ellipsometer [68]

3.5.2 X-Ray Diffraction

The deposited and irradiated thin films are analyzed with X-ray diffraction, Fig. (3-7) shows the lab where the measurements are conducted in CAC center, Alnajaf, Iraq. The measurements are done by the diffraction system with (Cu Kα) radiation $\lambda = 1.5406\,\text{Å}$ in geometry of reflection. An operational voltage proportional counter of $30\,kV$ and a current of $20\,mA$. The data in this work are recorded with the diffraction angle 2θ, within the range 5^o—80^o.

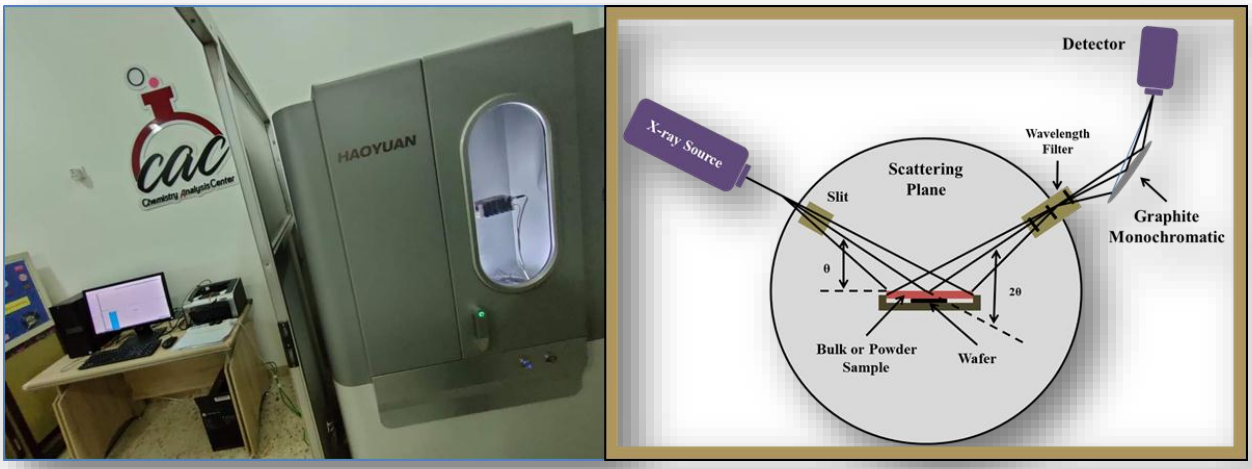

Figure 3-7: X-ray diffraction

3.5.3 FTIR Measurements

FTIR spectrometer which is located in the University of Babylon/ College of Engineering/ Polymer Department, was used to determine the spectral characterization of the prepared samples from the spectrum of $400 - 4000\,cm^{-1}$ utilizing KBr pellets as shown in Fig. (3-8).

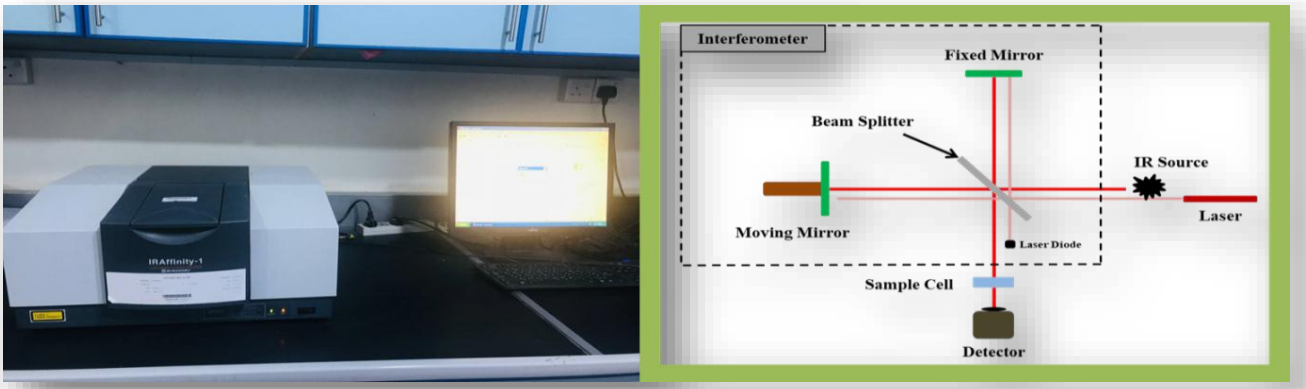

Figure 3-8: FTIR spectrometer

3.6.4 AFM Measurements

The atomic force microscope (AFM) measurements of AFM WORKSHOP type are achieved in Anwar Alraazi. Iraq-Baghdad, Fig. (3-9) shows the AFM schematic used to study the surface properties for both irradiated and non-irradiated thin films. AFM is employed to obtain topographic information in three dimensions (3D) of material.

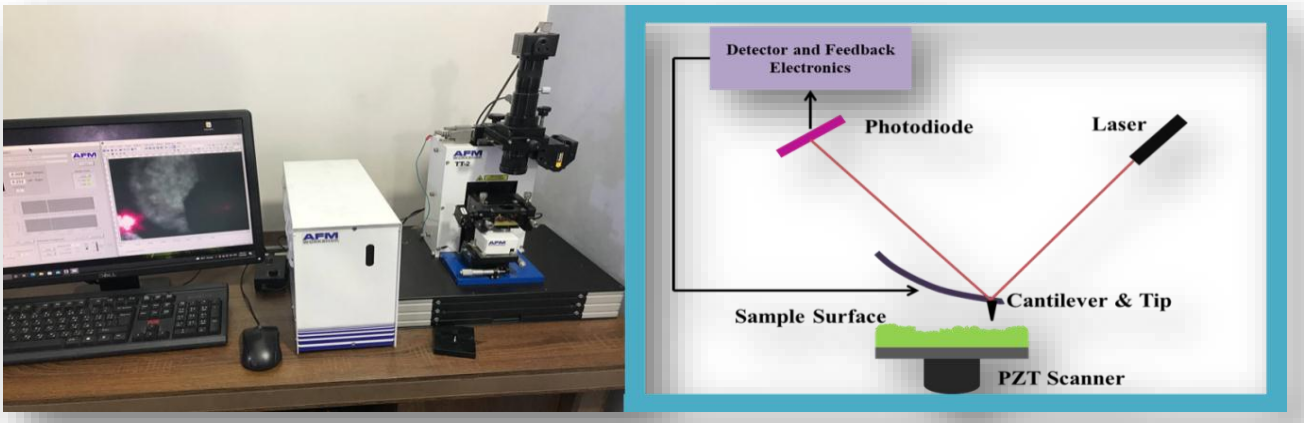

Figure 3-9: Atomic force microscope (AFM)

3.6.5 UV-Visible Absorption Spectroscopy

The optical properties of the prepared solutions and thin film are determined by UV-Visible spectrophotometer that located in the University of Babylon/ College of Science/ Physics Department. This spectrophotometer contains two light sources, deuterium and halogen lamps to provide the range of wavelength in the range $190 - 1100\ nm$. This gadget is a double-beam device, with one beam passing through the film under examination (optical measurements) and the other passing through the instrument's glass slide as seen in Fig.(3-10).

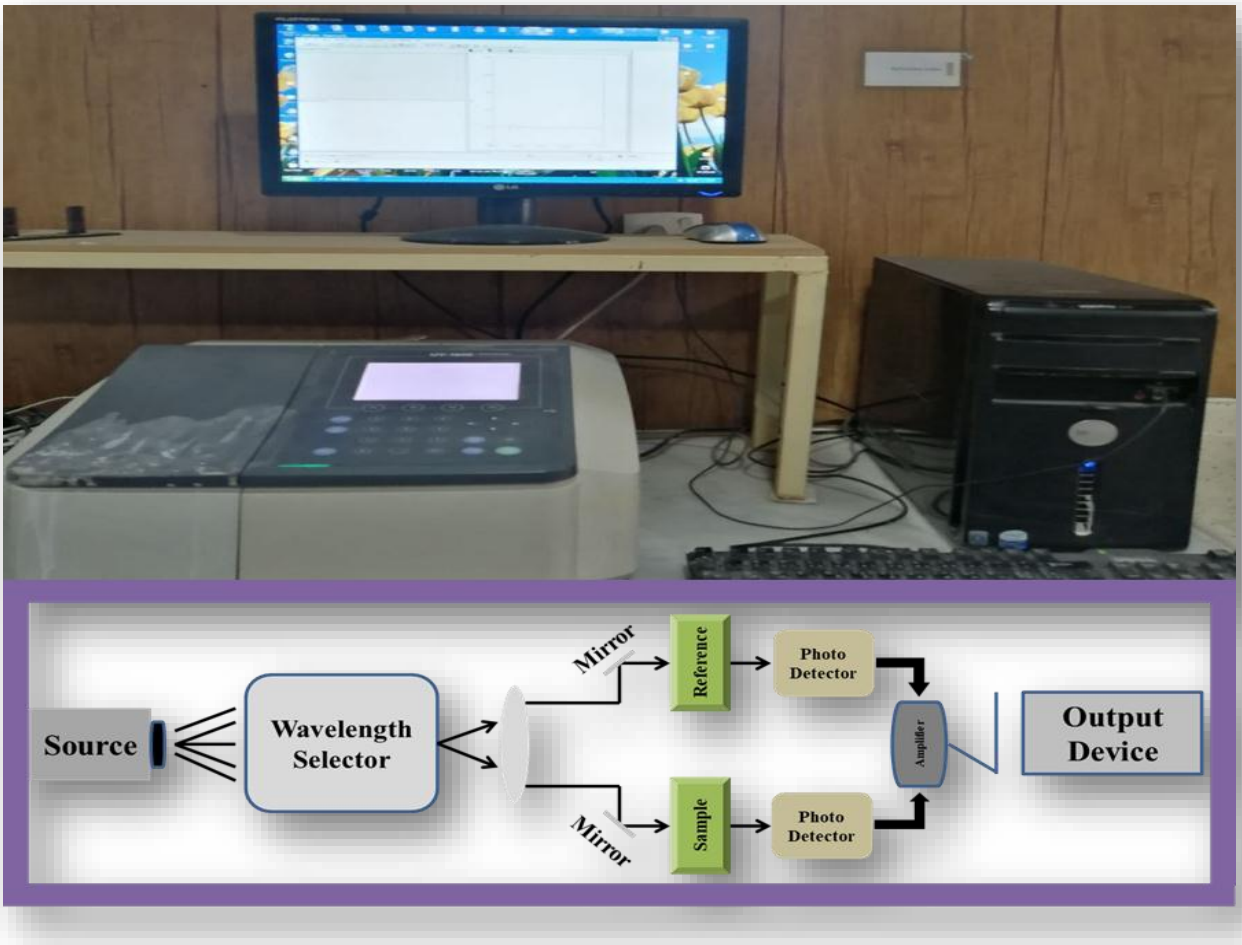

Figure 3-10: UV-visible spectrophotometer

3.6.6 Fluorescence Spectrophotometer

Fluorescence is based on photoluminescence, it is the physical process of light being released after being absorbed by a material. The amount of light (photons) released is indicated by the fluorescence intensity. It is the amount of emission that is determined by the excited states. The device is from SCINCO Fs-2, korea, in University of Babylon/ College of Education for Pure Sciences as shown in Fig. (3-11),

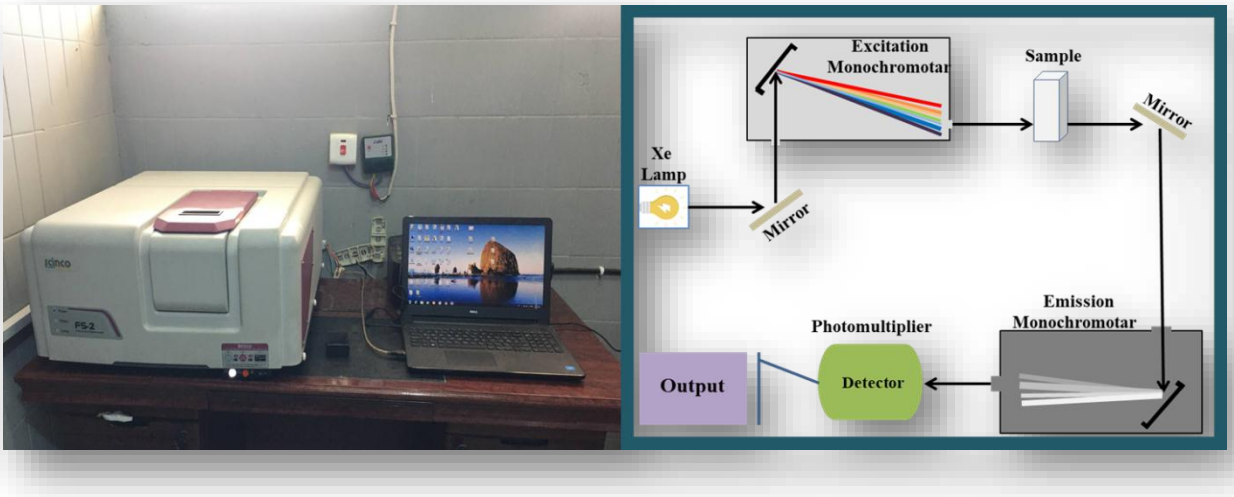

Figure 3-11: Fluorescence spectrophotometer

CHAPTER FOUR

RESULTS & DISCUSSION

4 Introduction

This chapter includes the results of experimental measurements of copper phthalocyanine (CuPc) blue as solution and thin films. Thin films are prepared by spin coating method on glass substrates at room temperature. Samples are irradiated with different laser wavelengths for different times. The linear optical properties and structural properties measurements are recorded to characterize the solution and the thin films.

4.2 X-Ray Diffraction for CuPc Powder

The XRD results of the CuPc (α) powder are shown in Fig. (4-1).The highest diffraction peak occurs at about ($2\theta = 6.68^{o}$) with (d = 1.32 nm) and the Millar indices (100), the crystal system is triclinic. The calculated lattice parameters are found to be (a=12.886, b=3.769, and c=2.061) Å, with angles ($\alpha=96.22^{o}$, $\beta=90.62^{o}$, and $\gamma=90.32^{o}$) which are obtained by Match!3 software. It can be seen that X-ray diffraction for CuPc powder is polycrystalline [24]. From the observed X-ray diffraction patterns, the grain size of crystallite is calculated using Scherer's equation [70]. Table (4-1) shows the important data obtained from XRD measurements for CuPc powder.

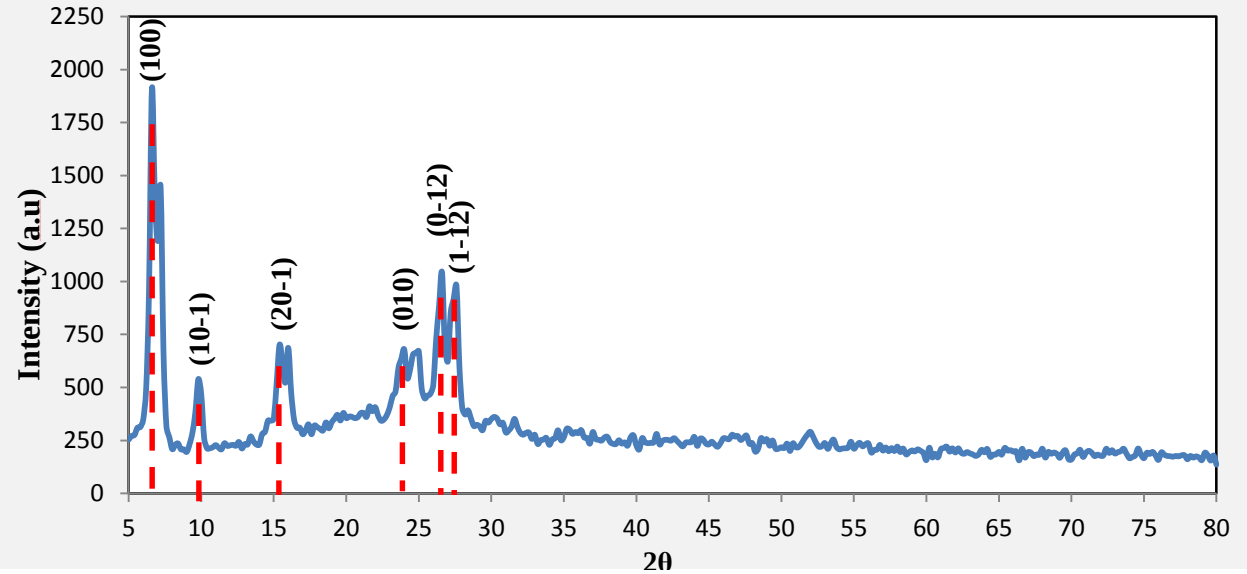

Figure 4-1: XRD for CuPc powder

Table 4-1. XRD measurement for CuPc powder

2θ	d(nm)	Height	I%	FWHM	Crystal Size (nm)
6.688	1.32058	1560	100	0.456	17
9.81	0.90088	340	21.8	0.477	17
15.46	0.57267	443	28.4	0.741	10
19.798	0.44807	112	7.2	1.283	6
21.628	0.41055	145	9.3	1.276	6
23.988	0.37067	419	26.9	1.567	5
26.571	0.33519	791	50.7	0.959	8

4.3 FTIR for CuPc Powder

The FTIR spectrum of CuPc powder has been measured at room temperature and shown in Fig. (4-2). FTIR spectrum is divided into four wavenumber regions: $400 - 1400\, cm^{-1}$ is called the finger print region which is unique for each compound includes the single bonds. The next region is in the range $1400 - 2000\, cm^{-1}$ which includes the double bonds. The third region shows the triple

bonds that are located in the region $2000 - 2300\ cm^{-1}$. The region of $2300 - 3500\ cm^{-1}$ configures the hydrogen bonds [28].

FTIR for CuPc powder shows the bond bending represented by the range $400 - 1500\ cm^{-1}$ while the bond stretching represented by the range $1500 - 3000\ cm^{-1}$. It is obviouse to notice a weak band in the range $624.94 - 942.26\ cm^{-1}$ indicating the presence of (metal-Nitrogen) bond vibration have been assigned for (Copper–Nitrogen).

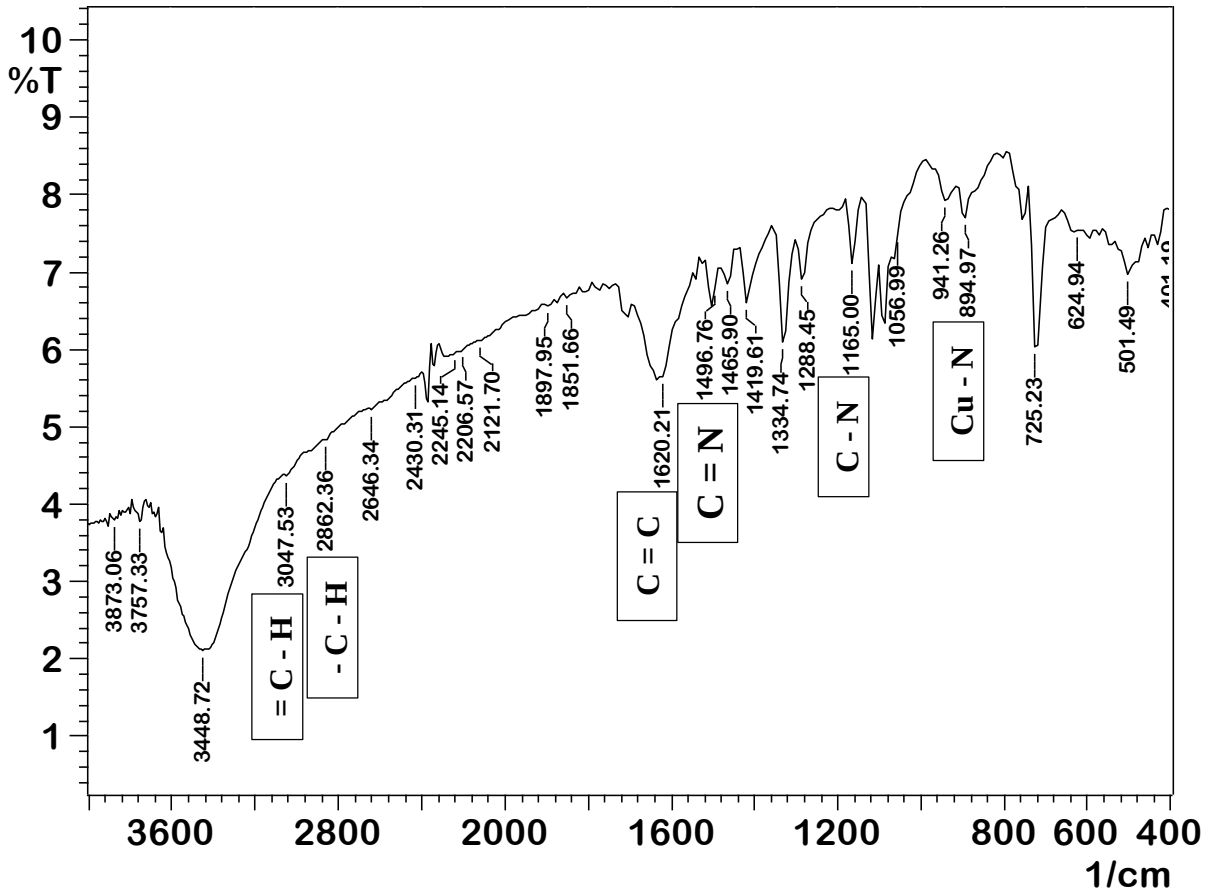

Figure 4-2: FTIR measurement for CuPc powder

4.4 Optical Properties of CuPc Solution

4.4.1 UV-Vis. Spectrum of CuPc Solution

The UV-Visible spectra include the absorbance, transmittance, reflectance, and the optical constants such as: absorption coefficient, refractive index, extinction coefficient and the real and imaginary dielectric constants, in addition to optical energy gap.

4.4.1.1 Time Irradiation Effect on the Optical Properties of CuPc Solution

The UV-Vis. Spectra are recorded for CuPc solution at concentration $0.15 g/l$. The results have been published in [71]. Figures (4-3a to 4-5a) illustrate the absorbance spectra in the wavelength range $290 - 800\ nm$. It can be seen that there are two observed bands. The first one is named as B-band Soret and appeared in the UV range while the second one is obtained in the visible region and called Q-band. This suggests that the spectrum range is from $\pi - \pi^*$ orbital's transition [28]. The measurements are taken for different irradiation times. Increasing the irradiating laser time leads to decrease the absorption of the solution obeying Beer – Lambert law as given in eq. $(2 - 1)$. The behaviour tends to behave like this due to the high energy laser which breaks the molecules bonding.

The measurements are taken for different laser irradiating times $0, 4, 8, and\ 16\ min.$ and different laser wavelengths $650, 532\ and\ 405\ nm.$ Figures (4-3b to 4-5b) show that the absorbance is higher for the non-irradiated sample and decreases with increasing the irradiation time of the solution. The reason for this is that longer laser exposure time, the greater the dissociation of bonds to the solution. As a result, the solution absorbance decreases [55].

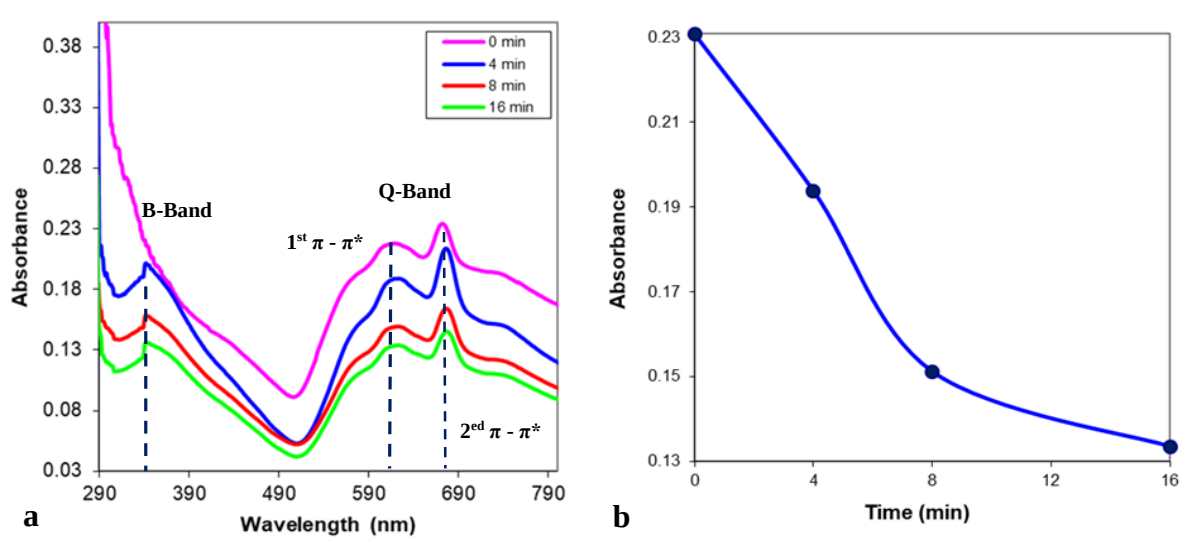

Figure 4-3: (a) Absorbance spectra with different irradiating laser times (0, 4, 8, and 16) min. using the red laser (650 nm) and solution concentration (0.15gm/l). (b) Maximum absorption vs. laser irradiating time at 667 nm

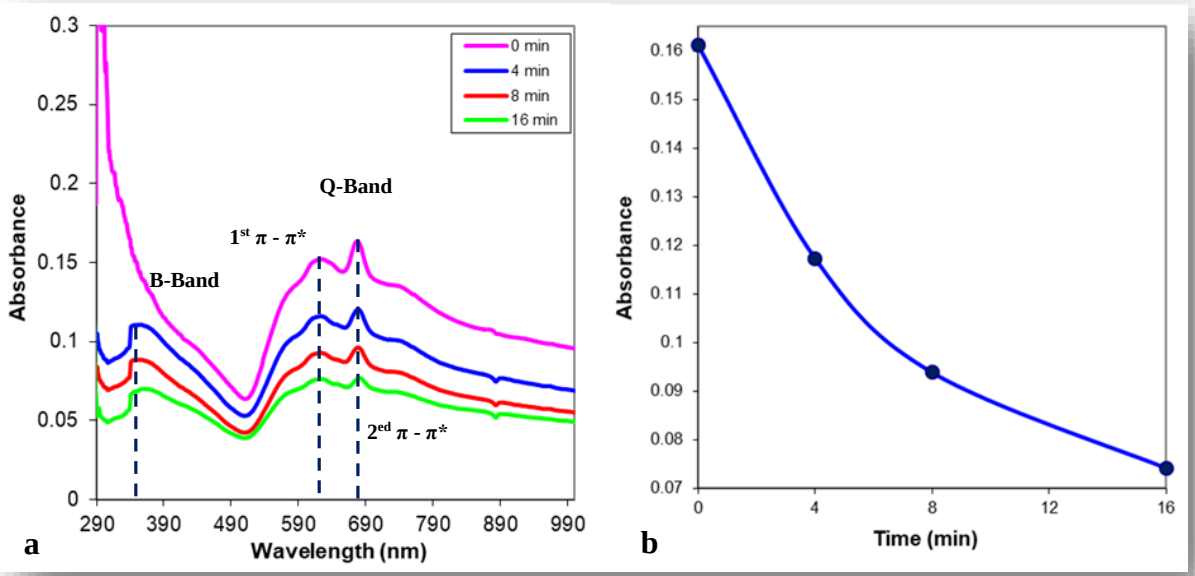

Figure 4-4: (a) Absorbance spectra with different irradiating laser times (0, 4, 8, and 16) min. at green laser (532 nm) and solution concentration (0.15gm/l). (b) Maximum absorption vs. laser irradiating time at 672 nm

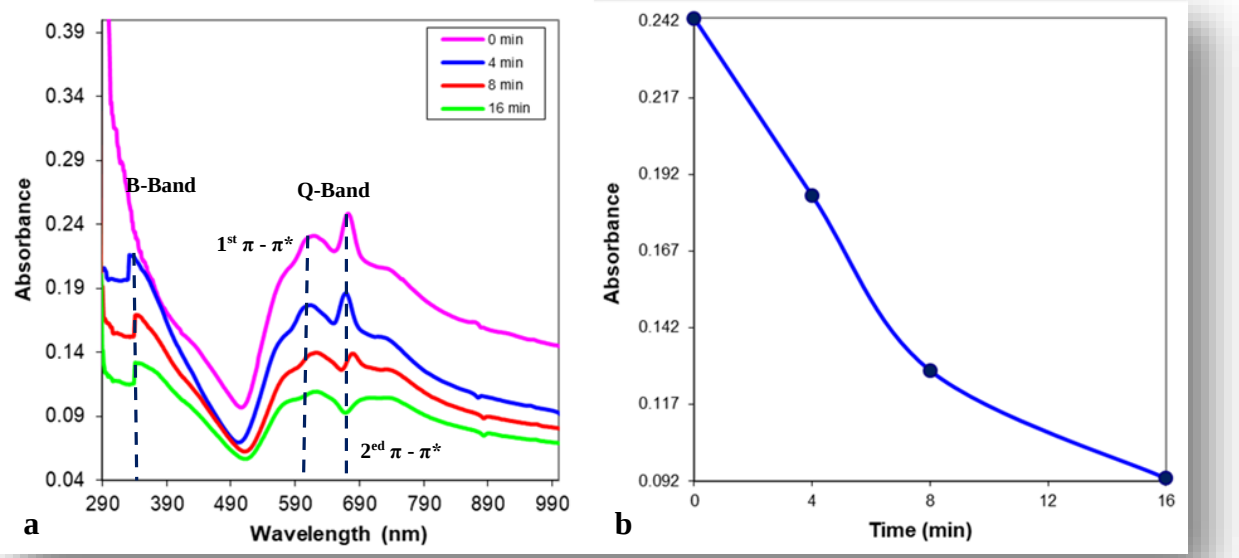

Figure 4-5: (a) Absorbance spectra with different irradiating laser times (0, 4, 8, and 16) min. using the violet laser (405 nm) and solution concentration (0.15gm/l). (b) Maximum absorption vs. laser irradiating time at 667 nm

Figures (4-6a to 4-8a) illustrate the reflection as a function of the wavelength at solution concentration $0.15 g/l$. The data are taken by varying the lasers irradiating times $0, 4, 8, and\ 16\ min$ for different laser wavelengths $650, 532, and\ 405\ nm$. Figures (4-6b to 4-8b) simply show that the maximum reflectance appears at the non-irradiated samples and decreases with increasing the laser irradiation times.

The energy gap is shown in Figs.(4-9a to 4-11a) which is excluded from $(\alpha hv)^{1/2}$ with the photon energy using Tauc equation. It is obvious to notice that the rapid increase in the absorption coefficient is where the absorption can be deduced. Figures (4-9b to 4-11b) show the band gap behavior with increasing laser irradiation time. Apparently, the energy gap increases with increasing the

irradiating time. This means the absorption edge shifted towards lower wavelengths which may be useful for UV sensors applications.

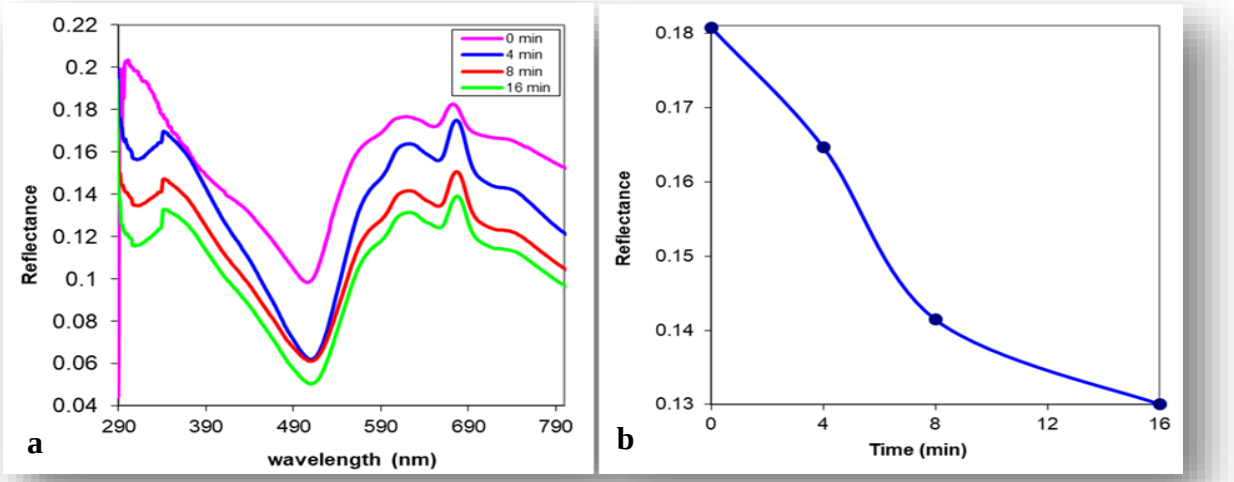

Figure 4-6: (a) Reflectance spectra with different irradiating laser times (0,4,8, and 16) min. using red laser (650 nm) and solution concentration (0.15gm/l). (b) Maximum reflectance vs. laser irradiating time at 666 nm

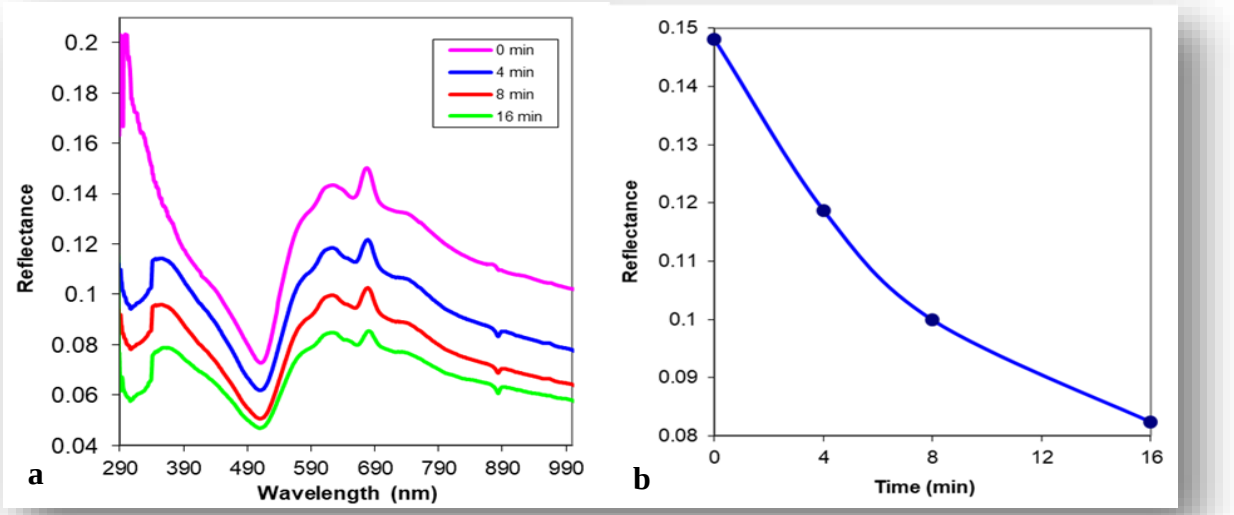

Figure 4-7: (a) Reflectance spectra with different irradiating laser times (0,4,8, and 16) min. using green laser (532 nm) and solution concentration (0.15gm/l). (b) Maximum reflection vs. laser irradiating time at 672 nm

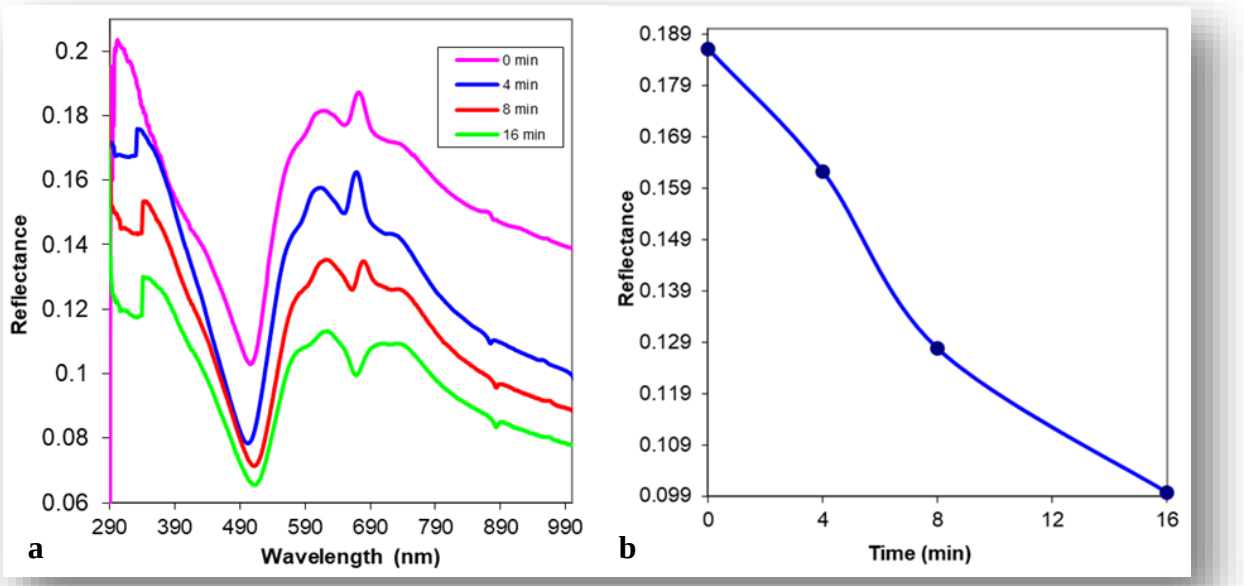

Figure 4-8: (a) Reflectance spectra with different irradiating laser times (0, 4, 8, and 16) min. using violet laser (405 nm) at concentration (0.15gm/l). (b) Maximum reflection vs. laser irradiating time at 667 nm

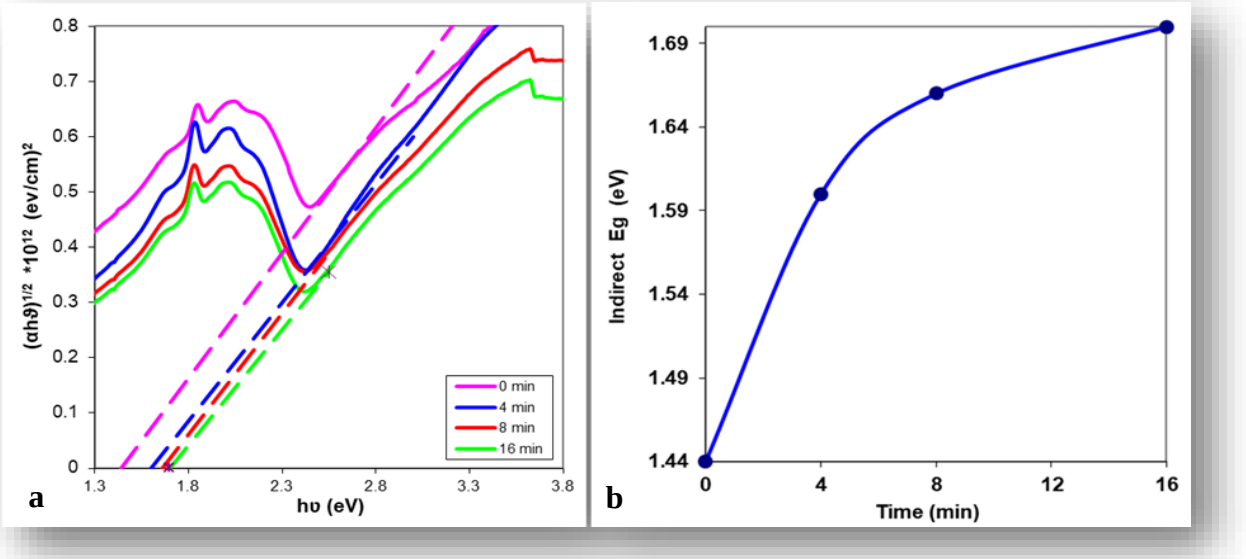

Figure 4-9: (a) $(\alpha h\upsilon)^{1/2}$ vs. photon energy for solution concentration (0.15g/l) at different laser irradiating times (0,4,8, and 16) min. using the red laser (650 nm). (b) Energy gap vs. red laser irradiating time

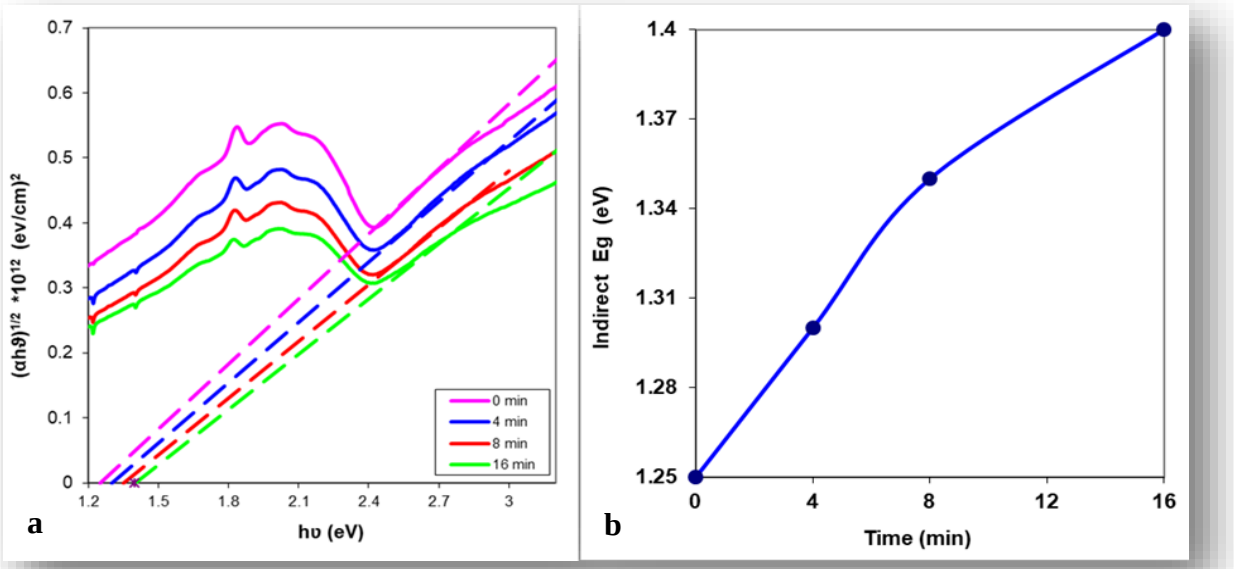

Figure 4-10: (a) $(\alpha h\upsilon)^{1/2}$ vs. photon energy at solution concentration (0.15g/l) at different laser irradiating times (0,4,8, and 16) min. for the green laser with wavelength (532 nm). (b) Maximum energy gap vs. green laser irradiating time

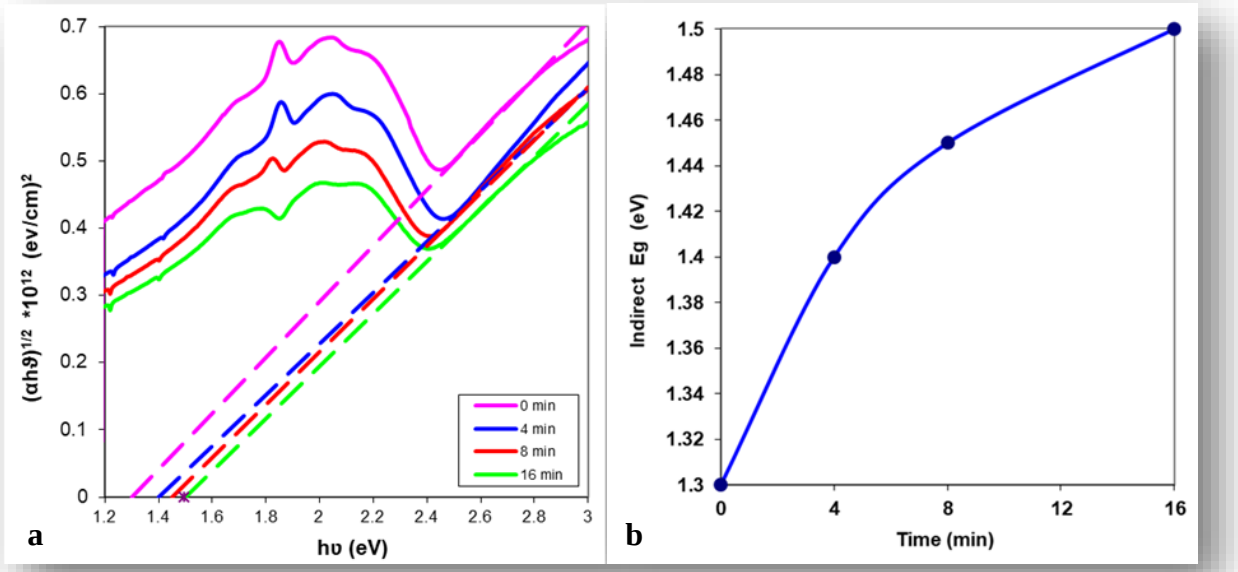

Figure 4-11: (a) $(\alpha h\upsilon)^{1/2}$ vs. photon energy at solution concentration 0.15g/l for different lasers irradiating times 0,4,8, and 16 min. for the violet laser 405 nm. (b) Maximum energy gap vs. violet laser irradiating time

The optical constants are calculated and displayed in Tables (4- 2).

Table 4-2. The optical parameters as (absorption coefficient, extinction coefficients, refractive index, dielectric constants and the optical conductivity) at sample exposed to red, green and violet lasers 650, 532, and 405 nm, at wavelength 667 nm

	Time (min)	a (l/g.cm)	ϵ (l/mol.cm)	α (cm^{-1})	n	K $*10^{-7}$	ε_{Real}	$\varepsilon_{im.}$ $*10^{-6}$	$\sigma_{Optical}$ (s^{-1})	Indirect Eg (eV)
Red Laser	**0**	1.526	879.26	0.229	2.324	12.1	5.401	5.64	0.127	1.44
	4	1.271	732.09	0.191	2.196	10.1	4.823	4.42	0.099	1.6
	8	0.994	572.37	0.149	1.988	7.90	3.954	3.14	0.071	1.66
	16	0.879	506.53	0.132	1.897	6.99	3.598	2.65	0.059	1.7
Green Laser	**0**	1.066	613.96	0.159	2.054	8.63	4.174	3.49	0.078	1.25
	4	0.776	447.12	0.116	1.822	6.28	3.289	2.26	0.050	1.3
	8	0.621	357.69	0.093	1.673	5.02	2.775	1.66	0.037	1.35
	16	0.491	282.95	0.074	1.546	3.97	2.367	1.21	0.027	1.4
Violet Laser	**0**	1.633	940.32	0.245	2.372	13.0	5.626	6.17	0.139	1.3
	4	1.239	713.29	0.186	2.164	9.86	4.682	4.27	0.096	1.4
	8	0.859	494.31	0.129	1.879	6.84	3.530	2.57	0.058	1.45
	16	0.619	356.98	0.091	1.665	4.94	2.771	1.64	0.037	1.5

4.4.1.2 Concentrations Effect on the Optical Properties for CuPc Solution Irradiated by laser Beam

The UV-Vis spectra are recorded for CuPc at concentrations $0.05, 0.1, and\ 0.2\ g/l$. Figures (4-12a to 4-21a) illustrate the absorbance spectra in the wavelength range $290 - 800\ nm$. It can be seen that there are two bands are obtained. The B-band (Soret) and appeared in the UV range in the region $\sim 300\ nm$ while the Q-band is obtained in the visible region with wavelength range

$\sim 673\ nm$ [30]. This suggests that the spectrum range is from $\pi - \pi^*$ orbital's transition [28]. Increasing the concentration leads to increase the absorption of the solution obeying Beer–Lambert law eq. (2 – 1). As the increase in the concentration of the solution leads to the emergence of secondary levels between the valence band and conduction band, these levels cause an decrease in the energy gap [55]. The measurements are taken for different laser irradiating times 0, 4, 8, and 16 min. with different laser wavelengths $650, 532, and\ 405\ nm$ for all concentrations. Figures (4-12b to 4-21b) show that the absorbance is higher at the highest concentration sample and decreases with decreasing the concentration at laser irradiation time $0, 4, 8, and\ 16\ min$, with wavelength $650, 532, and\ 405\ nm$.

Figures (4-22a to 4-31a) illustrate the reflectance spectra when varying the solution concentration $0.05, 0.1, and\ 0.2\ g/l$, simply it is shown that the reflectance spectra is higher in Q and B bands. The maximum reflectance appears at the highest concentration sample and decrease with decreasing the concentration at laser irradiation times $0, 4, 8, and\ 16\ min.$ with wavelengths $650, 532, and\ 405\ nm$. Figures (4-22b to 4-31b) show the maximum reflectance spectra against the concentrations $0.05, 0.1, and\ 0.2\ g/l$. Obviously, the reflectance is higher at the highest concentration sample and decreases with decreasing the concentration for the samples.

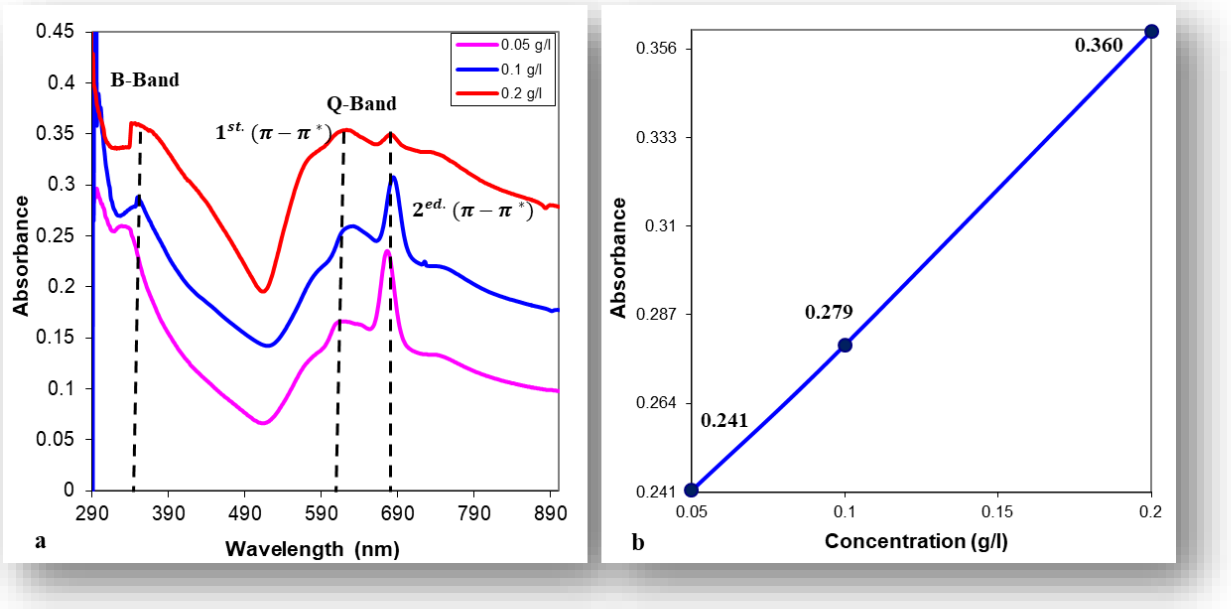

Figure 4-12: (a) Absorbance spectra with different CuPc solution concentrations 0.05, 0.1, and 0.2 g/l for non-irradiated samples. (b) Maximum absorption vs. the concentration of solution at 345 nm

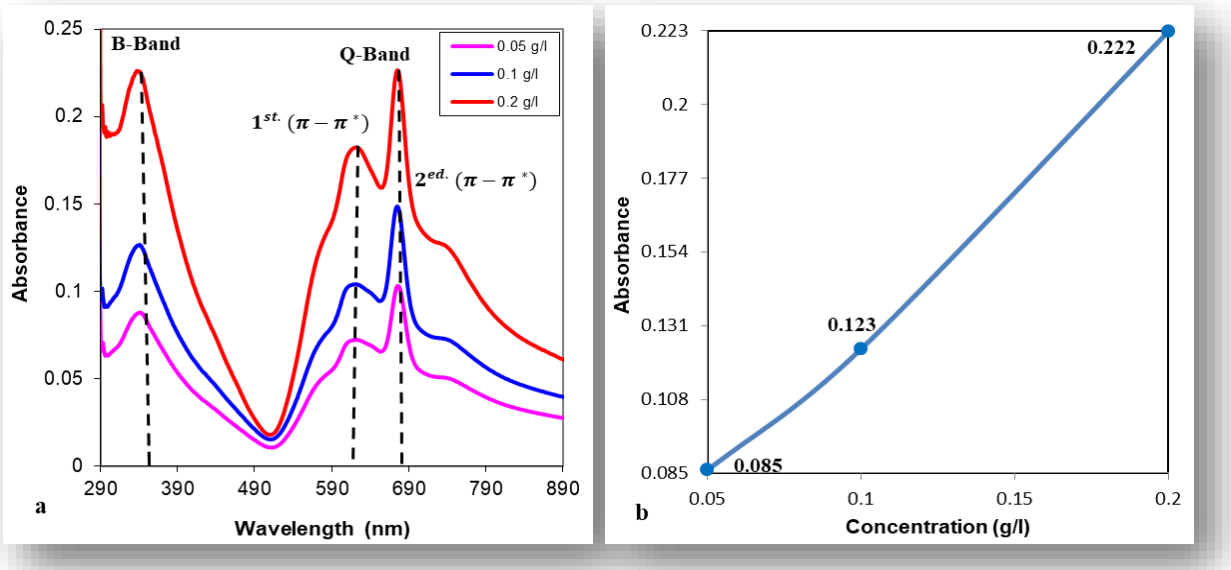

Figure 4-13: (a) Absorbance spectra with different CuPc solution concentrations 0.05, 0.1, and 0.2 g/l for 650 nm laser wavelength and 4 min irradiation time. (b) Maximum absorption vs. the concentration of solution at wavelength 335 nm

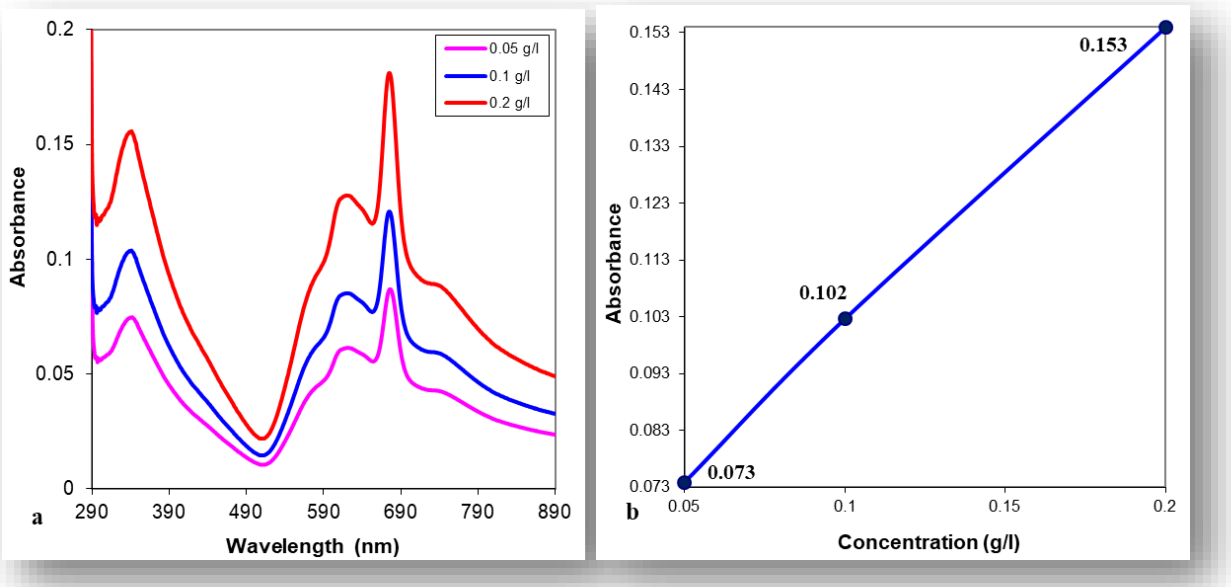

Figure 4-14: (a) Absorbance spectra with different CuPc solution concentrations 0.05, 0.1, and, 0.2 g/l for 650 nm laser wavelength and 8 min irradiation time. (b) Maximum absorption vs. the concentration of solution at wavelength 335 nm

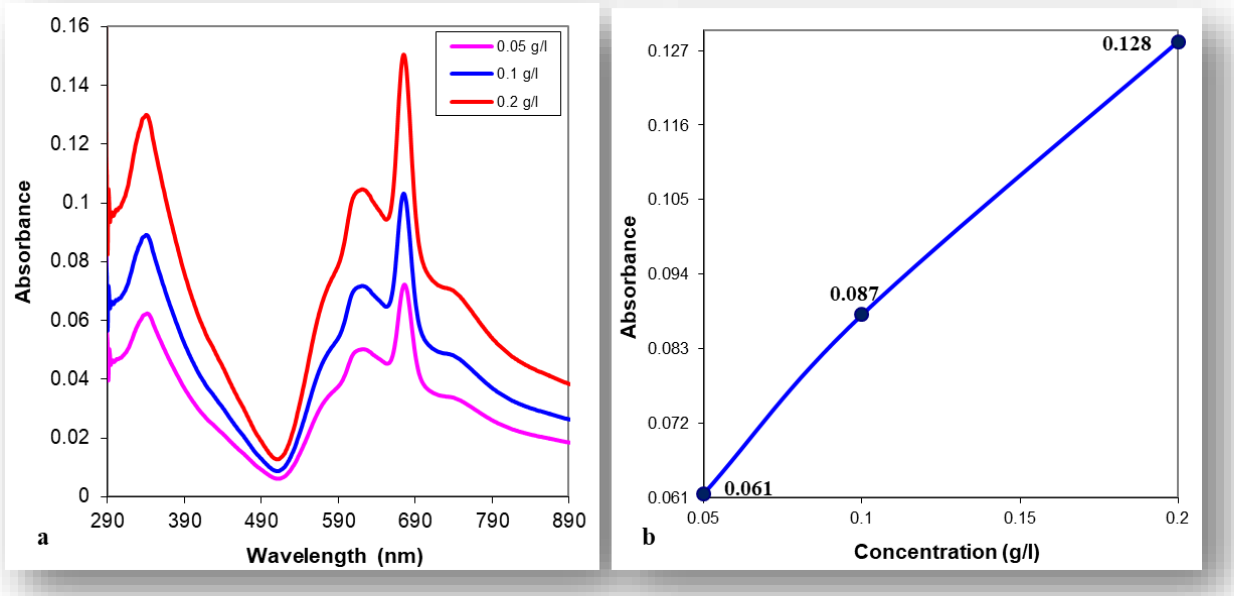

Figure 4-15: (a) Absorbance spectra with different CuPc solution concentrations 0.05, 0.1, and 0.2 g/l for 650 nm laser wavelength and 16 min irradiation time. (b) Maximum absorption vs. the concentration of solution at wavelength 335 nm

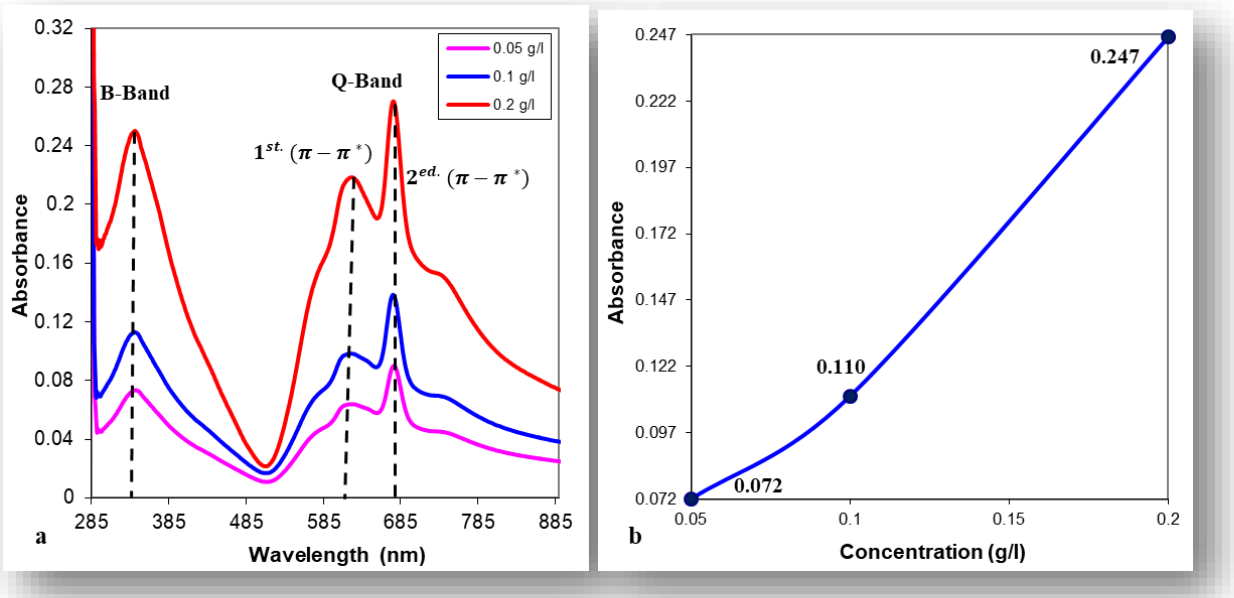

Figure 4-16: (a) Absorbance spectra with different CuPc solution concentrations 0.05, 0.1, and 0.2 g/l for 532 nm laser wavelength and 4 min irradiation time (b) Maximum absorption vs. the concentration of solution at wavelength 333 nm

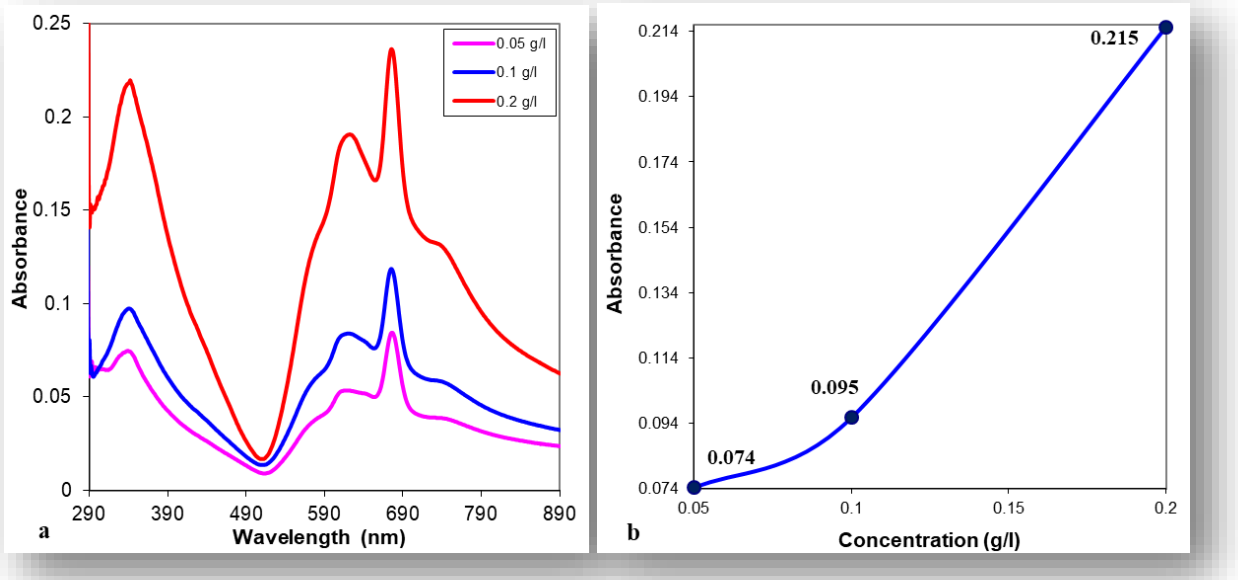

Figure 4-17: (a) Absorbance spectra with different CuPc solution concentrations 0.05, 0.1, and 0.2 g/l for 532 nm laser wavelength and 8 min irradiation time. (b) Maximum absorption vs. the concentration of solution at wavelength 333 nm

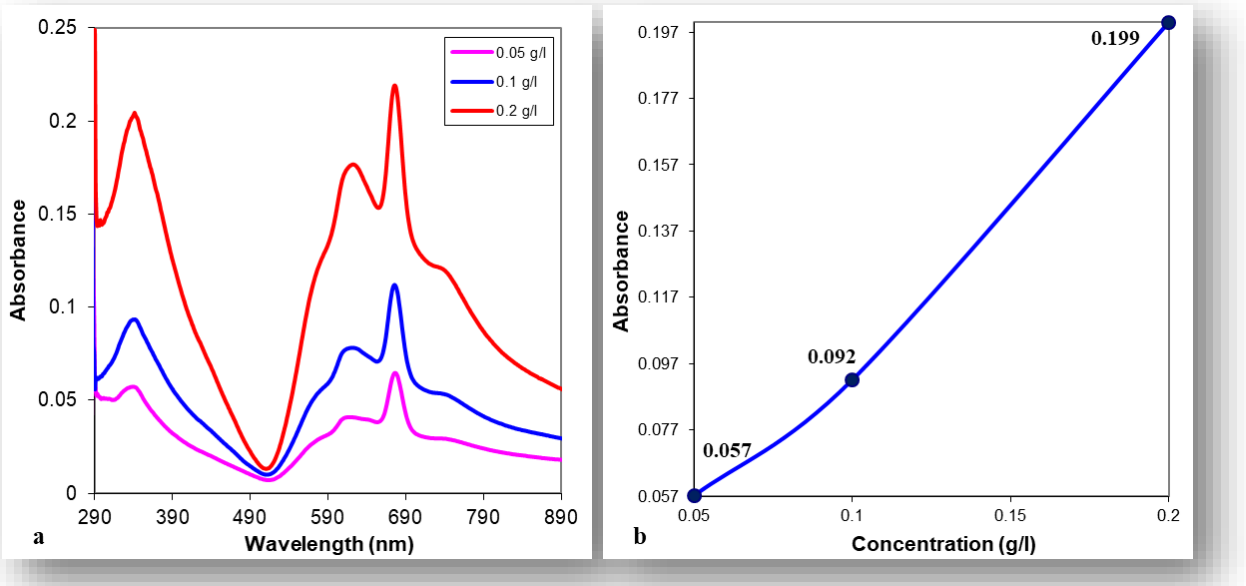

Figure 4-18: (a) Absorbance spectra with different CuPc solution concentrations 0.05, 0.1, and 0.2 g/l for 532 nm laser wavelength and 16 min irradiation time. (b) Maximum absorption vs. the concentration of solution at wavelength 333 nm

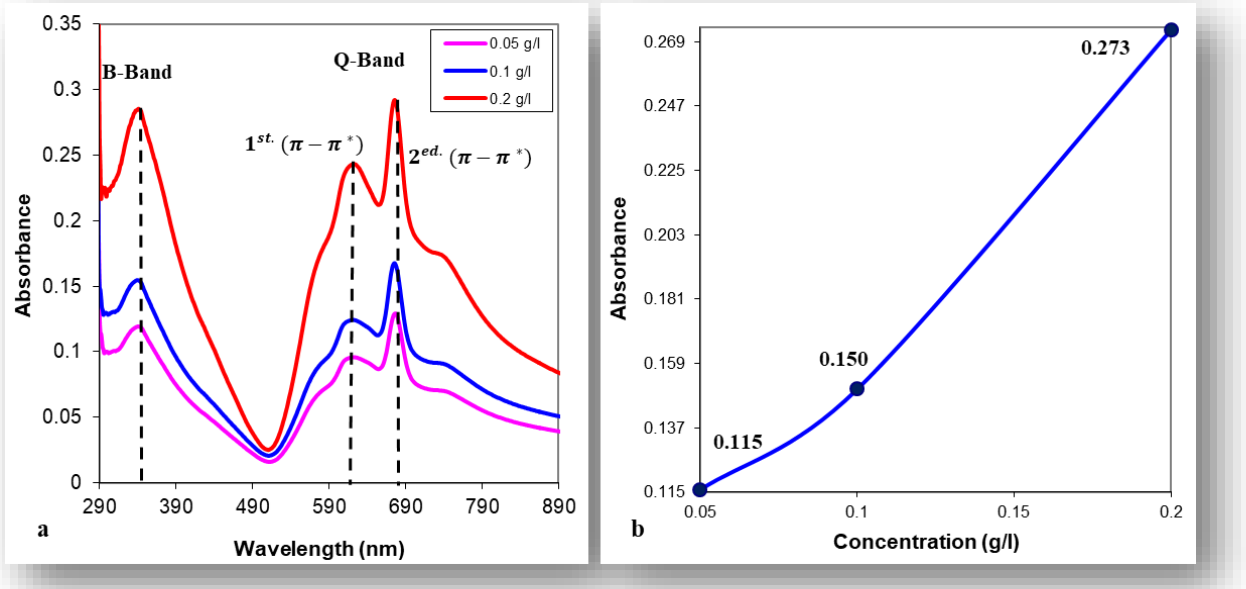

Figure 4-19: (a) Absorbance spectra with different concentrations 0.05, 0.1, and 0.2 g/l for 405 nm laser wavelength and 4 min irradiation time. (b) Maximum absorption vs. the concentration of solution at wavelength 330 nm

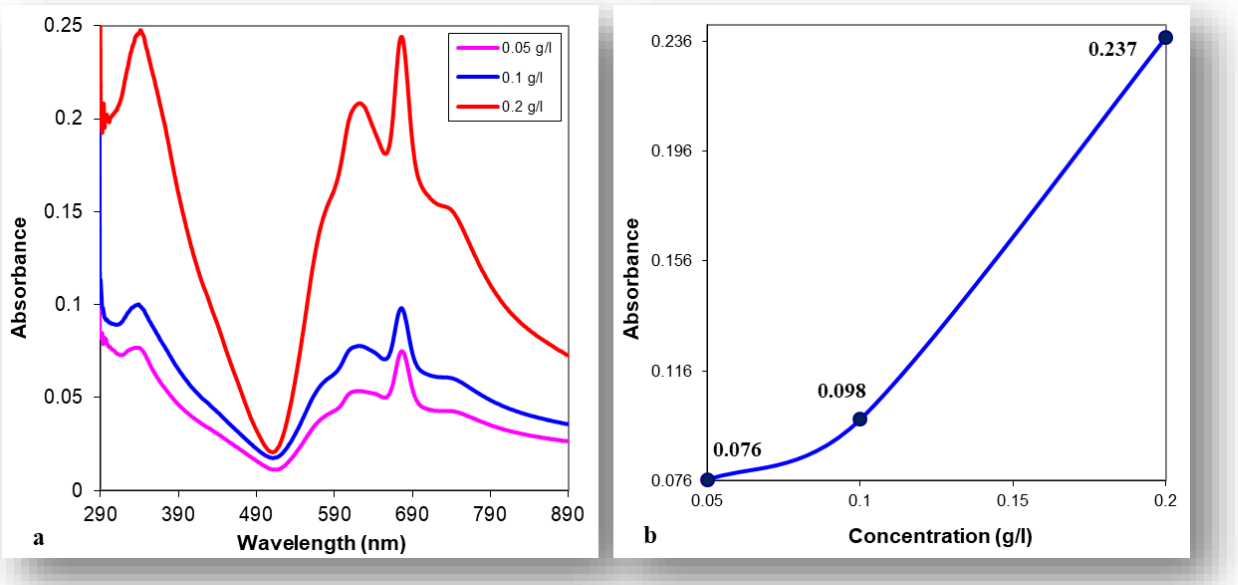

Figure 4-20: (a) Absorbance spectra with different CuPc solution concentrations 0.05, 0.1, and 0.2 g/l for 405 nm laser wavelength and 8 min irradiation time. (b) Maximum absorption vs. the concentration of solution at wavelength 330 nm

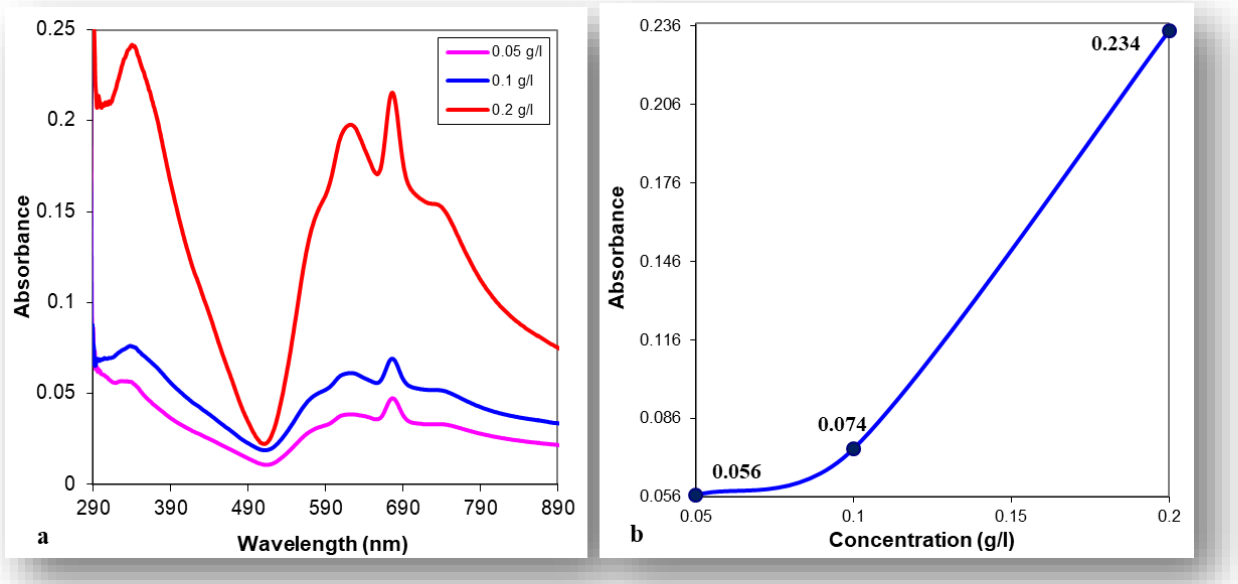

Figure 4-21: (a) Absorbance spectra with different CuPc solution concentrations 0.05, 0.1, and 0.2 g/l for 405 nm laser wavelength and 16 min irradiation time. (b) Maximum absorption vs. the concentration of solution at wavelength 330 nm

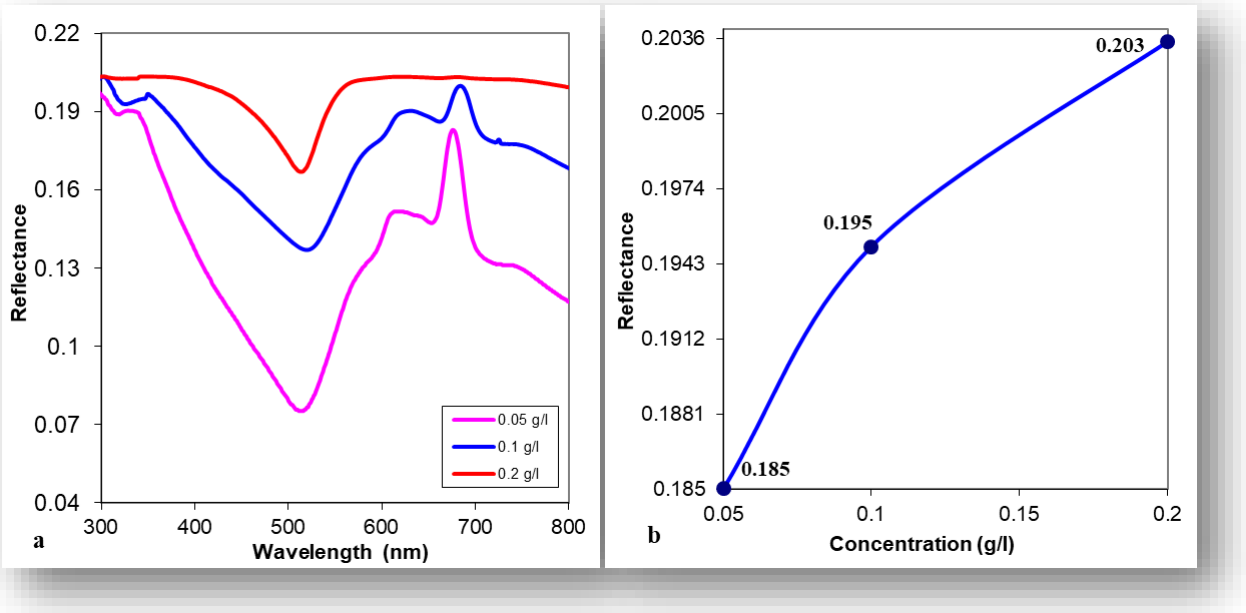

Figure 4-22: (a) Reflectance spectra with different CuPc solution concentrations 0.05, 0.1, and 0.2 g/l for the non-irradiated samples. (b) Maximum reflectance vs. the concentrations of solution at wavelength 345 nm

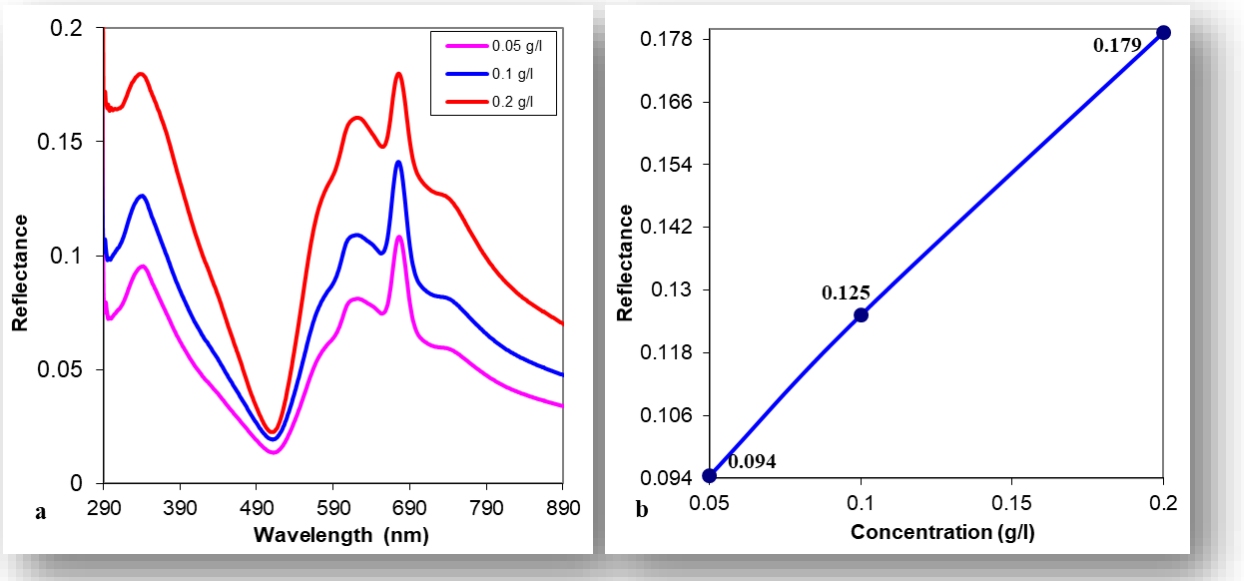

Figure 4-23: (a) Reflectance spectra with different concentrations 0.05, 0.1, and 0.2 g/l for 650 nm laser wavelength and 4 min irradiation. (b) Maximum reflection vs. the concentration of solution at wavelength 335 nm

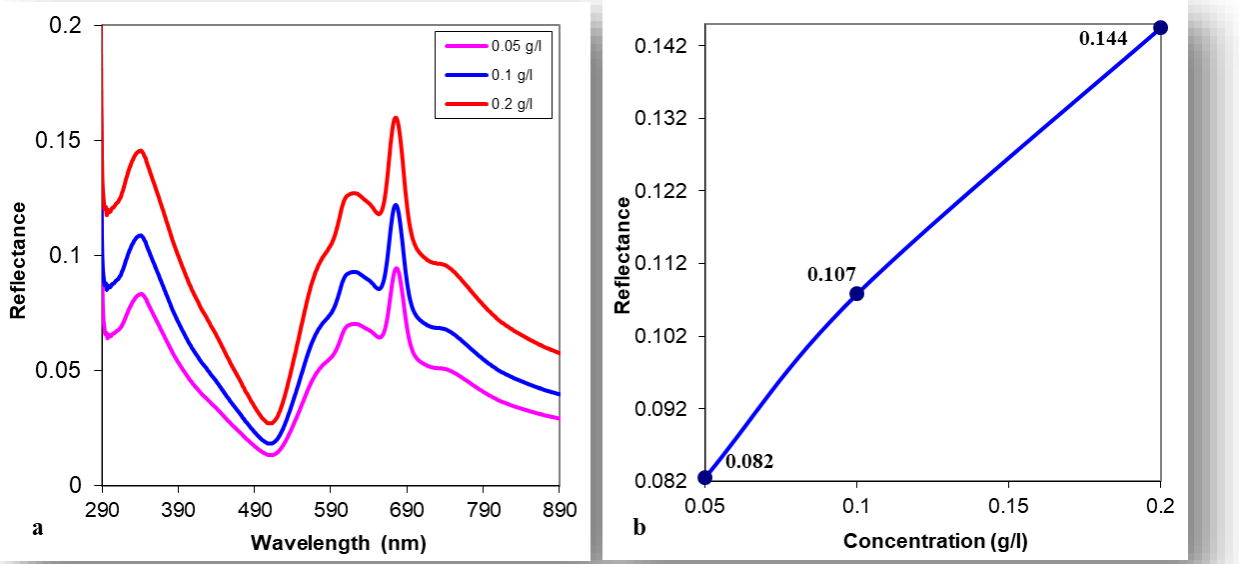

Figure 4-24: (a) Reflectance spectra with different concentrations 0.05, 0.1, and 0.2 g/l for 650 nm laser wavelength and 8 min irradiation. (b) Maximum reflection vs. the concentration of solution at wavelength 335 nm

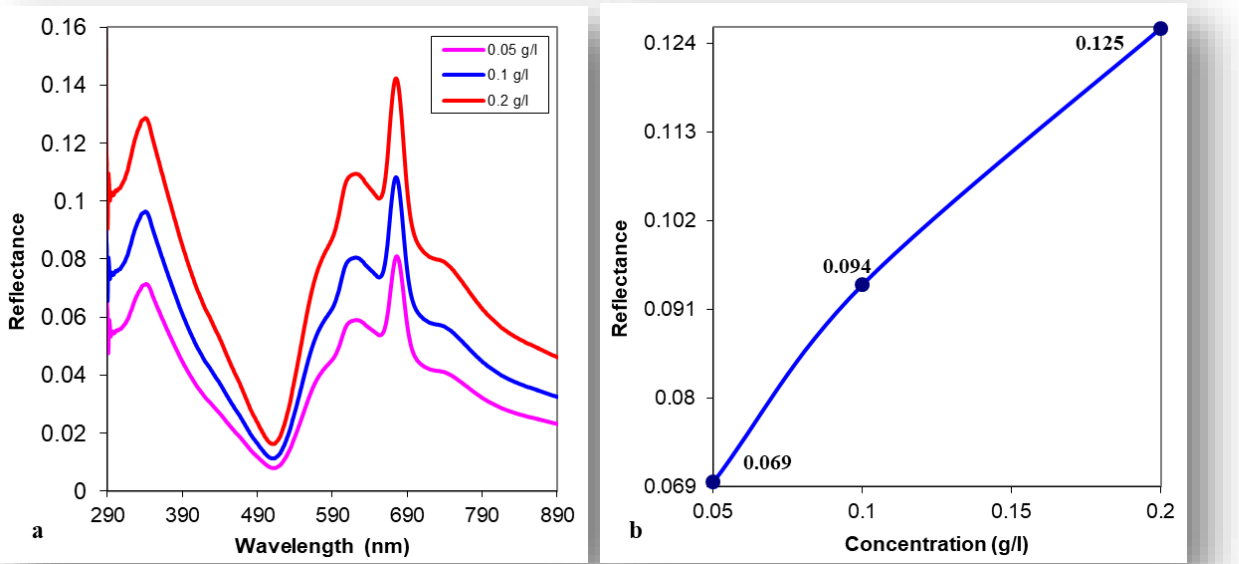

Figure 4-25: (a) Reflectance spectra with different concentrations 0.05, 0.1, and 0.2 g/l for 650 nm laser wavelength and 16 min irradiation. (b) Maximum reflection vs. the concentration of solution at wavelength 335 nm

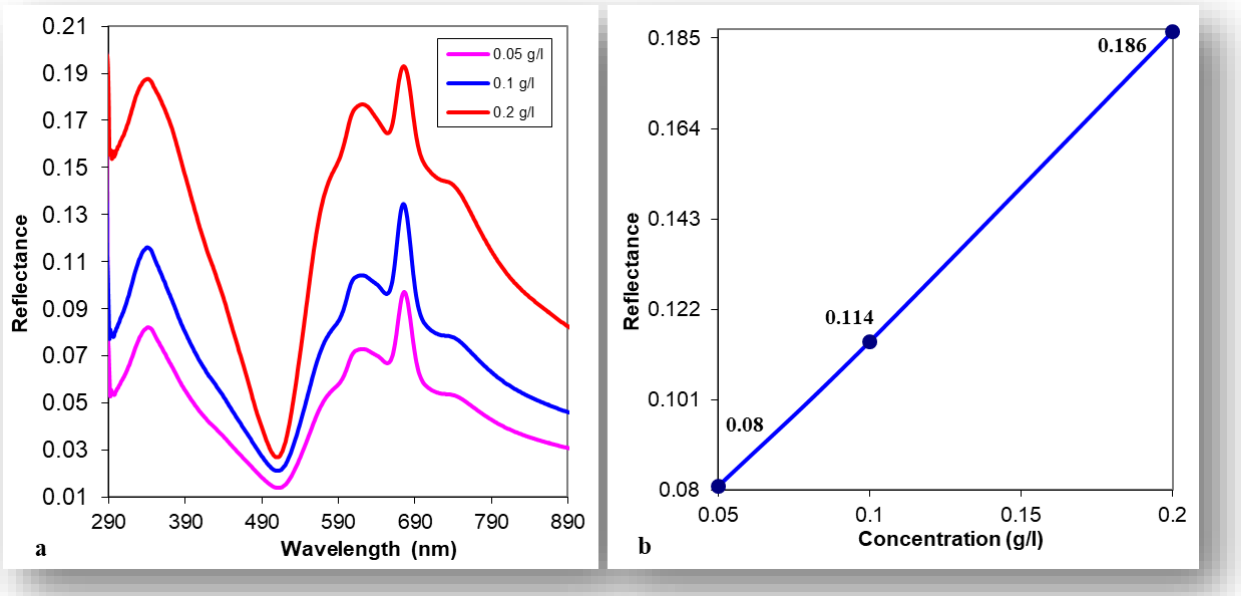

Figure 4-26: (a) Reflectance spectra with different concentrations 0.05, 0.1, and 0.2 g/l for 532 nm laser wavelength and 4 min irradiation. (b) Maximum reflection vs. the concentration of solution at wavelength 333 nm

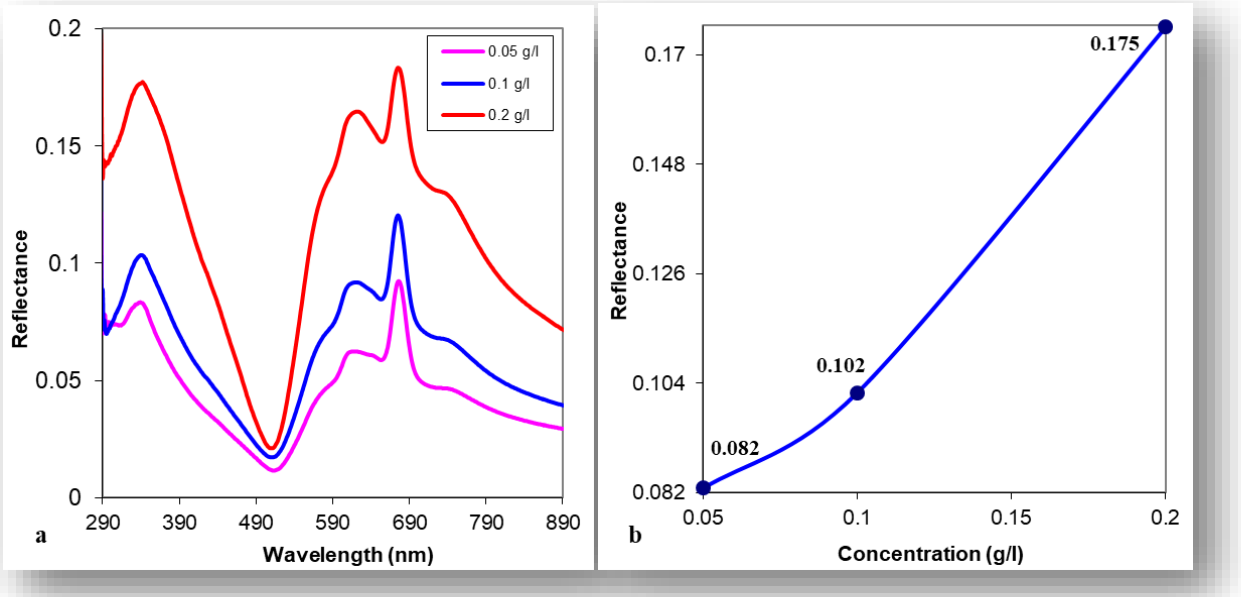

Figure 4-27: (a) Reflectance spectra with different concentrations 0.05, 0.1, and 0.2 g/l for 532 nm laser wavelength and 8 min irradiation. (b) Maximum reflection vs. the concentration of solution at wavelength 333 nm

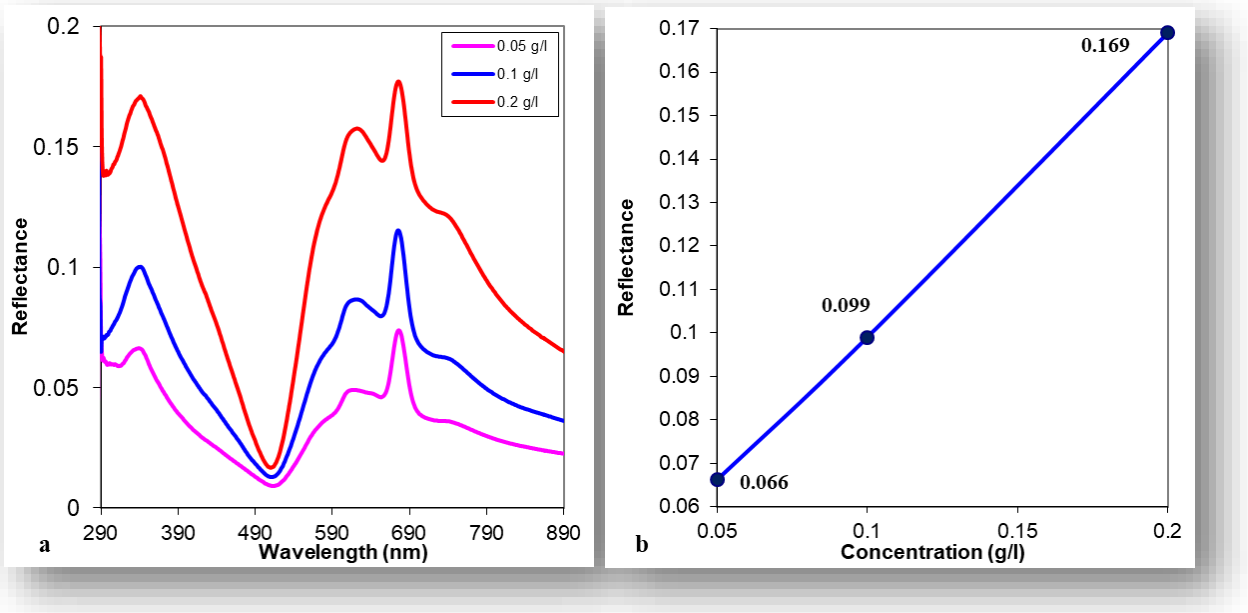

Figure 4-28: (a) Reflectance spectra with different concentrations 0.05, 0.1, and 0.2 g/l for 532 nm laser wavelength and 16 min irradiation. (b) Maximum reflection vs. the concentration of solution at wavelength 333 nm

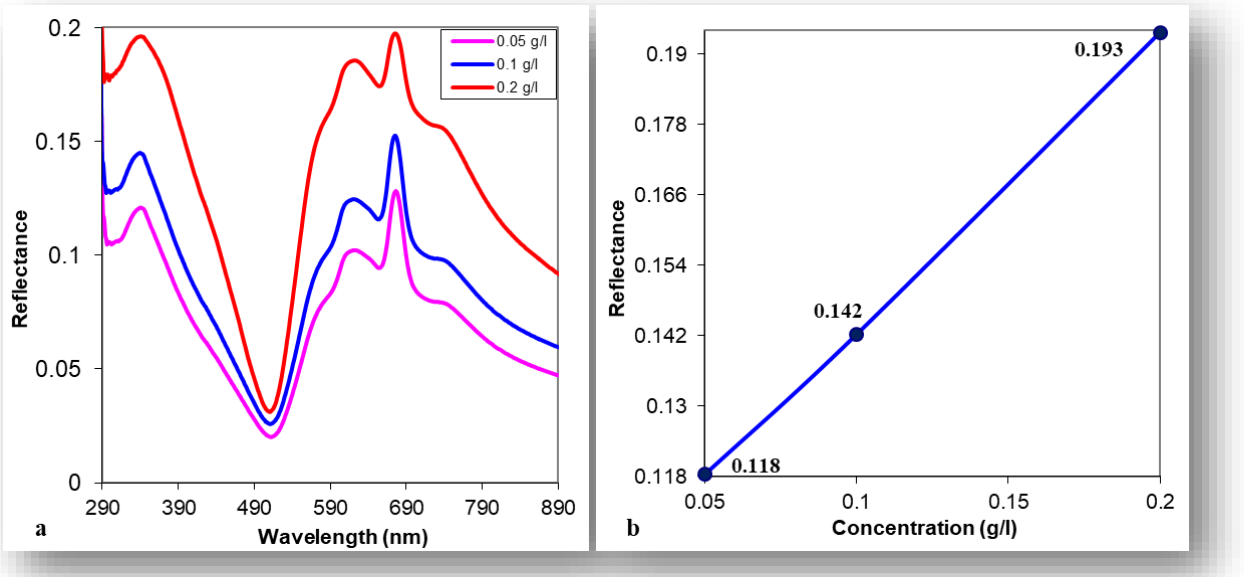

Figure 4-29: (a) Reflectance spectra with different concentrations 0.05, 0.1, and 0.2 g/l for 405 nm laser wavelength and 4 min irradiation. (b) Maximum reflection vs. the concentration of solution at wavelength 330 nm

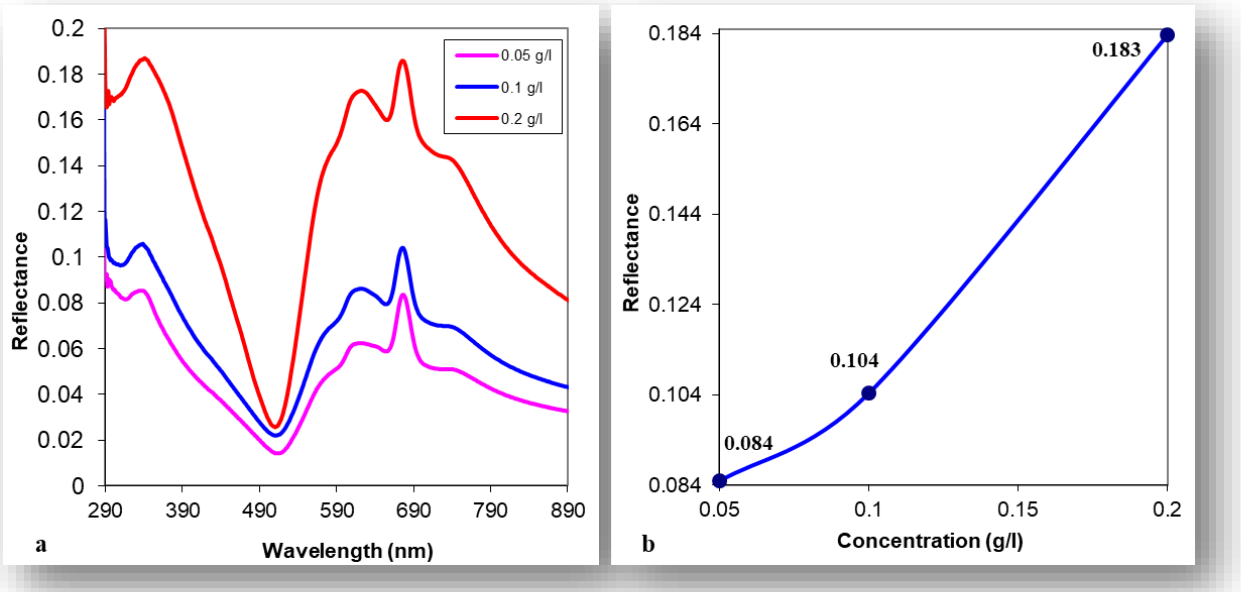

Figure 4-30: (a) Reflectance spectra with different concentrations 0.05, 0.1, and 0.2 g/l for 405 nm laser wavelength and 8 min irradiation. (b) Maximum reflection vs. the concentration of solution at wavelength 330 nm

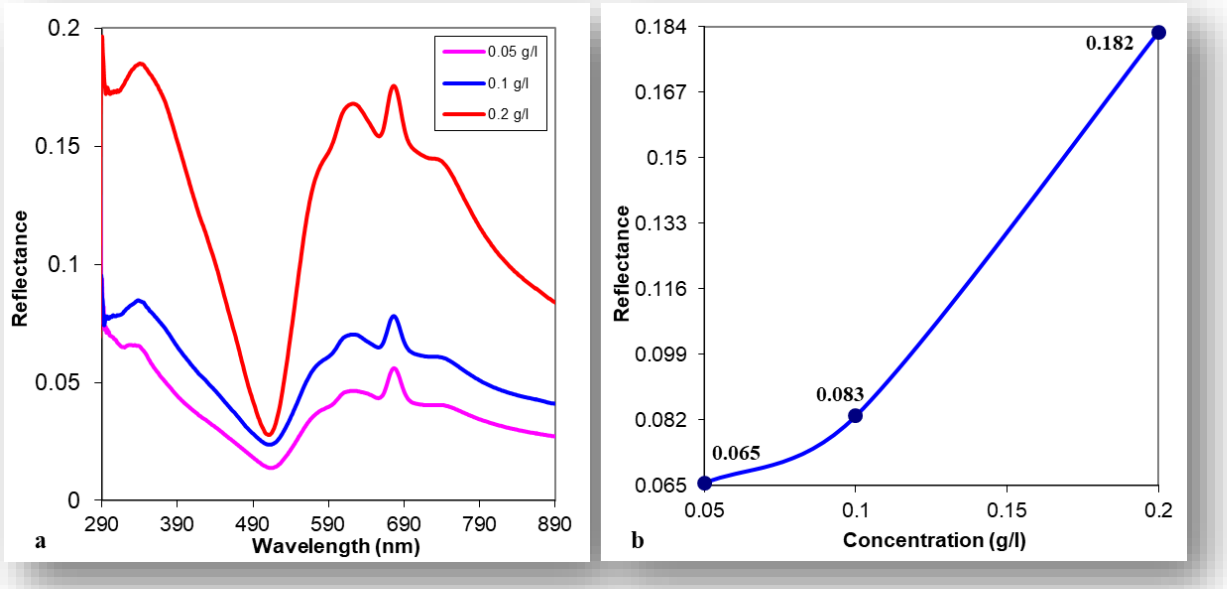

Figure 4-31: (a) Reflectance spectra with different concentrations 0.05, 0.1, and 0.2 g/l for 405 nm laser wavelength and 16 min irradiation. (b) Maximum reflection vs. the concentration of solution at wavelength 330 nm

Figures (4-32a to 4-41a) show the energy gap evaluated from $(\alpha h\nu)^{(1/2)}$ with the photon energy using Tauc equation. These figures illustrate the band gap behavior with increasing the concentration. As a result, the energy gap decreases with increasing the concentration for the red, green, and violet lasers. $650, 532, and\ 405\ nm$, this is due the pigment with the lowest energy gap works on assisting the electron to excite from valence band to the conduction band with very low energy and very short time. This is very important for its use in many photovoltaic applications.

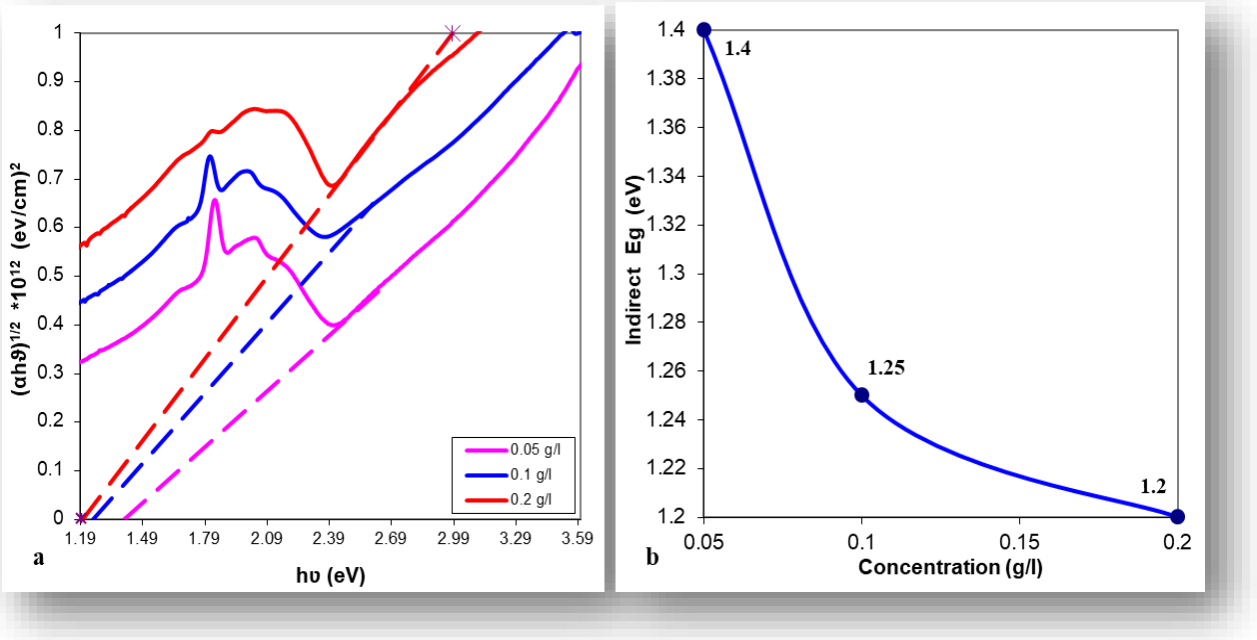

Figure 4-32: (a) Energy gap vs. photon energy at solution concentrations 0.05, 0,1, and 0.2 g/l at non-laser irradiation time. (b) Indirect Eg eV vs. concentration g/l

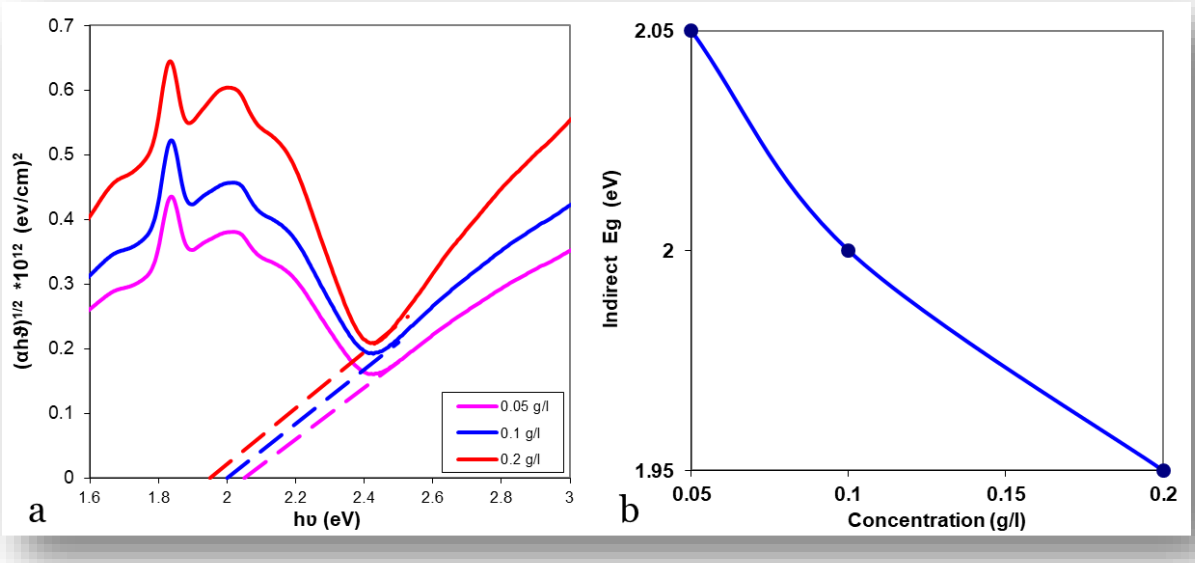

Figure 4-33: (a) Energy gap vs. photon energy at solution concentrations 0.05, 0,1, and 0.2 g/l at laser irradiation time 4 min and wavelength 650 nm. (b) Indirect Eg (eV) vs. concentration g/l

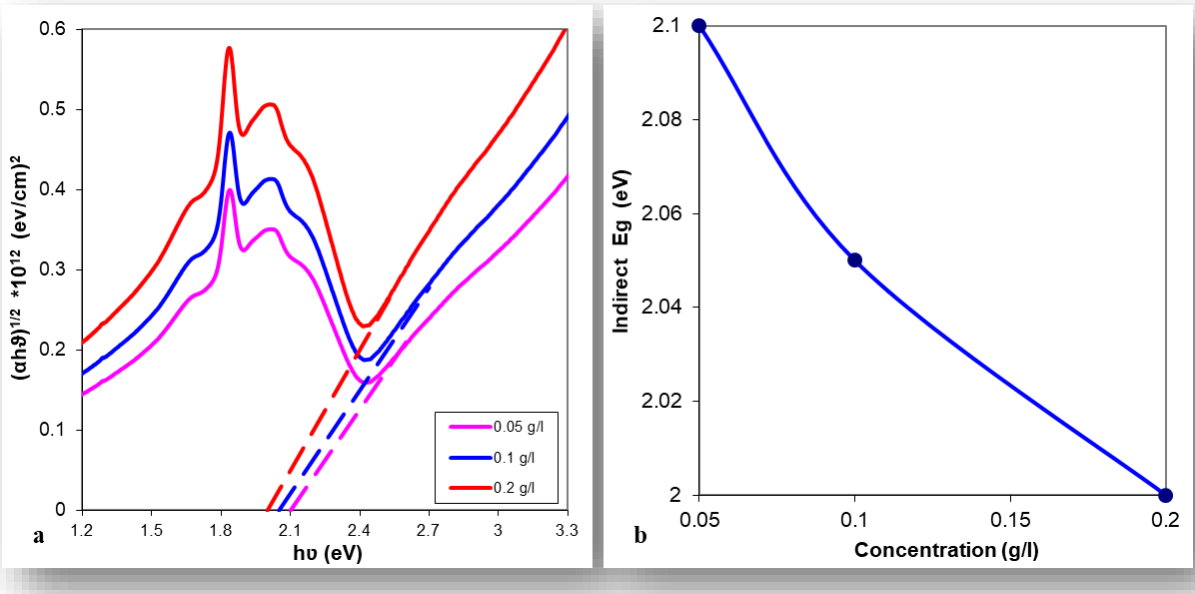

Figure 4-34: (a) Energy gap vs. photon energy at solution concentrations 0.05, 0,1, and 0.2 g/l at laser irradiation time8 min and wavelength (650 nm). (b) Indirect Eg eV vs. concentration g/l

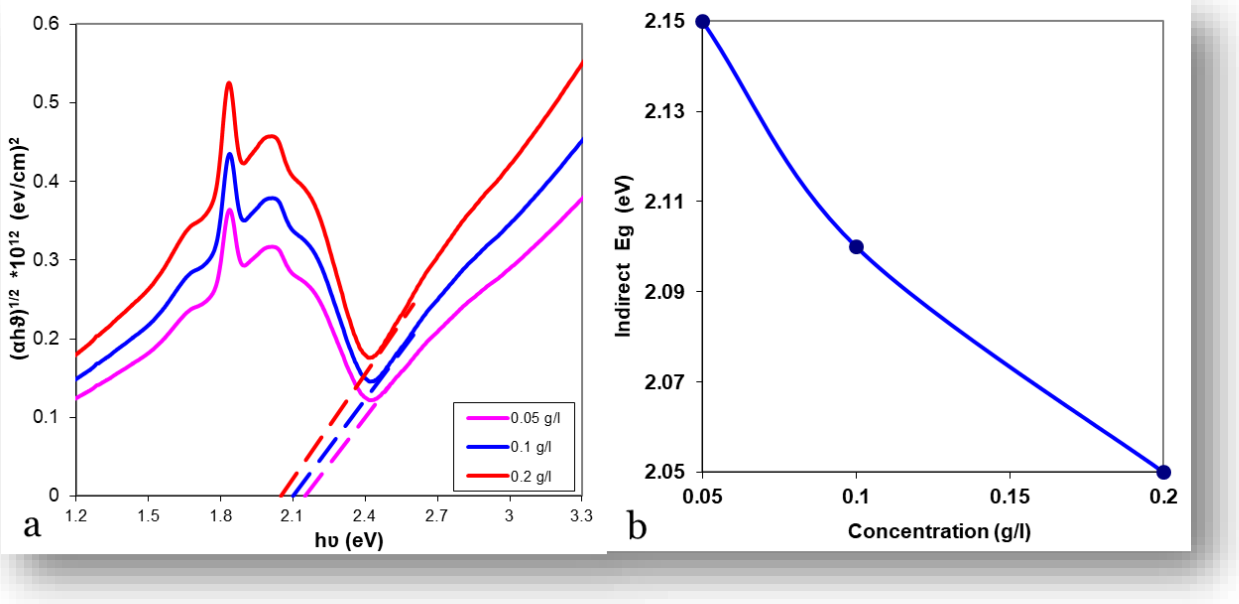

Figure 4-35: (a) Energy gap vs. photon energy at solution concentrations 0.05, 0,1, and 0.2 g/l at laser irradiation time 16 min and wavelength 650 nm. (b) Indirect Eg eV vs. concentration g/l

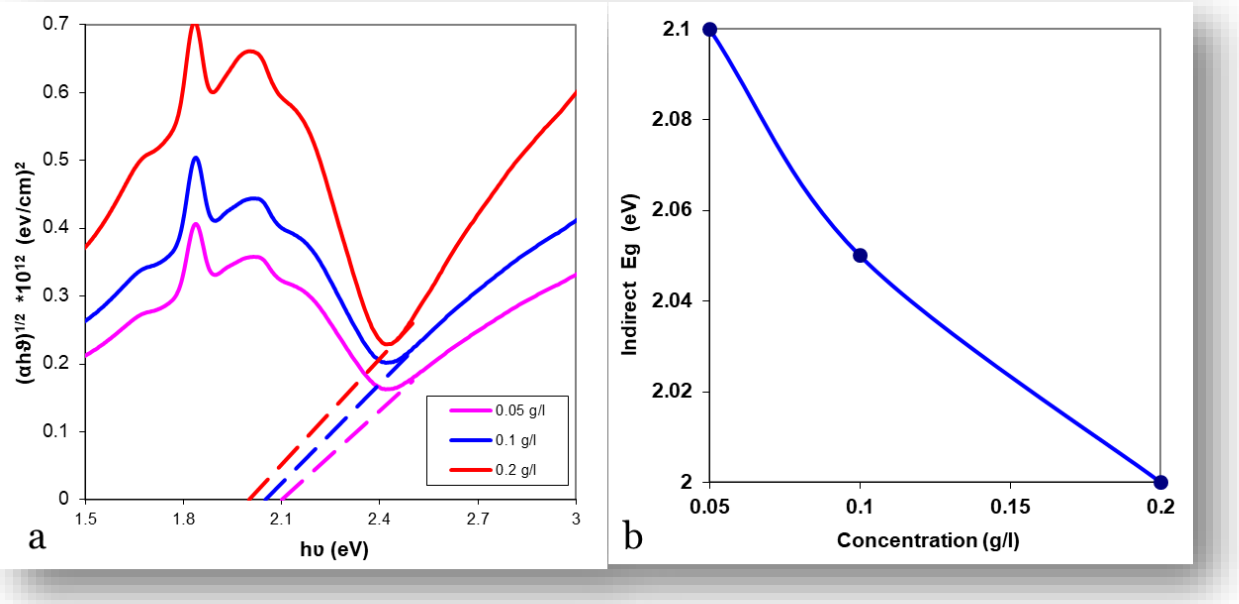

Figure 4-36: (a) Energy gap vs. photon energy at solution concentrations 0.05, 0,1, and 0.2 g/l at laser irradiation time 4 min and wavelength 532 nm. (b) Indirect Eg eV vs. concentration g/l

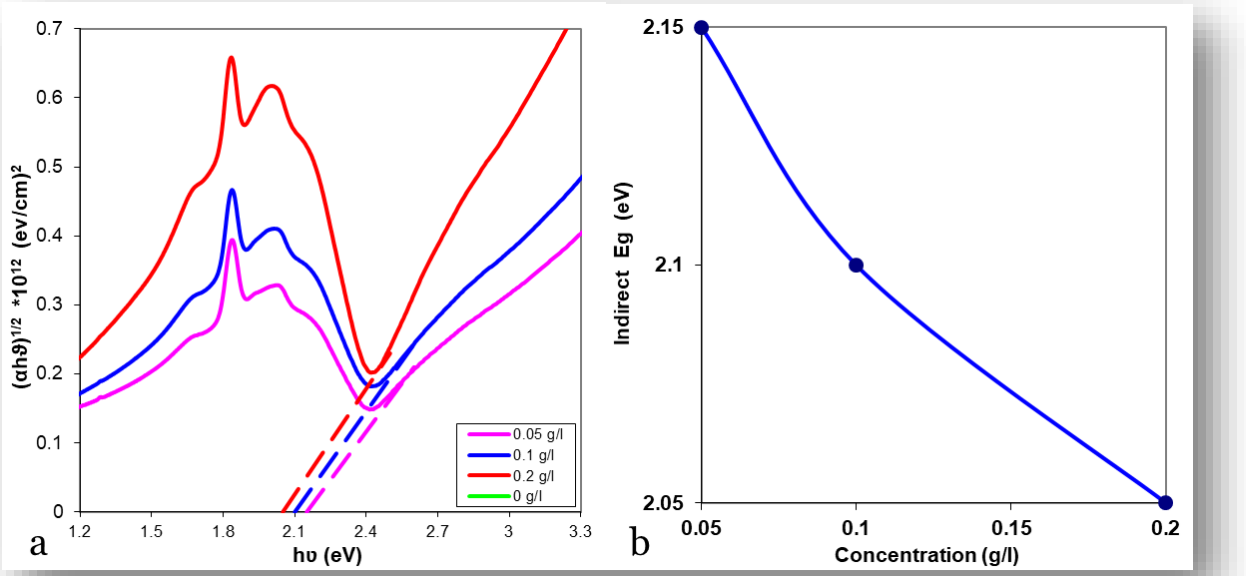

Figure 4-37: (a) Energy gap vs. photon energy at solution concentrations 0.05, 0,1, and 0.2 g/l at laser irradiation time 8 min and wavelength 532 nm. (b) Indirect Eg eV vs. concentration g/l

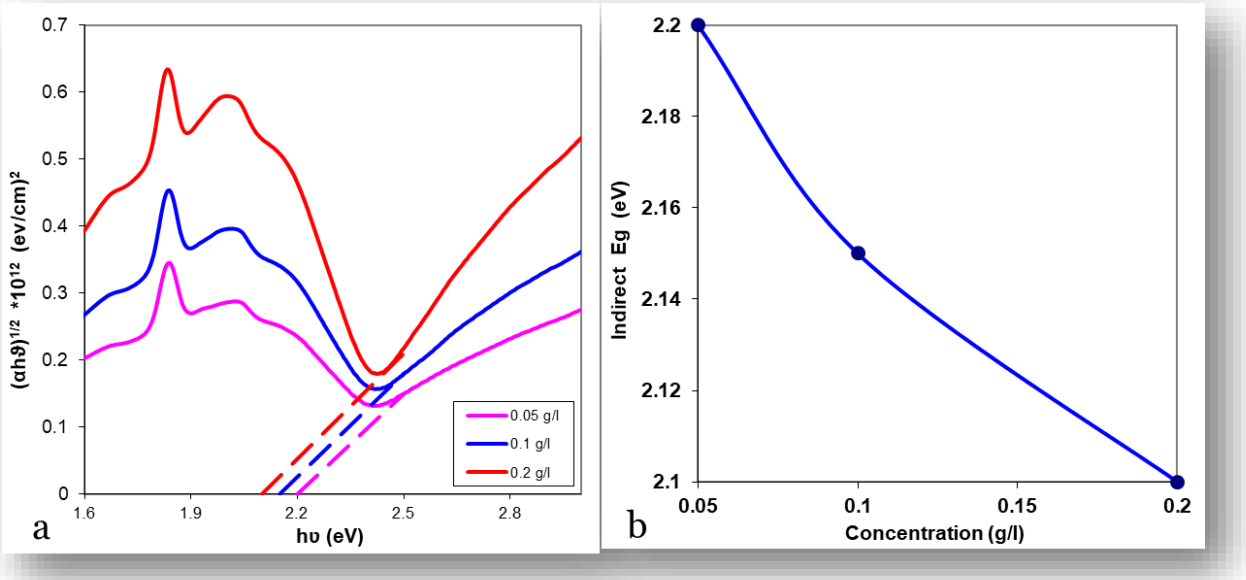

Figure 4-38: (a) Energy gap vs. photon energy at solution concentrations 0.05, 0,1, and 0.2 g/l at laser irradiation time 16 min and wavelength 532 nm. (b) Indirect Eg eV vs. concentration g/l

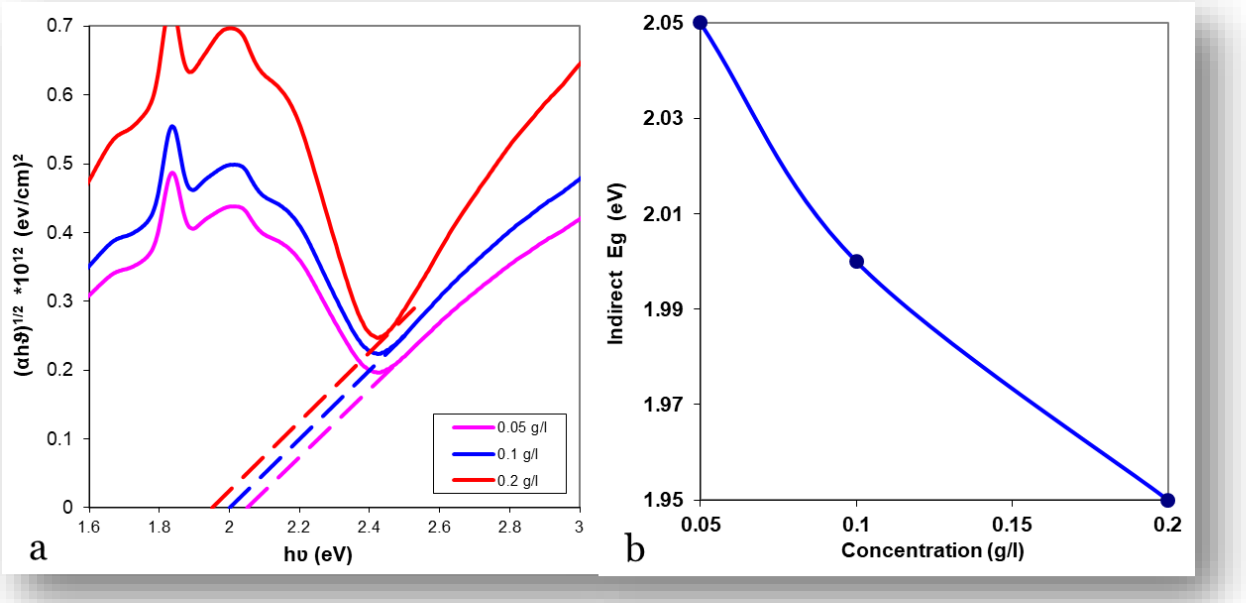

Figure 4-39: (a) Energy gap vs. photon energy at solution concentrations 0.05, 0,1, and 0.2 g/l at laser irradiation time 4 min and wavelength 405 nm. (b) Indirect Eg eV vs. concentration g/l

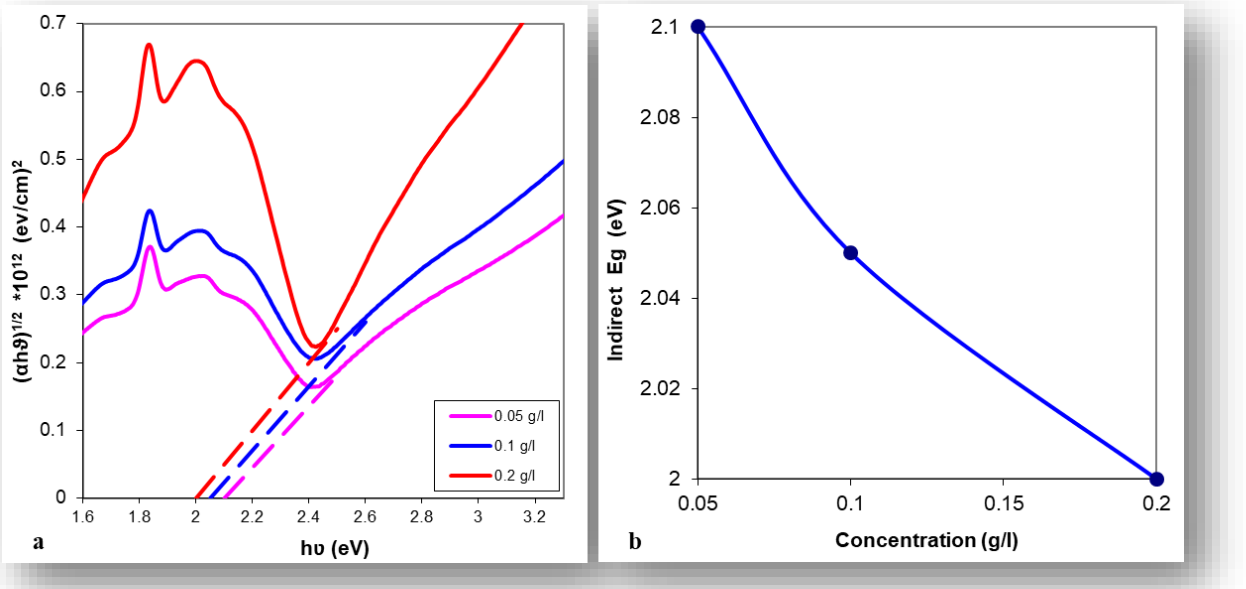

Figure 4-40: (a) Energy gap vs. photon energy at solution concentrations 0.05, 0,1, and 0.2 g/l at laser irradiation time 8 min and wavelength 405 nm. (b) Indirect Eg eV vs. concentration g/l

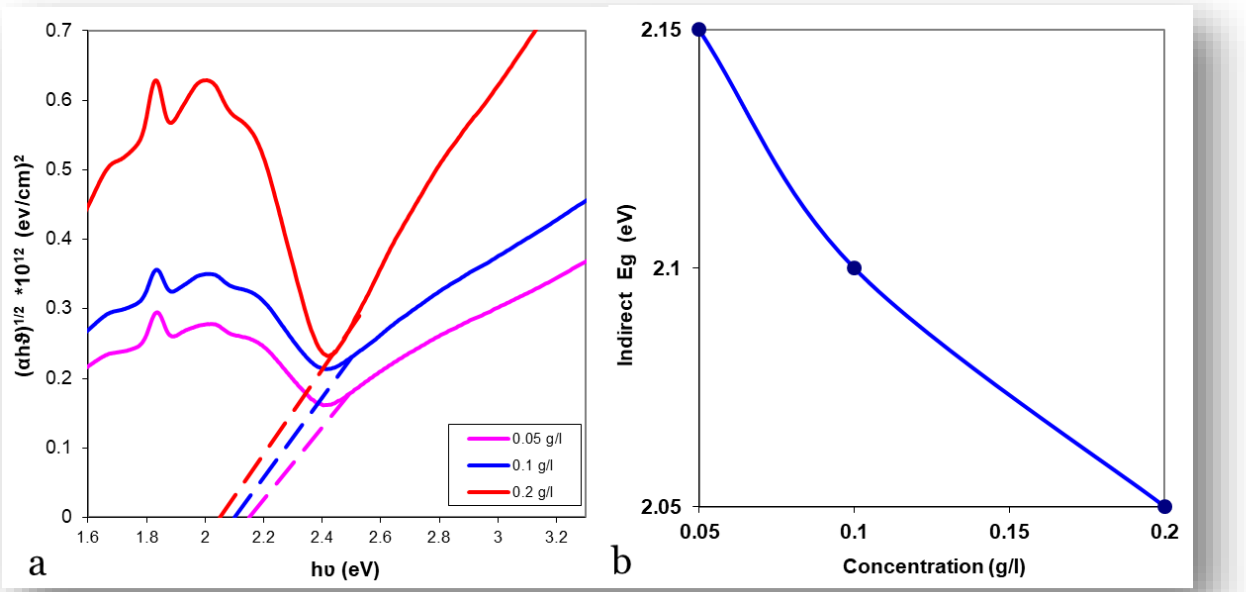

Figure 4-41: (a) Energy gap vs. photon energy at solution concentrations 0.05, 0,1, and 0.2 g/l at laser irradiation time 16 min and wavelength 405 nm. (b) Indirect Eg eV vs. concentration g/l

The optical parameters (absorptivity, molar absorptivity, absorption coefficient, refractive index, extinction coefficient, dielectric constants, optical conductivity and indirect energy gap) are listed in Tables (4-3 to 4-6).

Table 4-3. The optical parameters as absorption coefficient, extinction coefficients, refractive index, dielectric constants and the optical conductivity at laser irradiated time 0 min at wavelength 345 nm

Concentration (g/l)	a (l/g.cm)	ϵ (l/mol.cm)	α (cm^{-1})	n	k $*10^{-7}$	ε_{real}	$\varepsilon_{im.}$ $*10^{-6}$	$\sigma_{Optical}$ (s^{-1})	Indirect Eg (eV)
0.05	4.828	2781.50	0.241	2.362	6.63	5.579	3.132	0.136	1.4
0.1	5.583	3216.71	0.279	2.452	7.67	6.016	3.762	0.163	1.25
0.2	7.209	4153.16	0.360	2.532	9.90	6.415	5.015	0.218	1.2

Table 4-4. The optical parameters as absorption coefficient, extinction coefficients, refractive index, dielectric constants and the optical conductivity at laser irradiated time 4, 8, and 16 min with red laser 650 nm at wavelength 335 nm

	Concentration (g/l)	A (l/g.cm)	ϵ (l/mol.cm)	α (cm^{-1})	n	k $*10^{-7}$	ε_{real}	$\varepsilon_{im.}$ $*10^{-7}$	$\sigma_{optical}$ (s^{-1})	Indirect Eg (eV)
4 min	0.05	1.738	1001.43	0.086	1.625	2.32	2.643	7.53	0.033	2.05
	0.1	2.503	1442.06	0.125	1.860	3.34	3.460	12.4	0.055	2
	0.2	4.498	2591.46	0.224	2.310	6.00	5.340	27.7	0.124	1.95
8 min	0.05	1.477	851.08	0.073	1.539	1.97	2.371	6.06	0.027	2.1
	0.1	2.051	1182.06	0.102	1.727	2.74	2.983	9.45	0.042	2.05
	0.2	3.077	1773.10	0.153	2.013	4.10	4.053	16.5	0.074	2
16 min	0.05	1.231	709.65	0.061	1.456	1.64	2.119	4.78	0.021	2.15
	0.1	1.759	1013.79	0.087	1.634	2.35	2.672	7.67	0.034	2.1
	0.2	2.566	1478.45	0.128	1.876	3.42	3.522	12.8	0.057	2.05

Table 4-5. The optical parameters as absorption coefficient, extinction coefficients, refractive index, dielectric constants and the optical conductivity at laser irradiated time 4, 8, and 16 min with green laser 532 nm at wavelength 333 nm

	Concentration (g/l)	A (l/g.cm)	ϵ (l/mol.cm)	α (cm^{-1})	n	K $*10^{-7}$	ε_{real}	$\varepsilon_{im.}$ $*10^{-7}$	$\sigma_{optical}$ (s^{-1})	Indirect Eg (eV)
4 min	0.05	1.422	819.45	0.071	1.521	1.89	2.314	5.73	0.025	2.1
	0.1	2.188	1260.69	0.109	1.771	2.90	3.138	10.2	0.046	2.05
	0.2	4.845	2791.51	0.242	2.364	6.42	5.591	30.3	0.136	2
8 min	0.05	1.475	850.25	0.073	1.539	1.96	2.369	6.02	0.027	2.15
	0.1	1.892	1090.34	0.094	1.678	2.51	2.817	8.42	0.037	2.1
	0.2	4.250	2448.49	0.212	2.267	5.63	5.143	25.5	0.115	2.05
16 min	0.05	1.134	653.82	0.056	1.422	1.50	2.022	4.27	0.019	2.2
	0.1	1.812	1043.94	0.091	1.655	2.40	2.739	7.95	0.035	2.15
	0.2	3.938	2268.73	0.196	2.208	5.22	4.876	23.1	0.103	2.1

Table 4-6. The optical parameters as absorption coefficient, extinction coefficients, refractive index, dielectric constants and the optical conductivity at laser irradiated time 4, 8, and 16 min with violet laser 405 nm at wavelength 330 nm

	Concentration (g/l)	A (l/g.cm)	ϵ (l/mol.cm)	A (cm^{-1})	n	k $*10^{-7}$	ε_{real}	$\varepsilon_{im.}$ $*10^{-7}$	$\sigma_{optical}$ (s^{-1})	Indirect Eg (eV)
4 min	**0.05**	2.317	1335.30	0.115	1.805	3.05	3.258	10.9	0.049	2.05
	0.1	3.004	1730.95	0.150	1.997	3.95	3.990	15.7	0.071	2
	0.2	5.460	3145.39	0.273	2.441	7.17	5.958	35.0	0.159	1.95
8 min	**0.05**	1.525	878.88	0.076	1.555	2.00	2.421	6.23	0.028	2.1
	0.1	1.966	1132.81	0.098	1.698	2.58	2.884	8.77	0.039	2.05
	0.2	4.746	2734.52	0.237	2.350	6.24	5.523	29.3	0.133	2
16 min	**0.05**	1.132	652.64	0.056	1.421	1.49	2.021	4.23	0.019	2.15
	0.1	1.488	857.48	0.074	1.544	1.96	2.385	6.04	0.027	2.1
	0.2	4.682	2697.65	0.234	2.340	6.15	5.477	28.7	0.131	2.05

4.4.2 Fluorescence Spectra for CuPc Solution

The fluorescence spectra for CuPc solution with concentrations $0.2\ g/l$ and irradiation time $4, 8, and\ 16\ min$ and laser wavelengths $650, 532, and\ 405\ nm$ are shown in Figs. (4-42 to 4-44). Also the comparison between the emission and excitation energy gap are illustrated in the Table (4-7). Through the results, There is a convergence of values between the calculated energy gap values using Tauc equation and that calculated by the fluorescence method.

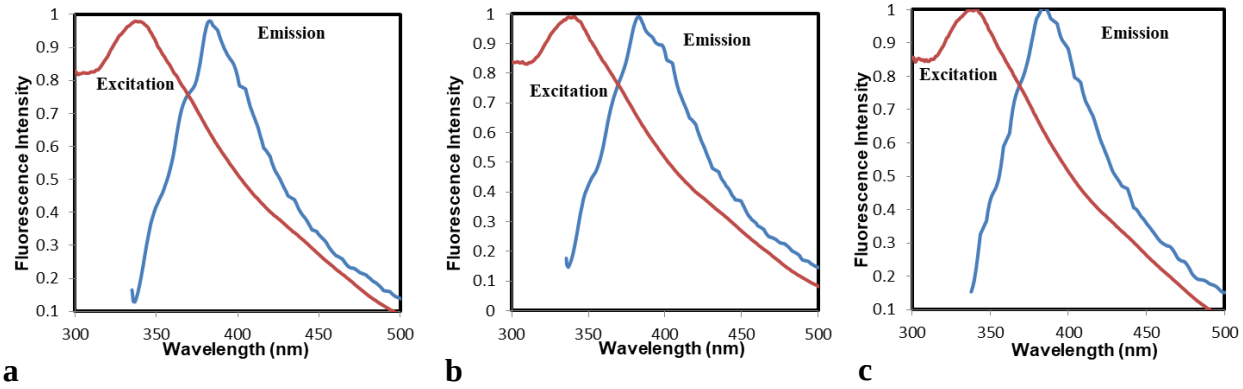

Figure 4-42: Emission and excitation spectrum for CuPc solution at concentration 0.2 g/l irradiated by red laser 650 nm at time (a) 4min, (b) 8 min, and (c) 16 min

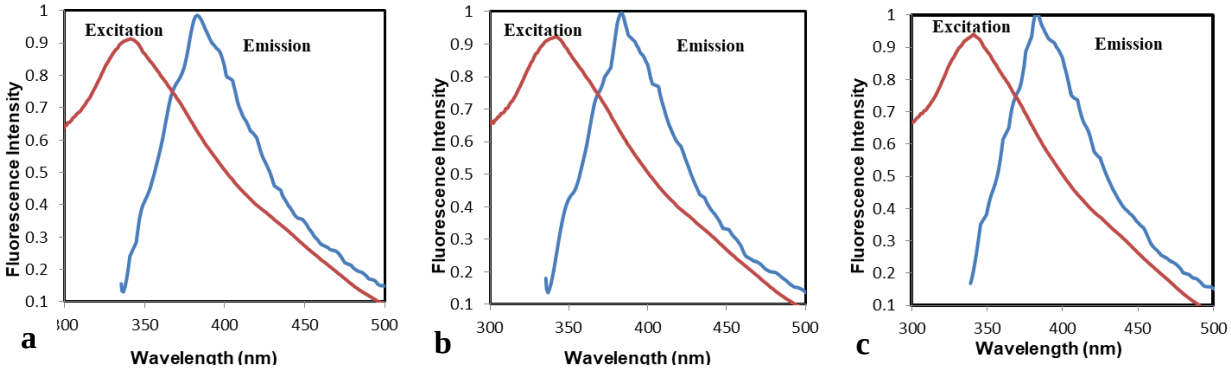

Figure 4-43: Emission and excitation spectrum for CuPc solution at concentration 0.2 g/l irradiated by green laser 532 nm at time (a) 4 min, (b) 8 min, and (c) 16 min

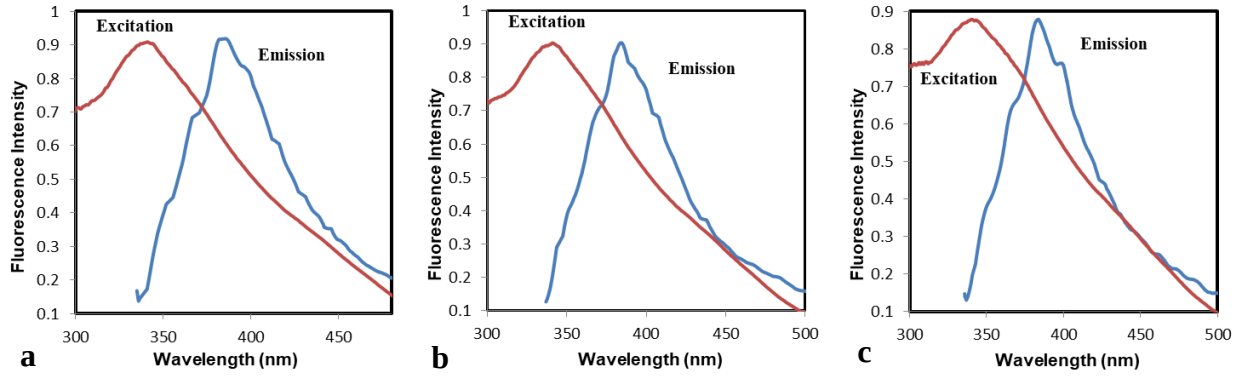

Figure 4-44: Emission and excitation spectrum for CuPc solution at concentration 0.2 g/l irradiated by violet laser 405 nm at time (a) 4min, (b) 8 min, and (c) 16 min

Table 4-7. Emission and excitation energy gap at concentration 0.2g/l with laser irradiation times 4, 8, and 16 min. and wavelengths 650, 532 and 405 nm

Wavelength (nm)	4 min.		8 min.		16 min.	
	Tauc eV	PL. eV	Tauc eV	PL. eV	Tauc eV	PL. eV
650	2.75	3.25	2.72	3.25	2.61	3.24
532	2.70	3.25	2.68	3.24	2.61	3.24
405	2.75	3.25	2.59	3.24	2.56	3.25

4.5 Optical and Structural Properties of CuPc Thin Film

4.5.1 Effect of the Irradiation Time on the Optical Properties of CuPc Thin Film

CuPc thin film is deposited by spin coating method at room temperature with thickness of $219.12\,nm$ on a glass substrate. Thin films are exposed to different laser beams of wavelengths $650, 532\ and\ 405\,nm$, for different laser irradiation times $0, 10, 20, and\ 30\ min$.

Copper phthalocyanine thin films have two main absorption bands in the visible/near-UV region to the spectrum. The first one is called B (Soret) band occurring at around 350 nm, and the second band, occurring at around 552 and 770 nm, known as the Q-band [72].

Figs. (4-45a to 4-47a) show the optical absorption spectra of CuPc thin film at different irradiation times with wavelengths $650, 532, and\ 405\,nm$. UV-Vis spectrum of MPcs arising from molecular orbitals within the aromatic 18 π-electron system and from overlapping orbital on the central metal [28]. It can also be noticed that this band shows the characteristic splitting (Davydov

splitting) present in all phthalocyanine derivatives, two absorption bands, centered at ~$630-700\,nm$, which correspond to the known Q-band. Then the first and second $\pi-\pi^*$ transition appear at $552\,and\,770\,nm$ respectively [73]. Figs. (4-45b to 4-47b) display the maximum absorbance of the B-band varying with the irradiation times $0, 10, 20, and\ 30\,min$. The measurements are taken with different wavelengths $650, 532, and\ 405\,nm$. In addition, the peak that assigned to aggregations of dimer and trimmer molecules in the thin films became more intense in comparison to monomer peak which was higher in the solution. That could be explained by the fact that, in the solid case, phthalocyanine tend to form more aggregation of dimer and trimmer chain of molecules instead being monomers [74]. The results show that the absorbance value is the highest for the non-irradiated samples $(t = 0\,min)$ and decreases with increasing the laser irradiation times.

Figs. (4-48a to 4-50a) show reflectance spectra to the thin film samples with thickness $219.12\,nm$ before and after laser exposure with wavelengths $650, 532, and\ 405\,nm$. Obviously, the reflectance spectrum behaves similar to the absorbance spectrum, which decreases with increasing the laser irradiation time $0, 10, 20, and\ 30\,min$. Fig. (4-48b to 4-50b) shows the maximum reflectance varies time irradiation.

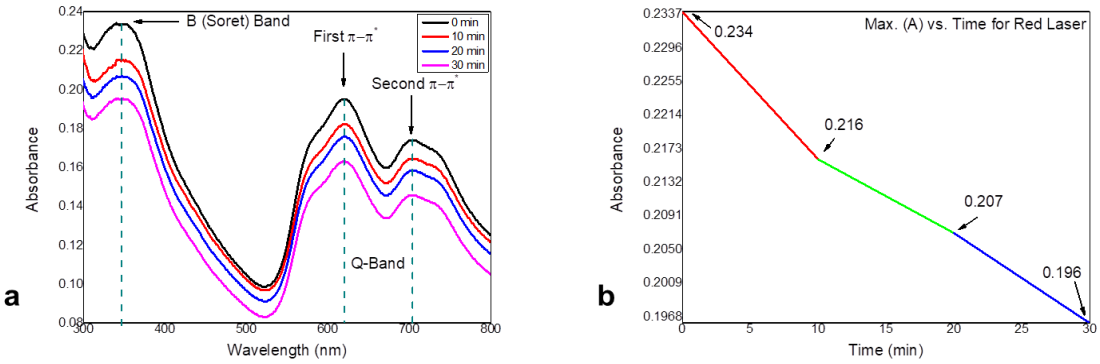

Figure 4-45: (a) Optical absorbance of CuPc thin film at different irradiation time 0, 10, 20, and 30 min, with red laser 650 nm. (b) Max. (A) vs. time irradiation of 350 nm

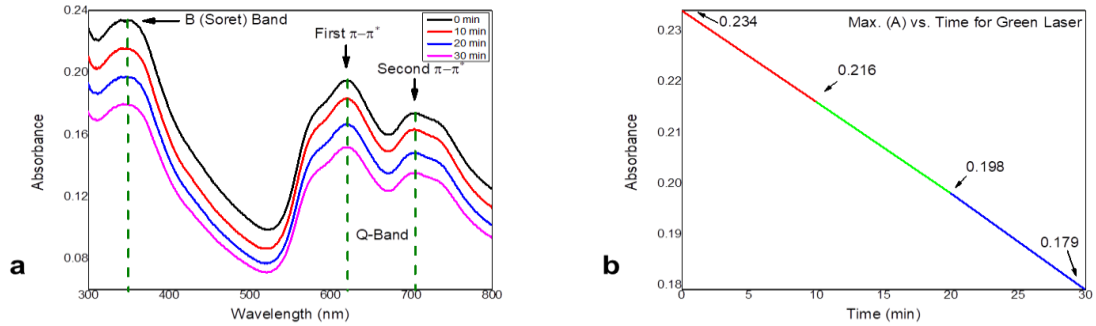

Figure 4-46: (a) Optical absorbance of CuPc thin film at different irradiation time 0, 10, 20, and 30 min, with green laser 532 nm. (b) Max. (A) vs. time irradiation of 350 nm

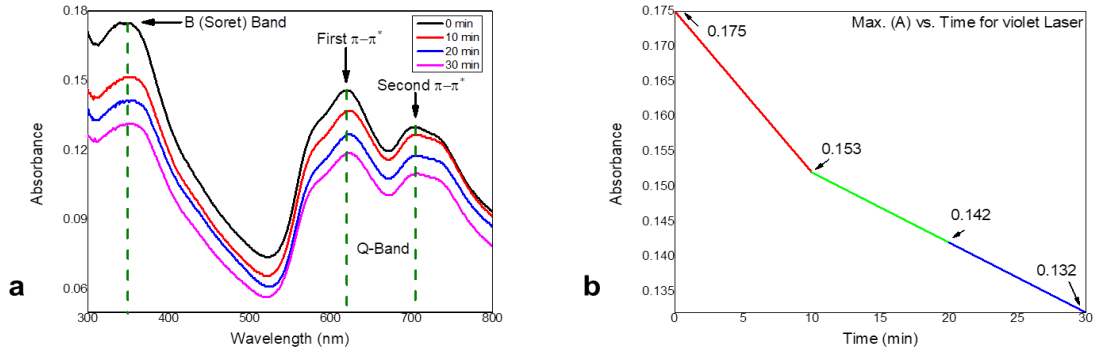

Figure 4-47: (a) Optical absorbance of CuPc thin film at different irradiation time 0, 10, 20, and 30min, with violet laser 405 nm. (b) Max. (A) vs. time irradiation of 350 nm

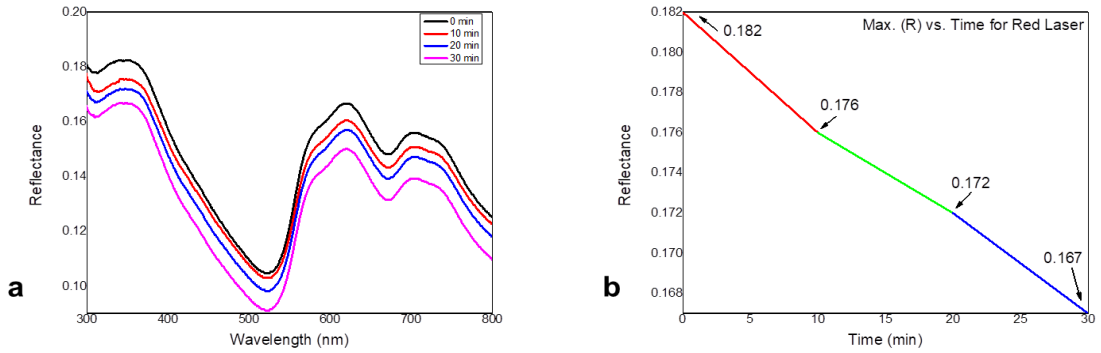

Figure 4-48: (a) Optical reflectance of CuPc thin film at different irradiation time 0, 10, 20, and 30 min, with red laser 650 nm. (b) Max. (R) vs. time irradiation of 350 nm

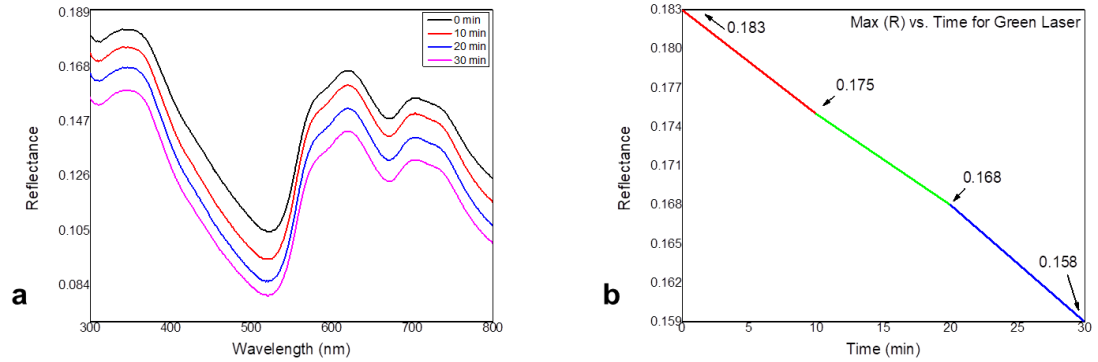

Figure 4-49: (a) Optical reflectance of CuPc thin film at different irradiation time 0, 10, 20, and 30 min, with green laser 532 nm. (b) Max. (R) vs. time irradiation of 350 nm

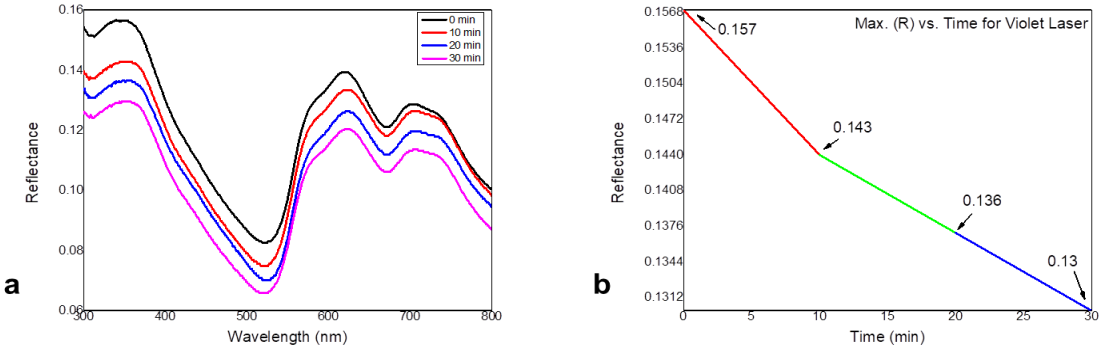

Figure 4-50: (a) Optical reflectance of CuPc thin film at different irradiation time 0, 10, 20, and 30 min, with violet laser 405 nm. (b) Max. (R) vs. time irradiation of 350 nm

The energy band gap (Allowed and Forbidden) with photon energy as shown in Fig. (4-51 to 4-53). the photon energy value of CuPc thin film of $\sim 219.12\ nm$ thickness irradiated at different lasers wavelength $650, 532, and\ 405\ nm$ at time $0, 10, 20, and\ 30\ min$. We notice that the optical energy gap increases slightly with the increase in the time irradiation. This means that there is a shift towards short wavelengths according to eq. (2-2). Optical parameters as (absorption coefficient, refractive index, extinction coefficient, dielectric constants, optical conductivity and direct energy gap) for CuPc thin film are listed in Table (4-8).

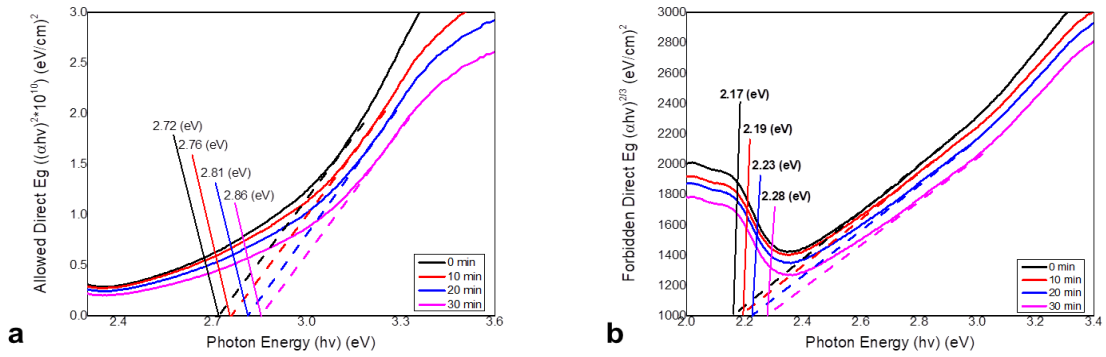

Figure 4-51: (a) Allowed band gap. (b) Forbidden band gap of CuPc thin film at irradiation time 0, 10, 20, and 30 min, with red laser 650 nm

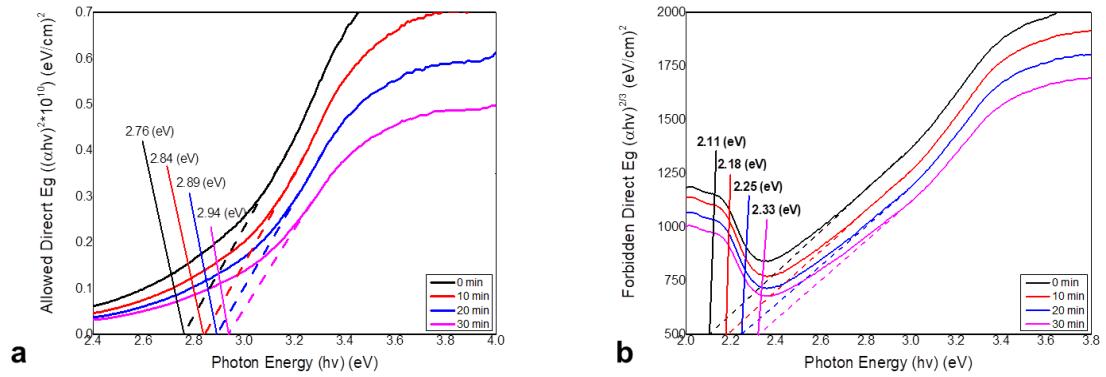

Figure 4-52: (a) Allowed band gap. (b) Forbidden band gap of CuPc thin film at irradiation time 0, 10, 20, and 30 min, with green laser 532 nm

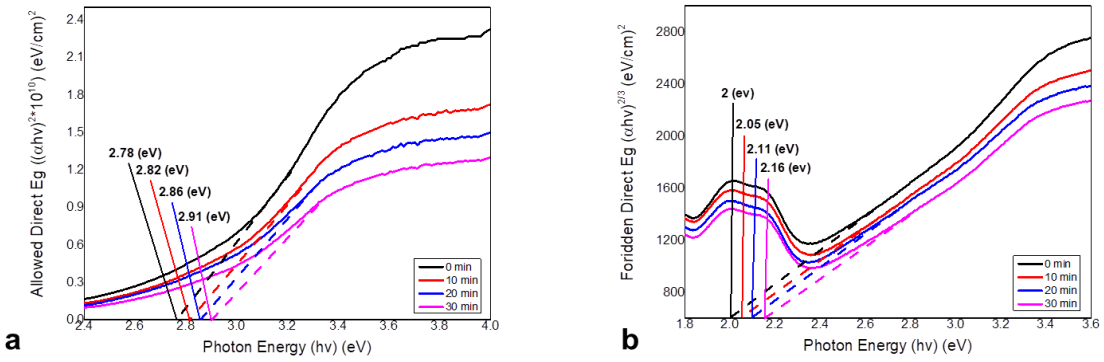

Figure 4-53: (a) Allowed band gap. (b) Forbidden band gap of CuPc thin film at irradiation time 0, 10, 20, and 30 min, with violet laser 405 nm

Table 4-8. Optical constants for CuPc thin film irradiation by red, green and violet laser wavelengths 650, 532, and 405 nm beam at time 0, 10, 20, and 30 min at wavelength 350 nm

	Time (min)	$(\alpha \times 10^4)$ (cm^{-1})	n	k	ε_{Real}	$\varepsilon_{im.}$	$(\sigma_{Optical})$ 10^{14} (s^{-1})	Allowed Eg (eV)	Forbidden Eg (eV)
Red Laser	0	2.456	2.342	0.068	5.480	0.321	1.374	2.72	2.17
	10	2.256	2.278	0.063	5.186	0.286	1.228	2.76	2.19
	20	2.169	2.248	0.061	5.048	0.272	1.165	2.81	2.23
	30	2.049	2.202	0.057	4.847	0.251	1.078	2.86	2.28
Green Laser	0	2.456	2.342	0.066	5.479	0.309	1.373	2.76	2.11
	10	2.263	2.280	0.061	5.197	0.278	1.233	2.84	2.18
	20	2.071	2.208	0.056	4.872	0.245	1.089	2.89	2.25
	30	1.886	2.133	0.051	4.549	0.216	0.958	2.94	2.33
Violet Laser	0	1.837	2.115	0.049	4.477	0.209	0.928	2.78	2
	10	1.576	1.994	0.042	3.974	0.169	0.750	2.82	2.06
	20	1.478	1.945	0.039	3.782	0.155	0.687	2.86	2.11
	30	1.367	1.887	0.037	3.560	0.139	0.616	2.91	2.16

4.5.2 Effect of the Irradiation Time on the Structural Properties of CuPc Thin Film

The structural properties are examined for the thin films including AFM and XRD. AFM test is conducted to identify the surface morphology. Results confirm that the laser irradiation has an obvious influence on the CuPc thin films, as shown in Figs. (4-57 to 4-66) for sample before and after exposing to different laser wavelengths $650, 532, and\ 405\ nm$ and different laser irradiation times $0, 10, 20, and\ 30\ min$. Some fluctuation in the surface roughness is attributed to the heterogeneity of the thickness of the thin film surface and some reasons go to the deposition preparation method [40]. The AFM results for each laser are listed in Table (4-9).

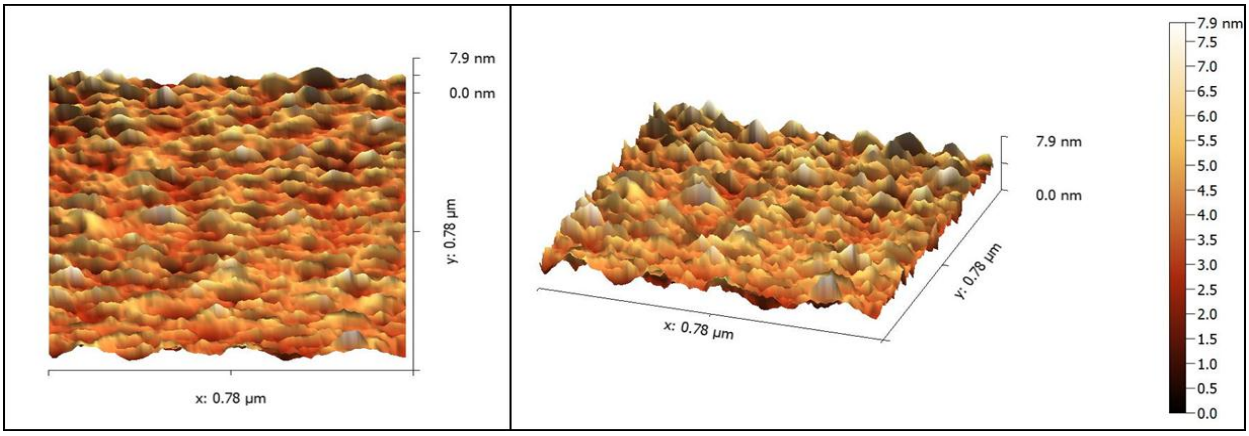

Figure 4-54: AFM for CuPc thin film for non-irradiated sample

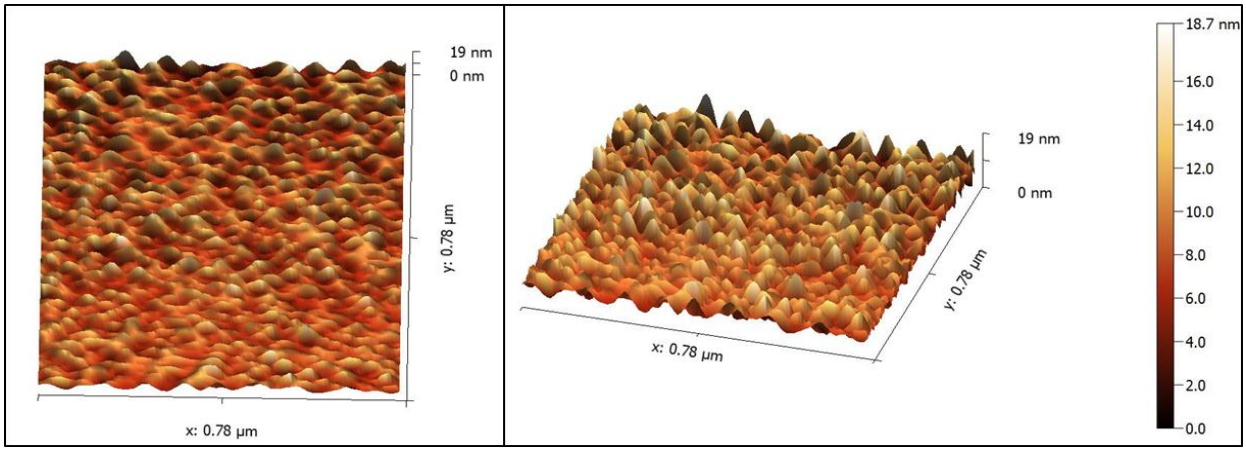

Figure 4-55: AFM for CuPc thin film with time irradiated 10 min by red laser 650 nm

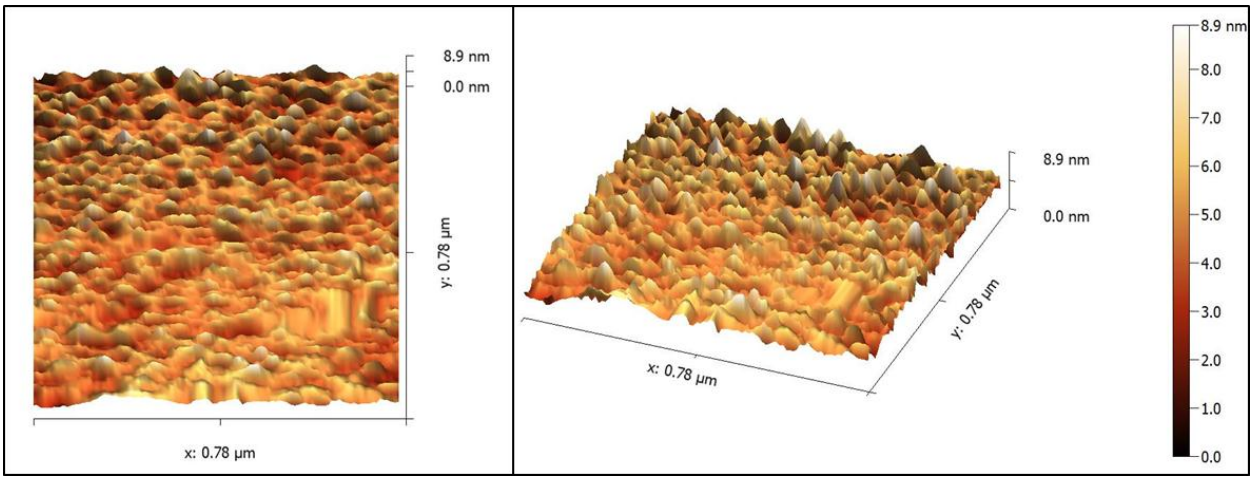

Figure 4-56: AFM for CuPc thin film with time irradiated 20 min by red laser 650 nm

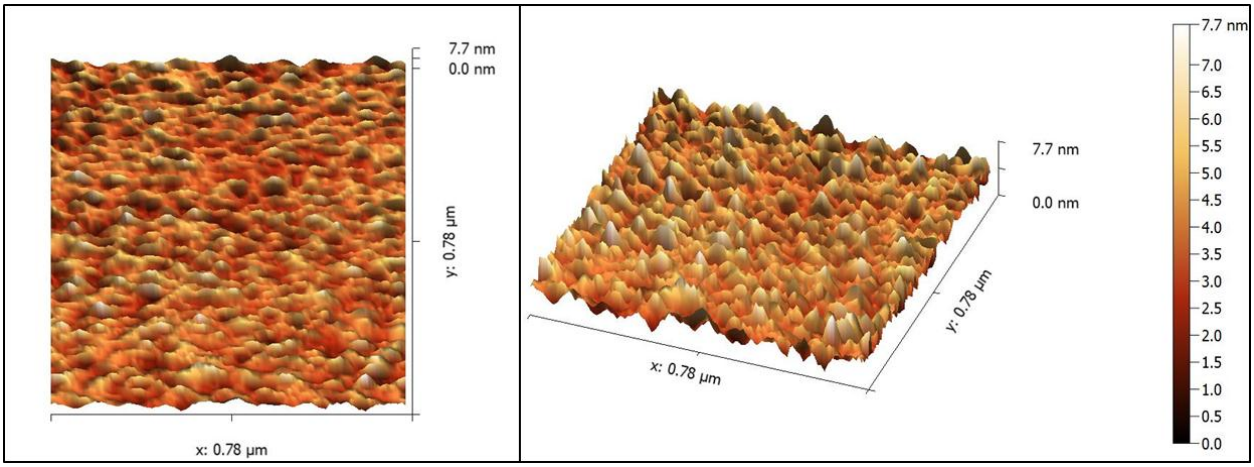

Figure 4-57: AFM for CuPc thin film with time irradiated 30 min by red laser 650 nm

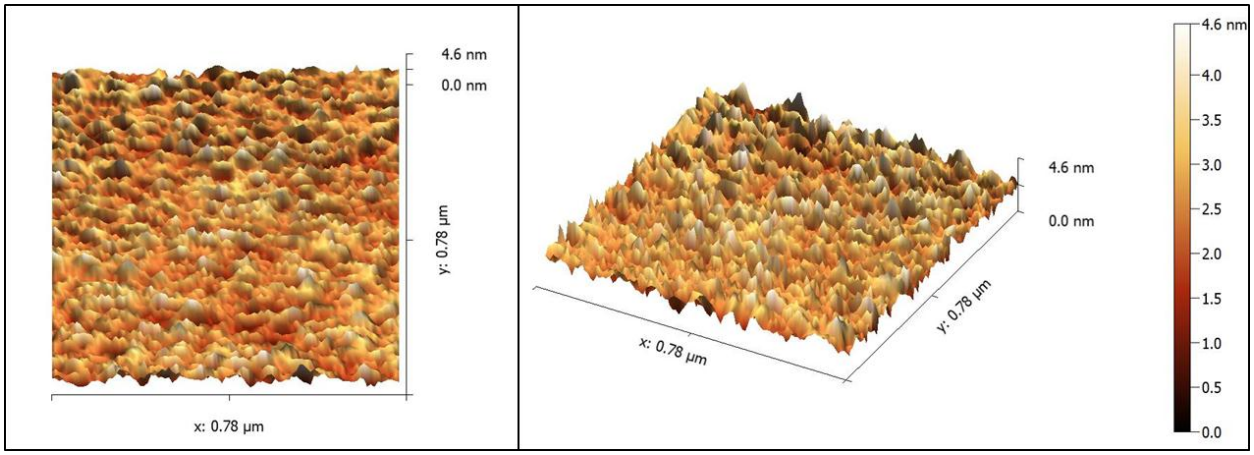

Figure 4-58: AFM for CuPc thin film with time irradiated 10 min by green laser 532 nm

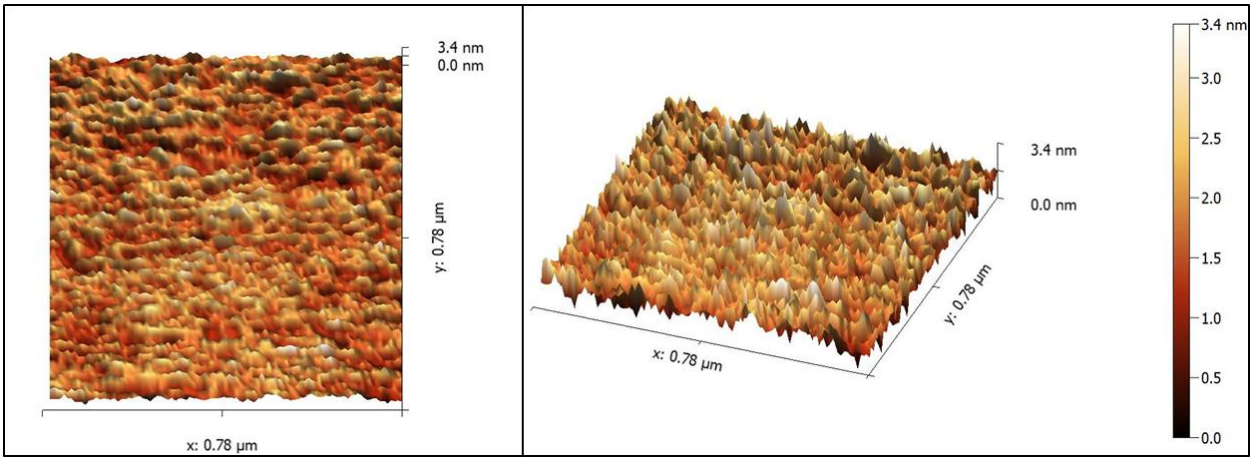

Figure 4-59: AFM for CuPc thin film with time irradiated 20 min by green laser 532 nm

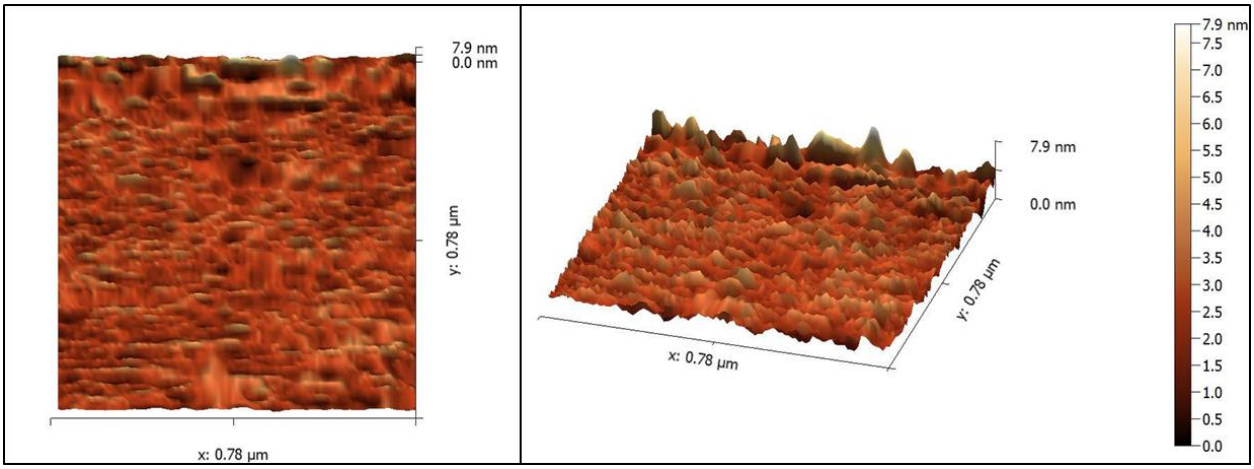

Figure 4-60: AFM for CuPc thin film with time irradiated 30 min by green laser 532 nm

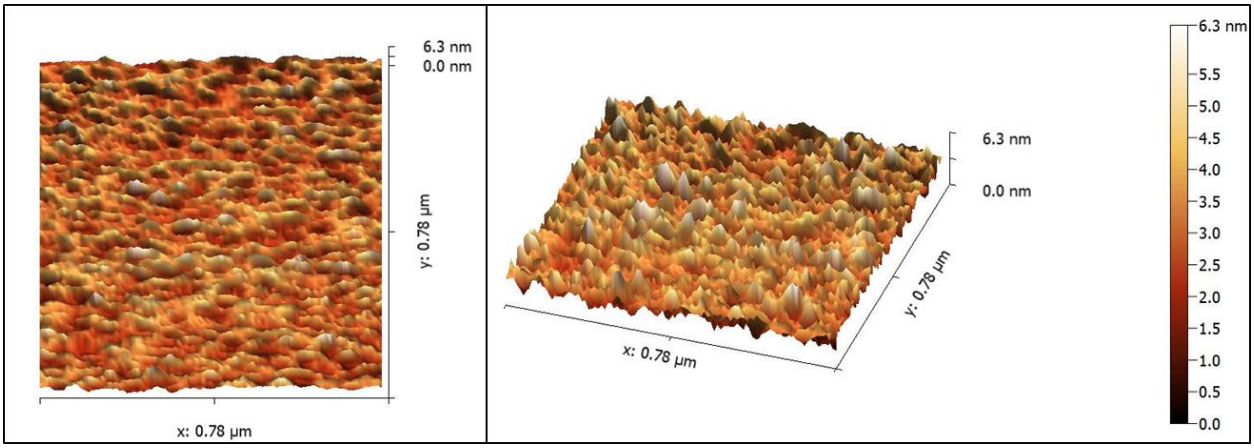

Figure 4-61: AFM for CuPc thin film with time irradiated 10 min by violet laser 405 nm

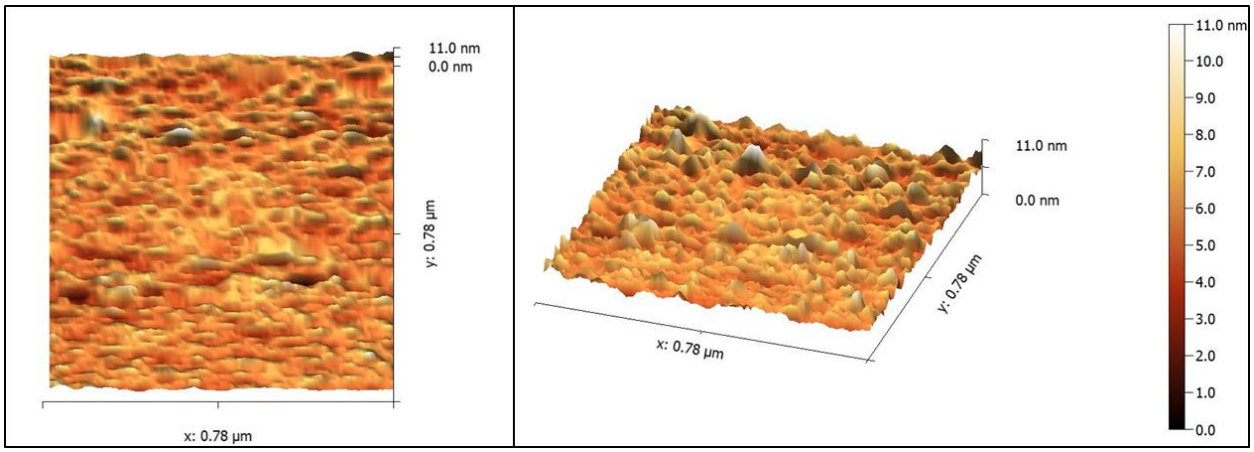

Figure 4-62: AFM for CuPc thin film with time irradiated 20 min by violet laser 405 nm

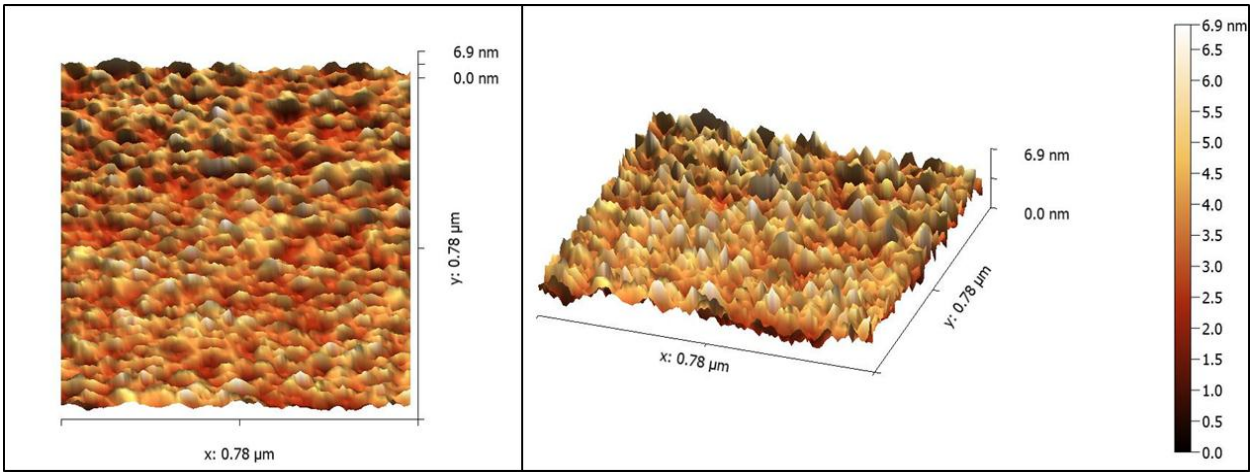

Figure 4-63: AFM for CuPc thin film with time irradiated 30 min by violet laser 405 nm

The histogram in the Figs. (4-64 to 4-66) shows the numerical distribution of particles on the sample, the number of particles for the specimen in the y-axis and the average diameter for the particles in the x-axis. It can be seen that the diameter of particles decreases with increasing time for all laser wavelengths, through this, we can observe that the surface roughness is high and decreases with increasing irradiation time.

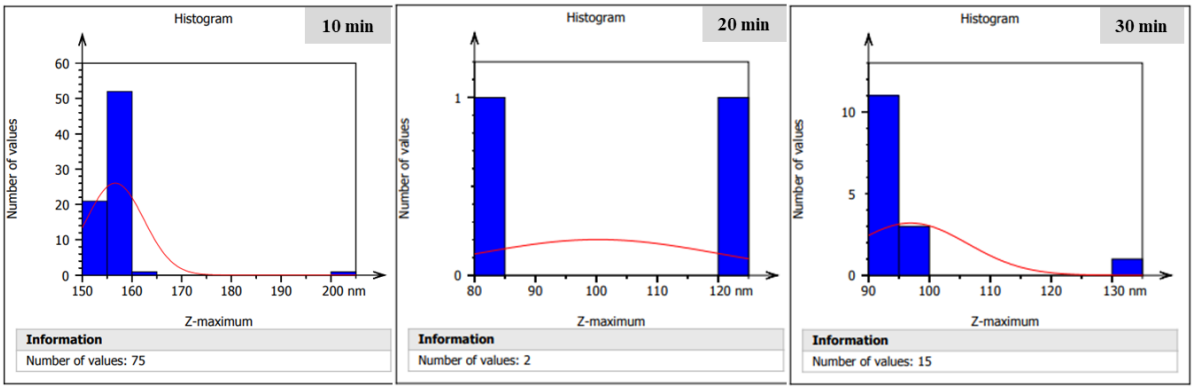

Figure 4-64: Number of particles vs. mean diameter for thin film irradiation by red laser 650 nm at time 10, 20, and 30 min

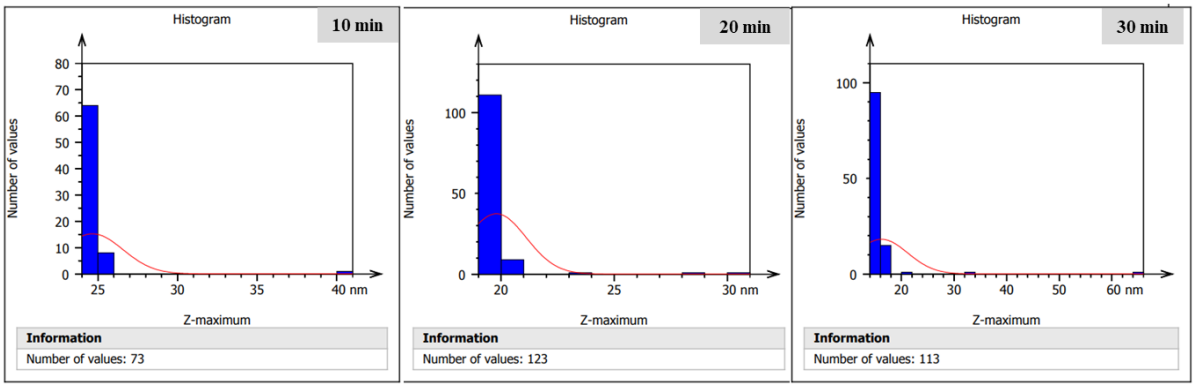

Figure 4-65: Number of particles vs. mean diameter for thin film irradiation by green laser 532 nm at time 10, 20, and 30 min

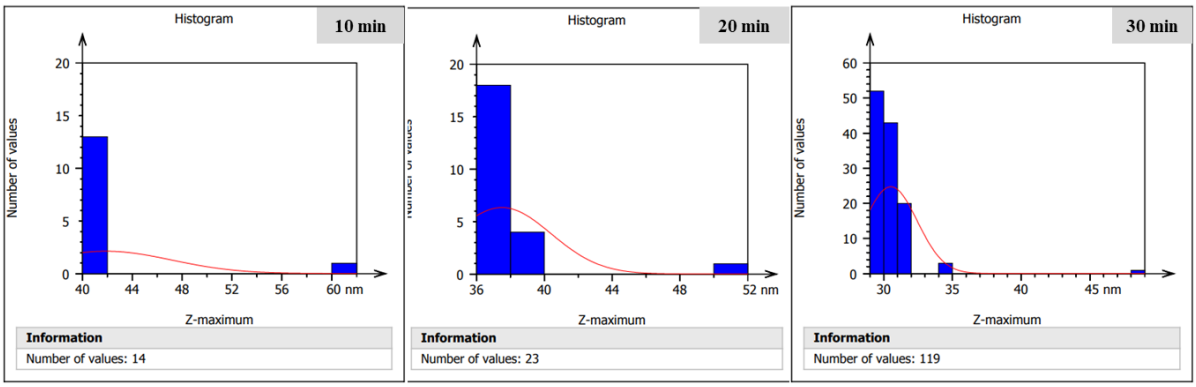

Figure 4-66: Number of particles vs. mean diameter for thin film irradiation by violet laser 405 nm at time 10, 20, and 30 min

Table 4-9. AFM measurements for CuPc thin film irradiated by red, green and violet laser wavelengths 650, 532, and 405 nm

	Time (min)	Average Diameter (nm)	Roughness (nm)	Average value (nm)	Root mean square (nm)
Red Laser	0	227.6	5.48	42.9	7.52
	10	156.6	1.99	13.54	2.56
	20	100.3	0.77	4.92	1.00
	30	96.91	0.82	4.44	1.05
Green Laser	0	227.6	5.48	42.9	7.52
	10	24.66	0.408	2.748	0.522
	20	19.79	0.456	2.939	0.578
	30	16.2	0.57	5.07	0.76
Violet Laser	0	227.6	5.48	42.9	7.52
	10	41.88	0.73	6.16	0.96
	20	37.5	0.775	4.529	0.979
	30	30.52	0.684	4.177	0.871

Figures (4-67 to 4-69) present the XRD to CuPc films of thickness 219.12 nm deposited on the glass substrata at room temperature. XRD gauge are taken for the thin films before and after laser irradiating with different wavelengths $650, 532, and\ 405\ nm$ and different laser irradiation times $0,10,20, and\ 30\ min$. X-ray results show that the peaks decrease with increasing irradiation times for red, violet and green laser. Also, longer laser exposure time of the samples leads to an increase in the breaking of the molecules bonds. Therefore, we can see from the result increasing in the FWHM with increasing the laser irradiation time this causes decreasing the crystal size, this means that the material is heading towards the Nano. Furthermore, a clear decrease in the peaks height is noticed in some areas which supports the optical results that are measured. The XRD results for each laser are listed in Tables (4-10 to 4-13).

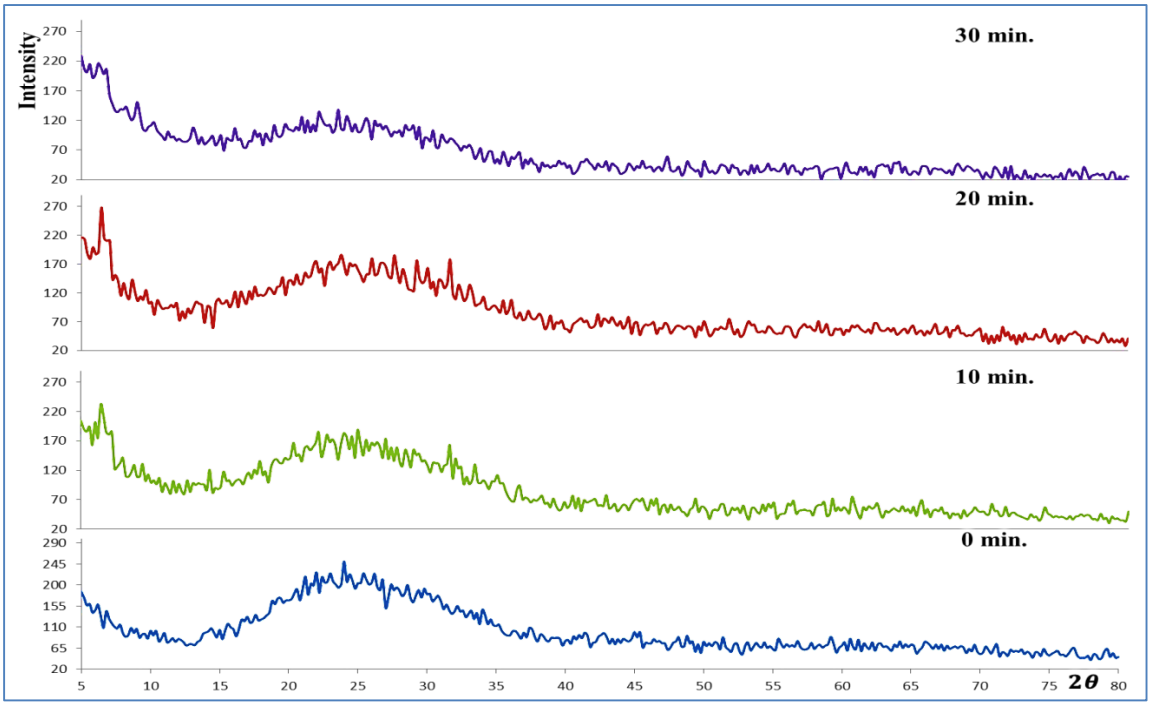

Figure 4-67: X-ray diffraction for CuPc thin film with time irradiated (0, 10, 20, and 30) min. by red laser (650 nm)

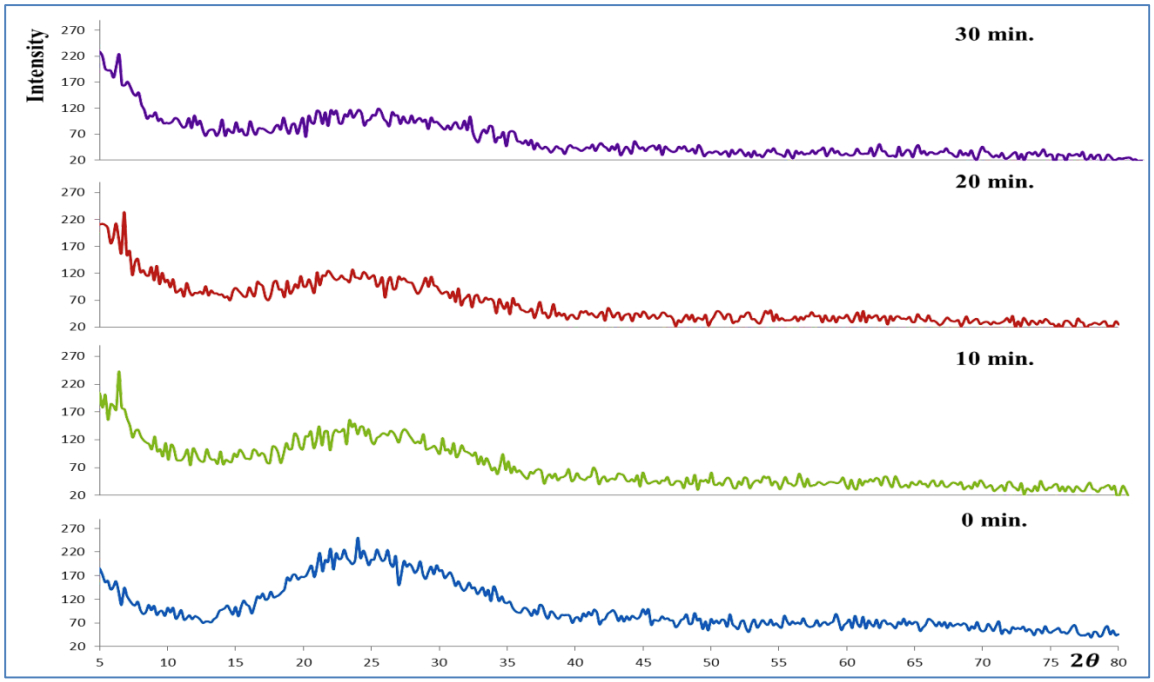

Figure 4-68: X-ray diffraction for CuPc thin film with time irradiated (0, 10, 20, and 30) min. by green laser (532 nm)

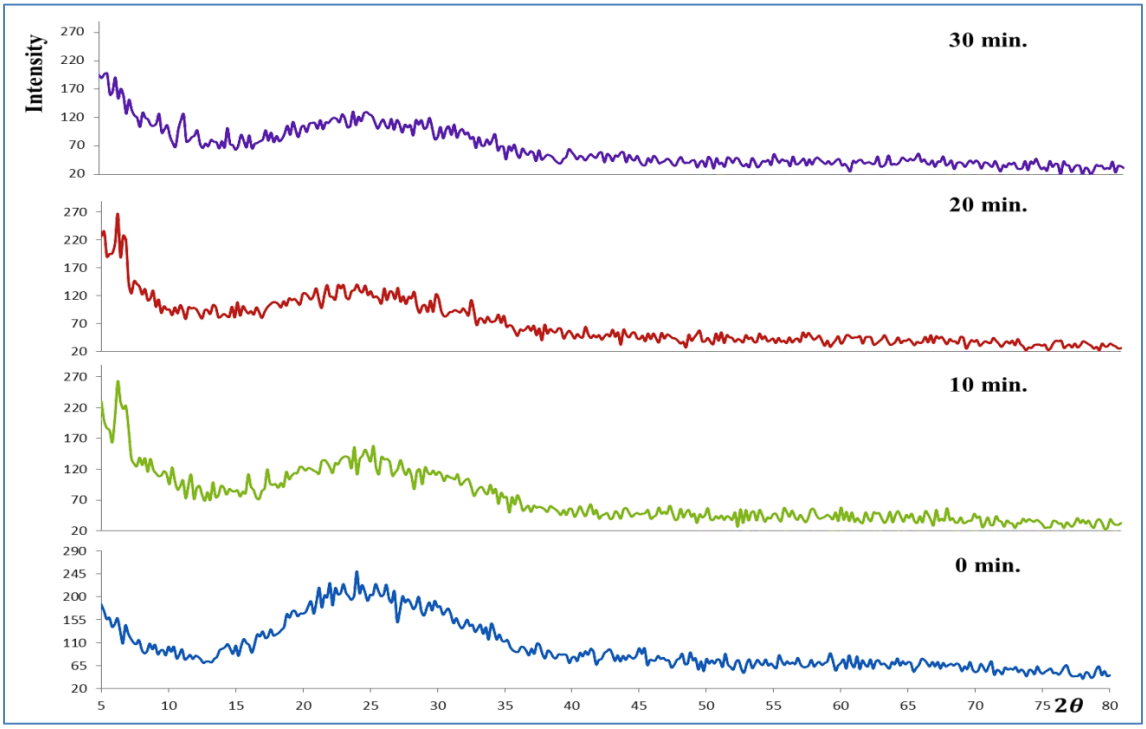

Figure 4-69: X-ray diffraction for CuPc thin film with time irradiated (0, 10, 20, and 30) min. by violet laser (405 nm)

Table 4-10. XRD measurements of CuPc thin film for non-irradiated sample

2θ	d(nm)	Height	I%	FWHM	Crystal Size (nm)
10.275	0.8602	44	74.6	0.375	22
15.445	0.57323	50	84.7	0.479	17
28.255	0.31559	59	100	0.487	17

Table 4-11. XRD measurements of CuPc thin film for the sample irradiated by red laser (650 nm).

Time (min)	2θ	d(nm)	Height	I%	FWHM	Crystal Size (nm)
10	6.464	1.36619	74	100	0.735	10
	31.428	0.28441	53	71.6	0.494	17
20	6.502	1.35825	100	100	0.541	15
	31.324	0.28533	63	63	0.461	18
30	23.411	0.37966	41	100	0.489	16
	46.951	0.19336	27	65.9	0.51	17

Table 4-12. XRD measurements of CuPc thin film for the sample irradiated by green laser (532 nm).

Time (min)	2θ	d(nm)	Height	I%	FWHM	Crystal Size (nm)
10	6.374	1.3856	54	100	0.435	17
	13.758	0.6431	34	63	0.34	24
20	6.454	1.36841	89	100	0.437	18
	21.097	0.42076	44	49	0.904	9
30	6.914	1.27734	95	100	0.302	22
	38.476	0.23378	25	28.4	0.326	27

Table 4-13. XRD measurements of CuPc thin film for the sample irradiated by violet laser (405 nm).

Time (min)	2θ	d(nm)	Height	I%	FWHM	Crystal Size (nm)
10	6.324	1.39637	95	100	0.673	12
	24.9	0.35729	46	48.4	0.65	12
20	6.286	1.40485	93	100	0.477	17
	32.244	0.27739	44	47.3	0.332	26
30	11.09	0.79716	49	100	0.538	15

4.5.3 Fluorescence Spectra for CuPc Thin Films

The fluorescence spectra for CuPc thin films with thickness $\sim 219.12\ nm$ and irradiation time $30\ min$ and laser wavelengths $650, 532, and\ 405\ nm$ shown in Fig. (4-70). Also the comparing between the emission and excitation energy gap are illustrated in Table (4-18). Through the results, it is found that there is a good agreement between the energy gap values calculated using the Tauc equation and the energy gap values calculated using the fluorescence method.

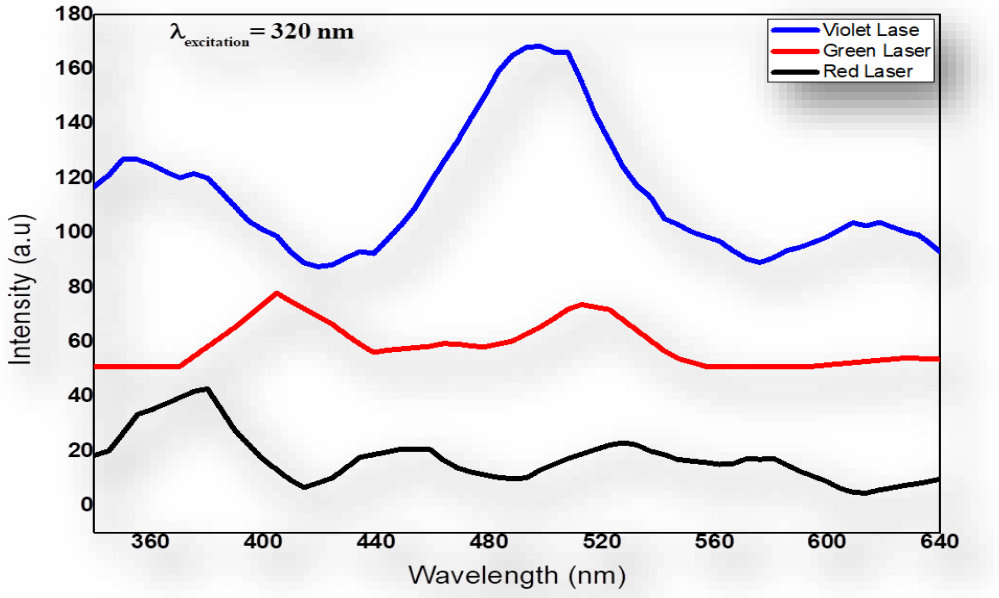

Figure 4-70: Fluorescence spectra for thin film irradiated by red, green and violet laser wavelengths 650, 532, and 405 nm for 30 min irradiation time

Table 4-14. Emission energy gap vs. excitation energy gap at thickness 220 nm and laser irradiation times 30 min. with wavelengths 650, 532 and 405 nm

Wavelength (nm)	Tauc (eV)	PL (eV)
650	2.6	3
532	2.5	3.5
405	2.4	3.2

CHAPTER FIVE

CONCLUSIONS & FUTURE WORKS

5 Introduction

This chapter presents the main conclusions that are acquired in our research and also some suggestions and recommendations for the future work.

5.2 Conclusions

The main results that were obtained during this research are concluded in the following:

1. The optical properties of the CuPc solution were studied before and after laser irradiation of different wavelengths $650, 532, and\ 405\ nm$ with different irradiation times $0, 4, , 8\ , and\ 16\ min$. The Results show the possibility to control the energy gap by laser. Also, increasing the energy gap with increasing the laser irradiation time for all laser wavelengths suggests the suitability for UV sensors applications.

2. The effect of the CuPc solution concentration $(0.05, 0.1,\ and\ 0.2\ g/l)$ on the optical properties was investigated before and after exposure to a laser beam of different wavelengths $650, 532, and\ 405\ nm$ for different laser irradiation times $0, 4, 8, and\ 16\ min$..In this experiment, the energy gap results suggest the ability to control the energy gap by varying the concentration. Decreasing the energy gap suggests the suitability for photovoltaic sensors applications.
3. The optical properties of the CuPc thin films were studied before and after laser irradiation by different laser wavelengths $650, 532, and\ 405\ nm$ for different irradiation times $0, 10, 20, and\ 30\ min$. Energy gap results show that it increases with increasing the laser irradiation times which indicate the ability for UV sensors applications.

4. The structural properties of the CuPc thin films were examined and the XRD data showed decreasing in the peaks height in the bands with increasing irradiation times. Also, the XRD data indicate the material tendency towards the nanomaterials behavior.
5. The AFM results of the thin films surface morphology before and after exposing to the laser beams showed a fluctuation in the values which it is might be to the heterogeneity of the thin films surface. The AFM results support the XRD results.

5.3 Future Works

There are many suggestions to the future projects, such as:

1. Study the impact of the laser irradiation times on the optical and structural properties for longer time periods (one hour and more).
2. Study the electrical properties of the laser irradiated thin films after electrical electrodes depositing.
3. Investigating the thin films that prepared in different methods such as Pulsed laser deposition and vacuum evaporating.
4. Study the nanomaterials properties after laser irradiation of CuPc thin films.
5. Study the dispersive properties of the CuPc thin films before and after laser irradiation.

Bibliography

[1] P. Singh and N. M. Ravindra, "Optical properties of metal phthalocyanines," *J. Mater. Sci.*, vol. 45, no. 15, pp. 4013–4020, doi: 10.1007/s10853-010-4476-6, 2010.

[2] B. Joseph and C. S. Menon, "Studies on the optical properties and surface morphology of Nickel phthalocyanine thin films," *Asian J. Chem.*, vol. 4, no. 1, pp. 255–264, 2007.

[3] M. Shah, M. H. Sayyad, and K. S. Karimov, "Fabrication and Study of Nickel Phthalocyanine based Surface Type Capacitive Sensors," *Sensors And Actuators*, pp. 392–394, 2008.

[4] M. M. El-Nahass, Z. El-Gohary, and H. S. Soliman, "Structural and optical studies of thermally evaporated CoPc thin films," *Opt. Laser Technol.*, vol. 35, no. 7, pp. 523–531, doi: 10.1016/S0030-3992(03)00068-9, 2003.

[5] O. Berger, W. J. Fischer, B. Adolphi, S. Tierbach, V. Melev, and J. Schreiber, "Studies on phase transformations of Cu-phthalocyanine thin films," *J. Mater. Sci. Mater. Electron.*, vol. 11, no. 4, pp. 331–346, doi: 10.1023/A:1008933516940, 2000.

[6] Y. L. Lee, C. Y. Sheu, and R. H. Hsiao, "Gas sensing characteristics of copper phthalocyanine films: Effects of film thickness and sensing temperature," *Sensors Actuators, B Chem.*, vol. 99, no. 2–3, pp. 281–287, doi: 10.1016/j.snb.2003.11.024, 2004.

[7] Y. L. Lee, W. C. Tsai, and J. R. Maa, "Effects of substrate temperature on the film characteristics and gas-sensing properties of copper phthalocyanine films," *Appl. Surf. Sci.*, vol. 173, no. 3–4, pp. 352–361, doi: 10.1016/S0169-4332(01)00019-8, 2001.

[8] R. Prabakaran, R. Kesavamoorthy, G. L. N. Reddy, and F. P. Xavier, "Structural investigation of copper phthalocyanine thin films using X-ray diffraction, Raman scattering and optical absorption measurements," *Phys. Status Solidi Basic Res.*, vol. 229, no. 3, pp. 1175–1186, doi: 10.1002/1521-3951(200202)229:3<1175::AID-PSSB1175>3.0.CO;2-K, 2002.

[9] L. Lozzi, S. Santucci, S. La Rosa, B. Delley, and S. Picozzi, "Electronic structure of crystalline copper phthalocyanine," *J. Chem. Phys.*, vol. 121, no. 4, pp. 1883–1889, doi: 10.1063/1.1766295, 2004.

[10] J. Sólyom, *Fundamentals of the Physics of Solids*, Volume 1. New York: Springer-Verlag Berlin Heidelberg 2007, 2007.

[11] A. Rockett, *The Materials Science of Semiconductors*, 1st ed. 233 Spring Street, New York, NY 10013, USA: Springer, 2008.

[12] M. C. Peter Y.Yu and Max-Planck-Institut, *Fundamentals of Semiconductors(Third edition)*. 2005.

[13] H. Naito, *Organic Semiconductors for Optoelectronics*, vol. 7, no. 1. Osaka, Japan: Wiley and Sons Ltd All, 2021.

[14] P. P. Manousiadis, K. Yoshida, G. A. Turnbull, and I. D. W. Samuel, "Organic semiconductors for visible light communications," *Philosophical Transactions of the Royal Society A: Mathematical, Physical and Engineering Sciences*, vol. 378, no. 2169. Royal Society Publishing, doi: 10.1098/rsta.2019.0186, Apr. 17, 2020.

[15] W. Brütting, *physics of organic semiconductors*. Germany: WILEY-VCH Verlag GmbH & Co. KGaA, Weinheim, 2005.

[16] Z. T. Liu, H. S. Kwok, and A. B. Djurišić, "The optical functions of metal phthalocyanines," *J. Phys. D. Appl. Phys.*, vol. 37, no. 5, pp. 678–688, doi: 10.1088/0022-3727/37/5/006, 2004.

[17] G. De La Torre, C. G. Claessens, and T. Torres, "Phthalocyanines: Old dyes, new materials. Putting color in nanotechnology," *Chem. Commun.*, no. 20, pp. 2000–2015, doi: 10.1039/b614234f, 2007.

[18] S. ARSLAN, "Phthalocyanines: Structure, Synthesis, Purification and Applications," *J. Life Sci.*, vol. 6, no. 2, pp. 188–197, 2016.

[19] M. T. Hussein, E. M. Nasir, and A. H. Al-Aarajiy, "Structural and Surface Morphology Analysis of Nickel Phthalocyanine Thin Films," *Adv. Mater. Phys. Chem.*, vol. 03, no. 01, pp. 113–119, doi: 10.4236/ampc.2013.31a014, 2013.

[20] A. Farooq, K. H. S. Karimov, F. Wahab, T. Ali, and S. Zameer Abbas, "Copper phthalocyanine and metal free phthalocyanine bulk heterojunction for temperature sensing," *J. Optoelectron. Adv. Mater.*, vol. 17, no. 5–6, pp. 822–826, 2015.

[21] K. Sakamoto and E. Ohno-Okumura, "Syntheses and functional properties of phthalocyanines," *Materials (Basel).*, vol. 2, no. 3, pp. 1127–1179, doi: 10.3390/ma2031127, 2009.

[22] C. J. Liu, J. J. Shih, and Y. H. Ju, "Surface morphology and gas sensing characteristics of nickel phthalocyanine thin films," *Sensors Actuators, B*

Chem., vol. 99, no. 2–3, pp. 344–349, doi: 10.1016/j.snb.2003.11.034, 2004.

[23] W. Herbst, K. Hunger, G. Wilker, H. Ohleier, and R. Winter, *Industrial Organic Pigments*, 3ed ed. Germany: Wiley-VCH, 2004.

[24] X. Ai, J. Lin, Y. Chang, L. Zhou, X. Zhang, and G. Qin, "Phase modification of copper phthalocyanine semiconductor by converting powder to thin film," *Appl. Surf. Sci.*, vol. 428, doi: 10.1016/j.apsusc.2017.09.146, 2018.

[25] B. Adolphi, O. Berger, and W. J. Fischer, "Angle-resolved XPS measurements on copper phthalocyanine thin films," *Appl. Surf. Sci.*, vol. 179, no. 1–4, pp. 102–108, doi: 10.1016/S0169-4332(01)00270-7, 2001.

[26] D. C. Dufour, G, C. Poncey, F. Rochet, H. Roulet, S. lacobucci, M. Sacchi, F. Yubero, N. Motta, M.N. Piancastelli, A. Sgarlata, "Metal phthalocyanines (MPc, M=Ni, Cu) on Cu(001) and Si(001) surfaces studied by XPS, XAS and STM," *J. Electron Spectros. Relat. Phenomena*, vol. 76, no. C, pp. 219–224, doi: 10.1016/0368-2048(95)02479-4, Dec. 1995.

[27] L. Reisz, Berthold, Belova, Valentina, Duva, Giuliano, Zeiser, Clemens, Hodas, Martin, Hagara, Jakub, Siffalovi, Peter, Pithan, A. Hosokai, Takuya, Hinderhofer, Alexander, Gerlach, and F. Schreiber, "Polymorphism and structure formation in copper phthalocyanine thin films," *J. Appl. Crystallogr.*, vol. 54, no. 1948, pp. 203–210, doi: 10.1107/S1600576720015472, 2021.

[28] A. A. M. Farag, "Optical absorption studies of copper phthalocyanine thin films," *Opt. Laser Technol.*, vol. 39, no. 4, pp. 728–732, doi: 10.1016/j.optlastec.2006.03.011, 2007.

[29] S. Karan and B. Mallik, "Effects of annealing on the morphology and optical property of copper (II) phthalocyanine nanostructured thin films," *Solid State Commun.*, vol. 143, no. 6–7, doi: 10.1016/j.ssc.2007.05.043, 2007.

[30] H. Hassan, N. B. Ibrahim, Z. Ibarahim, and K. Sopian, "The preparation of copper phthalocyanine thin film on silicon substrate for solar cell application," *IEEE Int. Conf. Semicond. Electron. Proceedings, ICSE*, pp. 326–330, doi: 10.1109/SMELEC.2008.4770334, 2008.

[31] M. Della Pirriera, J. Puigdollers, C. Voz, M. Stella, J. Bertomeu, and R. Alcubilla, "Optoelectronic properties of CuPc thin films deposited at different substrate temperatures," *J. Phys. D. Appl. Phys.*, vol. 42, no. 14, doi: 10.1088/0022-3727/42/14/145102, 2009.

[32] S. S. Mali, D. S. Dalavi, P. N. Bhosale, C. A. Betty, A. K. Chauhan, and P. S. Patil, "Electro-optical properties of copper phthalocyanines (CuPc) vacuum deposited thin films," *RSC Adv.*, vol. 2, no. 5, doi: 10.1039/c2ra00670g, 2012.

[33] C. Defeyt, P. Vandenabeele, B. Gilbert, J. Van Pevenage, R. Cloots, and D. Strivay, "Contribution to the identification of α-, β- And μ-copper phthalocyanine blue pigments in modern artists' paints by X-ray powder diffraction, attenuated total reflectance micro-fourier transform infrared spectroscopy and micro-Raman spectroscopy," *J. Raman Spectrosc.*, vol. 43, no. 11, pp. 1772–1780, doi: 10.1002/jrs.4125, 2012.

[34] H. A. Afify, A. S. Gadallah, M. M. El-Nahass, and M. Atta Khedr, "Effect of thermal annealing on the structural and optical properties of spin coated copper phthalocyanine thin films," *J. Mol. Struct.*, vol. 1098, doi: 10.1016/j.molstruc.2015.06.016, 2015.

[35] A. H. A. Jalaukhan, "Effect of Substrate Temperature on Optical Properties of Thermally Evaporated CuPc Thin Films," *J. Kerbala Univ.*, vol. 13, pp. 100–105, 2015.

[36] M. T. Hussein, K. A. Aadim, and E. K. Hassan, "Structural and Surface Morphology Analysis of Copper Phthalocyanine Thin Film Prepared by Pulsed Laser Deposition and Thermal Evaporation Techniques," *Adv. Mater. Phys. Chem.*, vol. 06, no. 04, pp. 85–97, doi: 10.4236/ampc.2016.64009, 2016.

[37] J. Xu, X. Liu, W. Hou, H. Guo, L. Yu, and H. Zhang, "Effect of solvent-vapour annealing on morphology, structure of copper(II) phthalocyanine thin films and device performance," *Bull. Mater. Sci.*, vol. 41, no. 4, doi: 10.1007/s12034-018-1618-y, 2018.

[38] M. T. Hussein and R. R. Mohammed, "Study the Nonlinearity Characteristics of Organic-Semiconductor (CuPc) Prepared Via Pulsed Laser Deposition Technique with Different Thickness," *Nano Hybrids Compos.*, vol. 27, doi: 10.4028/www.scientific.net/nhc.27.11, 2019.

[39] M. S. Hubert Gojzewski, Fatemeh Ghani, "Thin films of copper phthalocyanine deposited by solution processing methods," vol. 38, no. 1, pp. 79–90, doi: 10.2478/msp-2020-0007, 2020.

[40] A. F. Abdulameer, L. K. Abbas, N. S. Sadeq, and Z. G. Mohammadsalih,

"Structural, surface morphology and optical properties of annealing treated Copper Phthalocyanine doped Fullerene (CuPc: C60) thin films," in *Journal of Physics: Conference Series*, vol. 1795, no. 1, doi: 10.1088/1742-6596/1795/1/012068, 2021.

[41] R. R. Mohammed and M. T. Hussein, "Linear and Non-Linear Optical Properties for Organic Semiconductor (CuPc) Thin Films," *Iraqi J. Phys.*, vol. 19, no. 48, pp. 10–20, doi: 10.30723/ijp.v19i48.639, 2021.

[42] L. Vijayan, K. Shreekrishna Kumar, and K. B. Jinesh, "Influence of intensity on copper phthalocyanine based organic phototransistors," *Mater. Today Proc.*, vol. 47, no. xxxx, pp. 1099–1103, doi: 10.1016/j.matpr.2021.07.125, 2021.

[43] William M. Steen, *Laser Material Processing*, 4th ed. Michigan: Springer-Verlag London, 2008.

[44] N. A. Arreyndip, "Review of Laser Matter Interaction and Applications," 2014,[Online].Available:https://www.academia.edu/6490867/REVIEW_OF_LASER_MATTER_INTERACTION_AND_APPLICATIONS.

[45] F. G. Smith, *Optics and Photonics : An Introduction Second Edition*, vol. 69. 2007.

[46] J. Tang, "Unlocking Potentials of Microwaves for Food Safety and Quality," *J. Food Sci.*, vol. 80, no. 8, pp. E1776–E1793, doi: 10.1111/1750-3841.12959, 2015.

[47] K. a Nowakowski, "Laser beam interaction with materials for microscale applications," *Dissertation*, 2005.

[48] M. Cardona and P. Y. Yu, "Optical Properties of Semiconductors," in *Comprehensive Semiconductor Science and Technology*, vol. 1–6, 2011.

[49] J. R. Ferraro and L. J. Basile, *Fourier Transform Infrared Spectroscopy: Applications To Chemical Systems*. 1985.

[50] P. R. Griffiths, "Fourier transform infrared spectrometry," *Science (80-.).*, vol. 222, no. 4621, pp. 297–302, doi: 10.1126/science.6623077, 1983.

[51] B. C. Smith, *Fundamentals of Fourier Transform Infrared Spectroscopy*, Second Edi., vol. 10, no. 15. Taylor & Francis Group, 2011.

[52] M. M. El-Nahass, K. F. Abd-El-Rahman, and A. A. A. Darwish, "Fourier-transform infrared and UV-vis spectroscopes of nickel phthalocyanine thin films," *Mater. Chem. Phys.*, vol. 92, no. 1, pp. 185–189, doi:

10.1016/j.matchemphys.2005.01.008, 2005.

[53] E. V. S. Bass, Michael, Guifang Li, *HANDBOOK OF OPTICS*, 3rd ed. 2009.

[54] S. Faculty and S. Arabia, "Determination and Analysis the Influence of X-ray Irradiation on Optical Constant of Magnesium Phthalocyanin," *Aust. J. Basic Appl. Sci.*, vol. 5, no. 10, pp. 38–44, 2011.

[55] C. Kittel, *Introduction to Solid State Physics*, Eighth Edi., vol. 8, no. 9. California: John Wiley & Sons, Inc., 2005.

[56] R. E. Hummel, "Electronic properties of materials," *Journal of Chemical Information and Modeling*, vol. 53. p. 489, 2012.

[57] M. W. Kazem and R. K. Jamal, "Characterization of copper phthalocyanine-tetrasulfonic acid tetrasodium salt/graphene oxide," *Iraqi J. Sci.*, vol. 62, no. 6, doi: 10.24996/ijs.2021.62.6.15, 2021.

[58] J.Tauc, *Amorphous and Liquid Semiconductors*, 1st editio. New York: Plenum Publishing Corporation Ltd, 1974.

[59] H. A. Afify, A. S. Gadallah, M. M. El-Nahass, and M. Atta Khedr, "Effect of thermal annealing on the structural and optical properties of spin coated copper phthalocyanine thin films," *J. Mol. Struct.*, vol. 1098, pp. 161–166, doi: 10.1016/j.molstruc.2015.06.016, 2015.

[60] G. Martinez, "Optical Properties of Semiconductors," in *Springer Science+Business Media Dordrecht*, 1st ed., vol. 228, Erice, Sicily, Italy: KluwerAcademic, p. 324 / 327, 1993.

[61] J. R. Lakowicz, *Principles of Fluorescence Spectroscopy*, Third edit., vol. 33, no. 1. 2006.

[62] L. B. S. S. Freund, *Thin Film Materials Stress*, vol. 19, no. 7. 2006.

[63] F. S. Ruggeri, T. Šneideris, M. Vendruscolo, and T. P. J. Knowles, "Atomic force microscopy for single molecule characterisation of protein aggregation," *Archives of Biochemistry and Biophysics*, vol. 664. Academic Press Inc., pp. 134–148, doi: 10.1016/j.abb.2019.02.001, Mar. 30, 2019.

[64] G. B. and C. F. Quate, "Atomic Force Microscope," *Handb. Phys. Med. Biol.*, no. 9, pp. 5-1-5–9, doi: 10.1201/9781420075250, 1986.

[65] H. K. Nguyen, D. Prevosto, M. Labardi, S. Capaccioli, M. Lucchesi, and P. Rolla, "Effect of confinement on structural relaxation in ultrathin polymer films investigated by local dielectric spectroscopy," *Macromolecules*, vol. 44, no. 16, pp. 6588–6593, doi: 10.1021/ma200440z, 2011.

[66] F. Variola, “Atomic force microscopy in biomaterials surface science,” *Phys. Chem. Chem. Phys.*, vol. 17, no. 5, pp. 2950–2959, doi: 10.1039/C4CP04427D, Feb. 2015.

[67] M. Vanderroost, F. Ronsse, K. Dewettinck, and G. Pieters, “Coating processes in fluidised beds: quality control model based on population balance theory.,” *Commun. Agric. Appl. Biol. Sci.*, vol. 73, no. 1, pp. 231–5, 2008, [Online]. Available: http://www.ncbi.nlm.nih.gov/pubmed/18831281.

[68] C. Negara, “Fast Polarization State Detection by Division-of-Amplitude in a Simple Configuration Setup Fast Polarization State Detection by Division-of-Amplitude in a Simple Configuration Setup Introduction,” pp. 75–89, 2019.

[69] S. Roy, A. Turner, and P. K. Bhattacharya, “Developing a Gaertner Ellipsometer for Thin Film Thickness Measurement,”, doi: 10.18260/1-2-620-38784, 2022.

[70] M. Yahia, I. S.Ganesh, V.Shkir, H. Y. Alfaify, S.Zahran, and A. M. Algarni, H.Abutalib, M. M.Al-Ghamdi, Attieh A.El-Naggar, A. M.Albassam, “An investigation on linear and non-linear optical constants of nano-spherical CuPc thin films for optoelectronic applications,” *Phys. B Condens. Matter*, vol. 496, doi: 10.1016/j.physb.2016.05.020, 2016.

[71] A. A. Ejam and N. A. A. Wahhab, “Laser Irradiation Time Effect on the Optical Properties of Copper Phthalocyanine Solution,” *NeuroQuantology*, vol. 20, no. 3, pp. 224–230, doi: 10.14704/nq.2022.20.3.nq22064, 2022.

[72] A. Louardi, T. Chtouki, A. Rmili, B. Elidrissi, and H. Erguig, “Effect of annealing temperature on the optical properties of Co3O4 thin films prepared by spray pyrolysis,” *Int. J. Appl. Eng. Res.*, vol. 11, no. 2, pp. 1432–1435, 2016.

[73] T. Sasaki, K. Tabata, K. Tsukagoshi, A. Beckel, A. Lorke, and Y. Yamamoto, “Control of molecular orientation and morphology in organic bilayer solar cells: Copper phthalocyanine on gold nanodots,” *Thin Solid Films*, vol. 562, doi: 10.1016/j.tsf.2014.03.090, 2014.

[74] A. A. Shaty and H. A. Banimuslem, “Optical Characterizations and Gas Detection Study of Metalo Phthalocyanine Thin Film Specie,” *J. Nanostructures*, vol. 12, no. 3, pp. 491–502, doi: 10.22052/JNS.2022.03.002, 2022.

الخلاصة

هذه الدراسة تصف تأثير التشعيع بالليزر على صبغة عضوية. حيث تأخذ القياسات لصبغة ثالوسيانين النحاس في حالة المحلول مرة وأغشية رقيقة مرة أخرى التي يتم تحضيرها بتقنية الترسيب بالطلاء الدوراني. تشعع هذه العينات بواسطة ليزرات بتغيير بعض المعلمات. يتم اخذ القياسات البصرية للمحاليل والاغشية. كما يتم دراسة الخواص التركيبية المتضمنة فحص XRD, FTIR المعاملات التركيبية التي يتم دراستها مثل الحجم الحبيبي، الخشونة، معدل الجذر التربيعي ويتم مقارنة هذه القياسات مع قياسات العينات غير المشعة.

يتم تحضيرمحلول ثالوسيانين النحاس بتراكيز مختلفة ٠,٠٥، ٠,١، ٠,١٥، ٠,٢ غرام لكل لتر. بعد ذلك يتم تحضيرالاغشية باستخدام تقنية الترسيب بالطلاء الدوراني وبأسماك مختلفة بحدود ١٢٠، ١٨٠ ، ٢٢٠ نانوميتر. كل من عينات المحاليل والاغشية يتم تشعيعها بليزرات ذات اطوال موجية مختلفة ٦٥٠، ٥٣٢، ٤٠٥ نانوميتر ولأزمان تشعيع مختلفة وهي ٠، ٤، ٨، ١٦ دقيقة لعينات المحلول و الزمن ٠، ١٠، ٢٠، ٣٠ دقيقة لعينات الاغشية الرقيقة.

الخواص البصرية لمحلول النحاس ثالوسيانين بتركيز ٠,١٥غم/لتر تظهر نقصان في طيف الامتصاصية والانعكاسية مع زيادة زمن التشعيع بينما يلاحظ زيادة في النفاذية. فجوة الطاقة تزداد مع زيادة زمن التشعيع. ان الثوابت البصرية الاخرى مثلا (الامتصاصية، الامتصاصية المولارية، معامل الامتصاص، معامل الانكسار، معامل الخمود، ثوابت العزل الحقيقية والخيالية، التوصيلية البصرية) تقل بزيادة زمن التشعيع بالليزر.

أن تغير تركيز المحلول له تأثيرعلى الخواص البصرية لمحلول ثالوسيانين النحاس قبل وبعد تعرض العينات للتشعيع بالليزر بأطوال موجية مختلفة ٦٥٠، ٥٣٢، ٤٠٥ نانوميتر ولأزمان تشعيع مختلفة ايضا ٠، ٤، ٨، ١٦ دقيقة. تبين النتائج بأن فجوة الطاقة تنخفض مع زيادة تركيز المحلول. يتم قياس فجوة الطاقة بأستخدام معادلة Tauc ويتم مقارنتها مع فجوة الطاقة التي تم قياسها من الفلورة عند التركيز ٠,٢ غم/لتر. لوحظ أن المعاملات البصرية تزداد بزيادة زمن التشعيع لكل التراكيز.

أن أغشية ثالوسيانين النحاس المرسبة على ارضيات زجاجية بسمك ٢١٩,١٢ نانو ميتر وبدرجة حرارة الغرفة يتم تشعيعها بليزرات ذات اطوال موجية مختلفة ٦٥٠، ٥٣٢، ٤٠٥ نانوميتر وبأزمان مختلفة ٠، ١٠، ٢٠، ٣٠ دقيقة. النتائج تبين نقصان في الامتصاصية والانعكاسية مع زيادة زمن التشعيع.

دراسة الخواص التركيبية عن طريق فحص بالحيود بالاشعة السينية XRD يبين نقصان في ارتفاع القمم مع زيادة زمن التشعيع. ايضا تشير النتائج الى ان المادة تتجه نحو العشوائية نتيجة تكسر الروابط الجزيئية. تبين نتائج الفحص AFM تأثير واضح للتشعيع بالليزر على سطح الغشاء الرقيق. تبين النتائج بوضوح تأثير التشعيع بالليزر على تركيب الغشاء.

جمهورية العراق

وزارة التعليم العالي و البحث العلمي

جامعة بابل / كلية العلوم

قسم الفيزياء

تأثير اشعاع الليزر على الخصائص التركيبية والبصرية لصبغة عضوية

رسالة مقدمة الى قسم الفيزياء كلية العلوم جامعة بابل وهي جزء من متطلبات نيل شهادة الماجستير في علوم الفيزياء

من قبل

احمد علي جاسم محمد

بأشراف

أ.م.د. نهال عبدالله عبدالوهاب

١٤٤٤هـ **٢٠٢٢م**